

Motility, Manipulation and Controlling of Unicellular Organisms

Using the example of Trypanosoma brucei brucei & Caulobacter crescentus

Inauguraldissertation

Zur

Erlangung der Würde eines **Doktors der Philosophie (PhD)**

vorgelegt der

Philosophischen-Naturwissenschaftlichen Fakultät
der Universität Basel

von

Axel Hochstetter

von Deutschland

Basel 2014

Originaldokument gespeichert auf dem Dokumentenserver der Universität Basel
edoc.unibas.ch



This work by Axel Hochstetter is licensed under a [Creative Commons Attribution-NonCommercial-ShareAlike 4.0 International License](https://creativecommons.org/licenses/by-nc-nd/4.0/). Die vollständige Lizenz kann unter creativecommons.org/licenses/by-nc-nd/4.0 eingesehen werden.

Genehmigt von der Philosophisch-Naturwissenschaftlichen Fakultät

auf Antrag von

Prof. Dr. Thomas Pfohl

&

Prof. Dr. Nico Bruns

Basel, den 11. November 2014

Prof. Dr. Jörg Schibler
Dekan der Philosophisch-
Naturwissenschaftlichen Fakultät

You are free to:

Share — copy and redistribute the material in any medium or format

Adapt — remix, transform, and build upon the material

The licensor cannot revoke these freedoms as long as you follow the license terms.

Under the following terms:



Attribution — You must give **appropriate credit**, provide a link to the license, and **indicate if changes were made**. You may do so in any reasonable manner, but not in any way that suggests the licensor endorses you or your use.



NonCommercial — You may not use the material for **commercial purposes**.



ShareAlike — If you remix, transform, or build upon the material, you must distribute your contributions under the **same license** as the original.

No additional restrictions — You may not apply legal terms or **technological measures** that legally restrict others from doing anything the license permits.

Notices:

You do not have to comply with the license for elements of the material in the public domain or where your use is permitted by an applicable **exception or limitation**.

No warranties are given. The license may not give you all of the permissions necessary for your intended use. For example, other rights such as **publicity, privacy, or moral rights** may limit how you use the material.

please find more information at <http://creativecommons.org/licenses/by-nc-sa/4.0/>

1	ABSTRACT.....	8
2	INTRODUCTION	9
2.1	GOALS AND SPECIFIC OBJECTIVES:	10
3	BACKGROUND KNOWLEDGE	11
3.1	PROPULSION OF SINGLE-CELLED ORGANISMS.....	11
3.1.1	<i>What are bacteria, amoeba and protozoa?</i>	11
3.1.2	<i>Means of motility</i>	13
	Cilia & flagella	13
	Pseudopods & pili.....	14
3.1.3	<i>Diffusion and Brownian motion</i>	15
3.2	MODEL ORGANISMS	20
3.2.1	<i>Trypanosoma brucei brucei</i>	20
	Taxonomy, life cycle and related disease.....	20
	Course of disease	21
	Sheathed flagellar propulsion.....	23
	Hydrodynamic clearing of VSG.....	25
3.2.2	<i>Caulobacter crescentus</i>	26
	Taxonomy, live cycle and habitat	26
	Caulobacter propulsion	28
3.3	MICROFLUIDICS	29
3.3.1	<i>Definition Microfluidics</i>	29
3.4	OPTICAL TWEEZERS	33
3.4.1	<i>Light and matter interactions</i>	33
3.4.2	<i>Optical trap</i>	34
4	MATERIALS AND METHODS.....	36
4.1	CELL CULTURE.....	36
	Cultivating caulobacter	36
	Cultivating trypanosomes.....	36
	Preparing cell and drug solutions	36
	Storing trypanosomes	37
	Thawing trypanosomes	37
	Preparing fixated trypanosomes	37
	Disposing trypanosomes.....	37
4.2	MICROFLUIDICS & SOFT LITHOGRAPHY	38
4.2.1	<i>Master preparation</i>	39
4.2.2	<i>Device preparation</i>	39
4.2.3	<i>Device mounting</i>	39
4.3	OPTICAL TRAPPING AND MICROSCOPY	40
4.3.1	<i>Calibration of the optical trap</i>	40

4.3.2	<i>Image recording and analysis</i>	42
	Tracking.....	42
	Aligning of Stacks (Registration).....	43
	Plot Profile.....	43
	CFD Simulations:.....	43
5	OPTICAL TRAPPING OF BACTERIA ON THE EXAMPLE OF <i>C. CRESCENTUS</i>	45
5.1	INTRODUCTION.....	45
5.2	MATERIALS AND METHODS.....	46
5.2.1	<i>Device design</i>	46
5.2.2	<i>Assessing the trap parameters for the force calculations</i>	46
5.2.3	<i>Assessment of photo-toxicity</i>	48
5.2.4	<i>Measuring escape probability and force</i>	48
5.2.5	<i>Induction of holdfast formation</i>	49
5.3	RESULTS.....	50
5.3.1	<i>Optical trap calibration for caulobacter</i>	50
5.3.2	<i>Photo-toxicity</i>	51
5.3.3	<i>Forces generated by caulobacter</i>	52
5.3.4	<i>Motility of caulobacter in the optical trap</i>	54
5.3.5	<i>Mechanically induced surface adhesion</i>	55
5.4	CONCLUSIONS.....	59
6	OPTICAL TRAPPING OF PROTOZOA, E.G. <i>TRYPANOSOMA BRUCEI BRUCEI</i>	60
6.1	INTRODUCTION.....	60
6.2	METHODS.....	60
6.3	RESULTS.....	61
6.3.1	<i>Optical trapping of trypanosomes</i>	61
6.3.2	<i>Dissipative energy of trypanosomes</i>	63
6.4	CONCLUSIONS.....	66
7	HYDRODYNAMIC IMPACT OF TRYPANOSOMES ON THEIR ENVIRONMENT	68
7.1	INTRODUCTION.....	68
7.2	METHODS.....	69
7.3	RESULTS.....	69
7.4	CONCLUSION.....	71
8	HYDRODYNAMIC MANIPULATION OF TRYPANOSOMES	72
8.1	INTRODUCTION.....	72
8.2	METHODS.....	74
8.3	RESULTS.....	77

8.4	DISCUSSION	80
8.5	CONCLUSION.....	82
9	MICROFLUIDICS-BASED SINGLE CELL ANALYSIS TO STUDY DRUG-DEPENDENT MOTILITY CHANGES IN TRYPANOSOMES	83
9.1	INTRODUCTION.....	83
9.2	RESULTS.....	85
9.2.1	<i>Design and function of drug testing device.....</i>	<i>85</i>
9.2.2	<i>Device operation.....</i>	<i>86</i>
9.2.3	<i>Drug diffusion</i>	<i>86</i>
9.2.4	<i>Microfluidics single cell motility analysis with glutaraldehyde.....</i>	<i>87</i>
9.2.5	<i>Microfluidics testing of 2DG on trypanosome motility</i>	<i>88</i>
9.2.6	<i>Impact of low dosages of 2DG on trypanosomes motility.....</i>	<i>90</i>
9.2.7	<i>Single cell analysis with suramin</i>	<i>92</i>
9.3	DISCUSSION	95
9.4	CONCLUSION.....	96
10	DISCUSSION	97
11	OUTLOOK AND PERSPECTIVES.....	101
12	APPENDIX A RECIPES.....	102
12.1	SOFT LITHOGRAPHY:	102
12.2	CELL CULTURE.....	103
12.2.1	<i>Media.....</i>	<i>103</i>
	HMI-9 culture medium (HMI-9; 1 litre):	103
	Culture medium for experiments (50 mL):.....	103
	Drug solution for experiments (20 mL):	103
	Freezing medium (100 mL).....	104
	Trypanosome dilution buffer TDB.....	104
	Trypanosome fixation buffer TFB.....	104
	Trypanosome sleeping buffer TSB.....	104
12.3	MATLAB CODES.....	105
12.3.1	<i>Plotting Trajectories in 3D:.....</i>	<i>105</i>
12.3.2	<i>Mean squared displacement (MSD) script.....</i>	<i>106</i>
13	REFERENCES	107
14	THANKS AND ACKNOWLEDGMENTS.....	114

List of abbreviations

2DG	2-Deoxy- <i>D</i> -Glucose
ACF	Auto Correlation Function
BSA	Bovine Serum Albumin
BSF	Bloodstream form
CC	Connecting Channel, between MC and chambers
caulobacter	<i>Caulobacter crescentus</i> / <i>C. crescentus</i>
FCS	Fetal Calf Serum (heat inactivated)
GA	Glutaraldehyde
GPI	Glycophosphatidylinositol
HAT	Human African Trypanosomiasis
NA	Numerical Aperture
MSD	Mean Square Displacement
OT	Optical Trap
PDMS	Polydimethylsiloxan; [C ₂ H ₆ OSi] _n
PFR	Paraflagellar Rod
RT	Room Temperature
trypanosomes	<i>Trypanosoma brucei brucei</i> / <i>T. b. brucei</i>
VSG	Variable surface Glycoprotein, a homodimeric GPI-anchored Protein; major <i>T.b.</i> surface antigen

Table of units and their abbreviations

fps	frames per second
mL	millilitre; (1mm) ³
mM	millimolar; 6.022 x 10 ⁻²⁰ molecules per litre
μM	micromolar; 6.022 x 10 ⁻¹⁷ molecules per litre
Pa	pascal
pN	piconewton; 10 ⁻¹² N
rpm	revolutions per minute
s	seconds
t	time

1 Abstract

Introduction: Motility is a measure for vitality of unicellular organisms. By using a microfluidic setup it is possible to analyse single-cell organisms and their motility. Thus it is possible to achieve several goals, from characterising the way of movement and the forces thereby generated to analysing drug effects and controlling pathogen displacement and spatial concentration to facilitate diagnosis. In order to do so, the microfluidic device as well as the manipulation and analysis tools have to be calibrated and adapted to the varying parameters as determined by the matter under study.

Methods: Using microfluidics in combination with optical trapping of unicellular organisms and high-speed microscopy, displacement trajectories were recorded and subsequently analysed using computer aided image analysis to characterise the flagellar propulsion of *Trypanosoma brucei brucei* and *Caulobacter crescentus*. Additionally, changes in the motility of *T. b. brucei* under the influence of drugs and different environments were determined and holdfast formation in *C. crescentis* was induced. The calibration parameters of the optical trap and the microfluidic devices were determined for different experimental setups in order to minimise phototoxic effects and maximise retention time of the organisms in the device.

Results: Swimming, *Caulobacter crescentus* generate an average force of 0.3 pN while being capable of a maximal force of 2.6 pN. *C. crescentis* and *Trypanosoma brucei brucei* rotate when they are inside an optical trap but for the trypanosomes this depends on the type of movement they were exhibiting directly before being trapped. The movement of *T. b. brucei* around the trap has a frequency of 15 Hz for the flagellar beat and a frequency of 1.5 Hz for the rotation itself.

The hydrodynamic interaction between swimming trypanosomes and the environment shows characteristic flow patterns around the trypanosome that reveal it to be a pusher and not a puller. Their random-walk like migration can be directed by the geometry of the microfluidic device in order to contain them inside the device.

In our experimental setup, *Caulobacter crescentus* exhibits a phototoxic reaction when trapped with a laser of the wavelength of 808 nm.

The combination of optical traps and microfluidic devices can be furthermore used as a versatile methodology to study the impact of drugs and chemicals on motile unicellular organisms. Due to diffusion driven drug control, dosage-dependent effects can be determined through a motility factor.

Conclusion: Microfluidics in combination with optical trapping of cells and high speed microscopy can be used to analyse, manipulate, and control the motility of unicellular organisms, thus providing us with an interdisciplinary toolset to study living soft matter in a complex fluidic environment.

2 Introduction

As we learn more and more about our world, we start looking at it on smaller scales. Thus the need arose to be able to investigate ever more complex systems on a smaller scale. The demand to study matter in small, often liquid-filled systems has given rise to the field of microfluidics. Moreover, microfluidics research has become ever more interdisciplinary, allowing us to integrate knowledge from several fields such as biology, chemistry, and physics simultaneously into research. With microfluidics, we are enabled to study soft matter, such as living cells, while it is still in its natural state and interacting with its environment. By explicitly shaping and controlling the environment we can study the matter's reaction to, and interaction with, its environment and thus learn more about the matter itself. Such investigations help us to better understand whole interaction systems.¹ Furthermore in combination with optical tweezers we are able to directly capture and control the matter we are aiming to study, which additionally presents us with a mean to examine influences generated by the matter on its environment.

However, the devices and traps have to be adapted to the matter under study. Living matter requires especially careful thought and consideration as it is comprised of a complex system of molecules and mechanisms that, when disturbed, can disintegrate, rendering it useless for study². Understanding these determinants, on the other hand, allows us to explore ways in which we can chemically and physically manipulate and control matter. At the example of pathogenic cellular organisms, gaining control means finding new ways to fight against them. Furthermore, the ability to study living matter in a complex system yet outside of the animal model, is a widely acknowledged need in various fields from biology to medicine.³ The ability to directly observe and experiment on matter in a controlled environment, not only allows us to bridge the gap between compound research and animal testing⁴ but also leaves us with the possibility to intervene more into the system and, by manipulating, understand it - something that is not possible in an animal model.

In order to understand the interaction of living cells with their environment, one first step is to understand what guides their behaviour and movement. This is especially interesting for single-cell organisms as they show a large variety of motility and behaviours, depending on the species, despite being comprised of only one single cell.⁵⁻¹⁰ A trypanosome for example, uses its motility not only for displacement, but also as a mechanism to clear its cell-surface of variable surface glycoproteins.¹¹ By making use of the flow field around its cell-body, the trypanosome manages to move proteins towards its cellular pocket where they can be endocytosed and digested. This enables the trypanosome to evade the host's immune system.¹¹ Another example of an important behaviour pertaining to motility is the ability of certain unicellular organisms, such as caulobacter, to form a strong bond with a surface and avoid displacement by the surrounding flow, which is

key to form biofilm colonies in food-rich environments.^{12,13} These examples show how the ability to move or to remain stationary plays a complex role for the survival of unicellular organism within their environment.

Understanding and even manipulating motility opens up the possibility for researchers to intervene in the system. By knowing how the motility and migration of living soft matter is determined in a given environment, it is possible to shape the circumstances so we can exert control over it. Furthermore, the understanding of the physical determinants of the cell's displacement within a complex fluid (e.g. blood) might open up possibilities to develop new methodology to find and thus diagnose pathogens within the liquids of the host body.

However, to do so we must understand the physical and methodological determinants of the traps and manipulation devices themselves, as well as their interaction with the living matter including variations in this interaction between different species of single cell organisms. When setting up an experimental design, careful consideration has to be given to the dimensions and geometry of the microfluidic device as well as to the calibration of the manipulation and recording tools.

2.1 Goals and specific objectives:

- To assess the forces and energy generated by flagellated unicellular swimmers on the example of *Caulobacter crescentus* and *Trypanosome brucei brucei*.
- To answer the question of whether the motility of caulobacter and trypanosomes is influenced by the optical trap.
- To see whether holdfast formation can be induced in *C. crescentus* by bringing the bacteria into close contact with a surface by an optical trap.
- To analyse the hydrodynamic flow field generated by a persistently swimming trypanosome and to classify trypanosomes as either pusher or puller.
- To assess in how far device geometry and presence or absence of flows, affect the detainment time of trypanosomes in confinement chambers.
- To explore the possibility for a passive cell sorting device suitable for the development into a diagnostic tool.
- To combine existing microfluidic devices and optical tweezers in order to create a methodology suitable for the testing of chemical substances on trypanosomes.
- To study the influence of varying doses of 2-deoxy-*D*-glucose and suramin on the motility of trypanosomes.

3 Background knowledge

3.1 Propulsion of single-celled organisms

3.1.1 What are bacteria, amoeba and protozoa?

Each life-form on this planet can be set into a relation to all other life-forms. One up-to-date system for categorizing all life forms is the system of the six kingdoms that share a common ancestor. This taxonomic system is based on a genetic meta-analysis of Ciccarelli *et al.*¹⁴ shown in Figure 3.1. Figure 3.1: The six kingdoms of biology, sharing a common ancestor¹⁵.

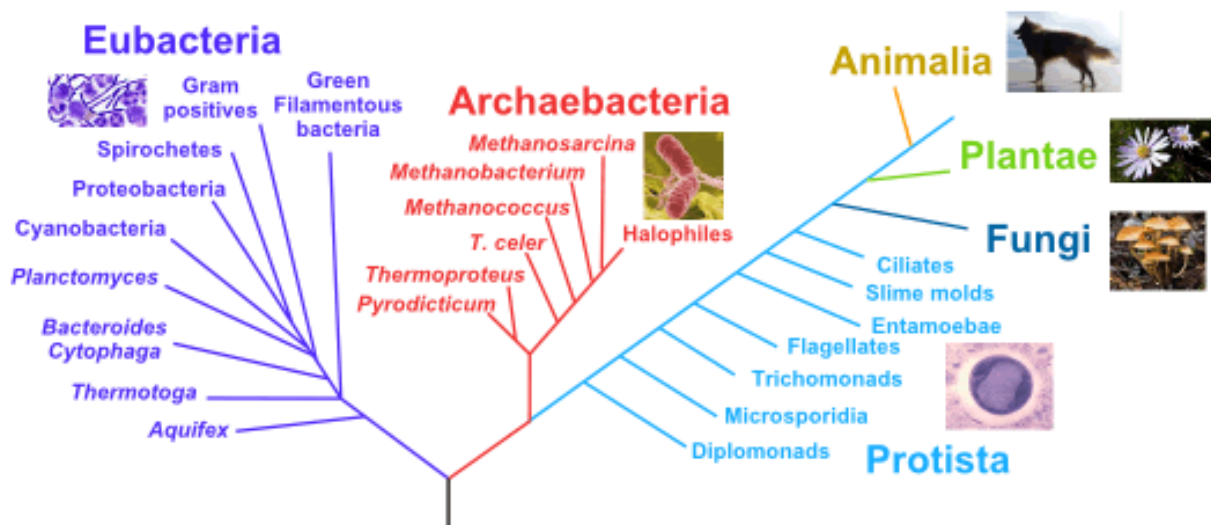


Figure 3.1: The six kingdoms of biology, sharing a common ancestor¹⁵

The six kingdoms can be sorted into the two groups of Eukaryota (protista, fungi, plantae and animalia), that possess a nucleus and other membrane-bound internal organelles, and Prokaryota (eubacteria and archaeobacteria) that do not possess any membrane bound organelles or nuclei (Figure 3.2)¹⁶.

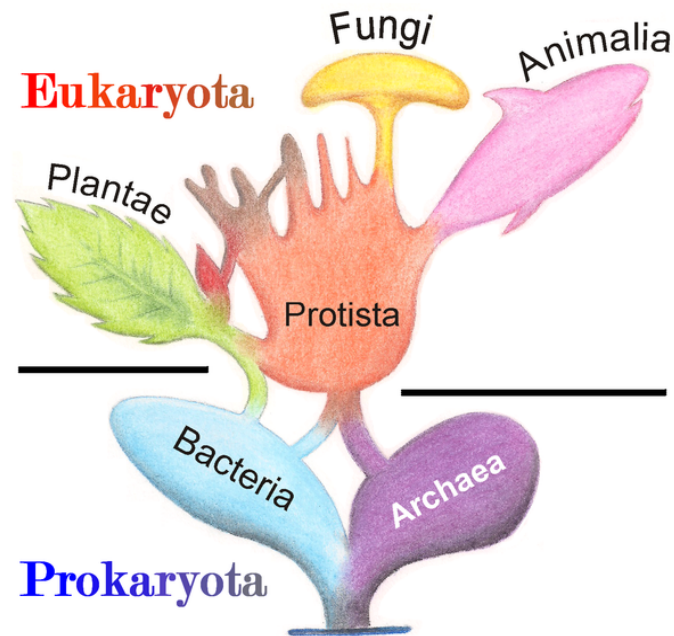


Figure 3.2: The six kingdoms in biology, assigned to Prokaryota and Eukaryota.¹⁷

For this work, where the motility of unicellular organisms is investigated, the "microscopic swimmers" are found in the kingdoms of eubacteria (for the *Caulobacter crescentus*) and protista (for the *Trypanosoma brucei brucei*, formerly protozoa) respectively. Throughout this work, the taxonomy of species is based on the works of Ciccarelli *et al.*¹⁴ and Adl *et al.*¹⁸ (Figure 3.1 and Figure 3.2).

The typical sizes for objects and organisms studied in microfluidics range from 1 and 100 μm . In this size regime we find exemplary three prototypes of cell motility: amoebae, bacteria (propelling themselves with pili) and flagellates.

3.1.2 Means of motility

Unicellular organisms have several structures to propel themselves, i.e. to crawl along a surface or swim in a surrounding liquid

Cilia & flagella

Eukaryotic cilia and flagella are whiplike structures that move either the cell itself or the surrounding medium. They share a common internal structure (Figure 3.3). From inside a basal body (kinetosome) the cilium/flagellum extends from the cell body. Surrounded by the extended plasma membrane, cilia/flagella consist of nine doublet microtubules that are arranged in a circle around a central pair of singlet microtubules (axoneme). This 9+2 arrangement extends to the distal end of the cilia/flagella. Arrays of dynein motor proteins anchored along one side of each microtubule (MT) doublet walk along the adjacent MT doublet, thereby producing the force for cell propulsion by MT bending.

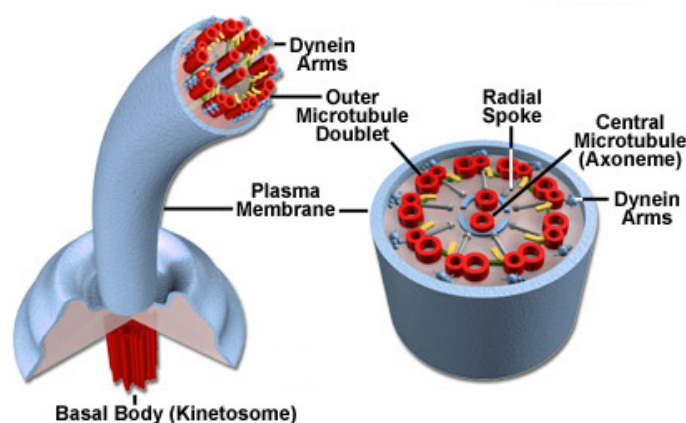


Figure 3.3: Structure of cilia and eukaryotic flagella

Adapted from <http://micro.magnet.fsu.edu/cells/ciliaandflagella/ciliaandflagella.html> by Michael W. Davidson.

The major differences between flagella and cilia are their length in comparison to the cell body (flagella are longer), their number (only one to a few flagella versus hundreds of cilia per cell), and how they beat.¹⁹

Cilia are very fast moving structures that, like a motor, produce a rotational movement. The beating of cilia has two phases: the effective stroke, where a cilium is elongated and moves forward, and a recovery stroke, where the cilium is bent while moving backwards (Figure 3.4 a). Due to this asymmetry in the beat, a net force is generated in the direction of the recovery stroke. The small asynchrony (phase shift) in a group of cilia that beat together results in a metachronal wave (Figure 3.4 b) that generates a net flow of the surrounding medium.²⁰

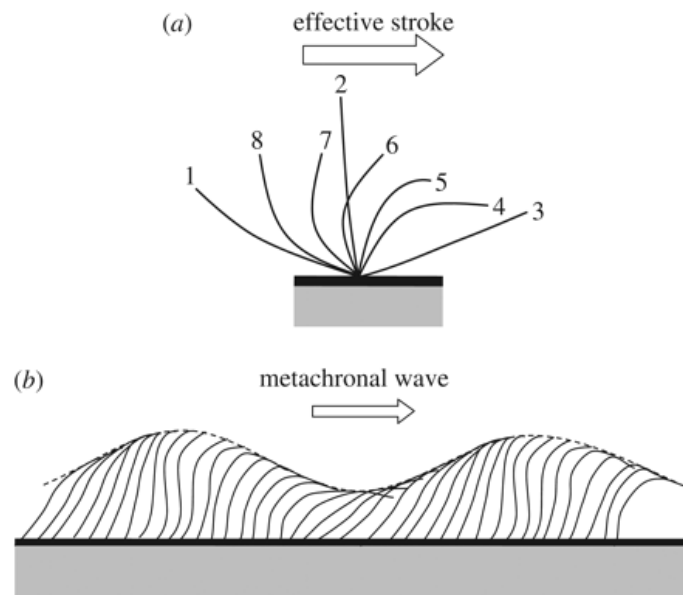


Figure 3.4: Cilia stroke pattern

(a): Effective stroke (1-3) and recovery stroke (4-8 → 1) of an individual cilium.

(b): Metachronal wave resulting from concerted beats of cilia. Images reproduced from T. Ishikawa²⁰.

There is no clear distinction between ciliary propulsion and eukaryotic flagellar propulsion.²⁰ Where the assembly of cilia together create a metachronal wave to propel the ciliate, eukaryotic flagellates swim by propagating planar or helical throughout their flagella.²⁰ In prokaryotes that do not have microtubules, flagella are helical filaments placed outside of the cytoplasmic membrane. Bacterial flagella are rotated relative to the cell body like a screw, driven by force that is produced by a basal motor complex.⁷ The rotation generates a helical wave that propagates to the distal tip of the flagellum, thus propelling prokaryotic flagellates.^{7,20}

Pseudopods & pili

Amoebae propel themselves by crawling along a surface. For each stride, they cycle through the following five steps (Figure 3.5): After an internal or external stimulus (1) the cell produces a finger-like protrusion (pseudopod) (2) that adheres to a remote spot of the substrate (3). The cell distorts and elongates by creating a contractile tension (4) and then moves closer to the targeted area by detaching and retracting the tail (5).

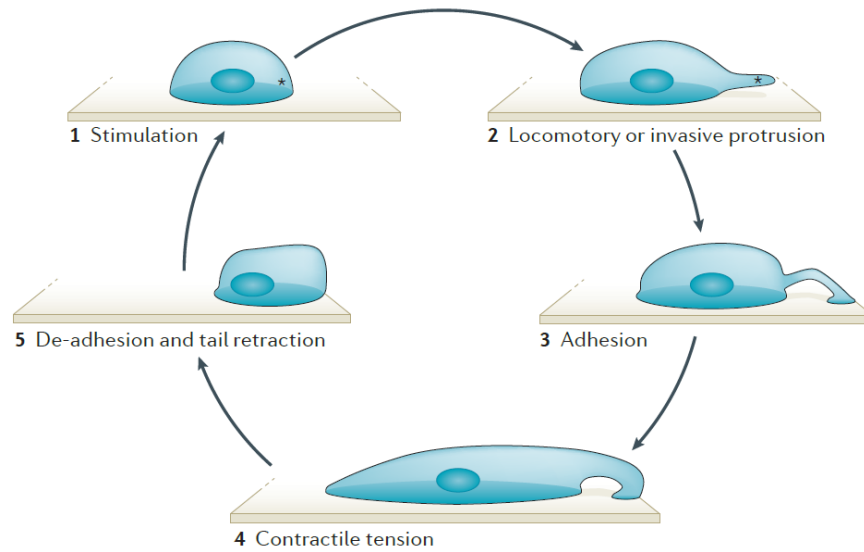


Figure 3.5: Cycle for amoeboid cell motility. Figure was originally published by J.J. Bravo-Cordero²¹.

Similar to amoeboid locomotion, cells can glide along a surface by using pili. Pili are long and thin, hair-like protrusions on bacteria, that serve multiple purposes. For example DNA uptake, protein secretion and propulsion are performed by type IV pili in gram positive bacteria.²² In the gram positive bacteria *Neisseria gonorrhoeae*, the force exerted by one type IV pili has been measured to be 50-100 pN.²³ By this force, *Neisseria gonorrhoeae* pull themselves²³ upwards in the urinary tract, where they cause inflammations in infected hosts²⁴.

3.1.3 Diffusion and Brownian motion

Even without active propulsion, micro-organisms in fluidic media still exhibit a steady displacement. This displacement was first described in 1785 by Jan Ingenhousz when investigating the stochastic movement of coal dust on alcohol and became popular when in 1827 the scottish botanist Robert Brown described the motion of pollen particles on water. In 1905, Albert Einstein proposed a set of equations as thermodynamic scaffold to Brown's observations.²⁵ He introduced D as the diffusion constant of particles, which depends on universal constants, the absolute temperature, the size of the particles and the viscosity of the fluid.

$$D = \frac{RT}{6N_A\pi\eta a} = \frac{k_bT}{6\pi\eta a} = \frac{k_bT}{\gamma_0} \quad (3.1)$$

where R is the gas constant, T is the temperature in Kelvin, $N_A = 6.022 \times 10^{23} \text{ mol}^{-1}$ is the Avogadro constant, η is the dynamic viscosity of the fluid, a the particle radius and $k_B = \frac{R}{N_A}$ is

Boltzmann's constant and γ_0 is the drag coefficient of a spherical particle moving relative to the surrounding fluid.

Eight years later Przi Bram²⁶ reported that the trajectories of moving protozoa can be described by *Brownian motion*. While the net displacement $x(t) - x(0)$ averages to zero, its square can be described by

$$\langle d(\tau)^2 \rangle = 2n_{dim}D\tau \quad (3.2)$$

where τ is time and n_{dim} is the number of dimensions in which the motion takes place.²⁷

Przi Bram also found, that the *random walks* of his investigated protozoa are much more influenced by the temperature than Einstein had stated.²⁷

An object that moves without persistence or preferred direction can be described by the random walk model. Popularly, this model is described as a drunken sailor trying to leave a tavern. After each step he takes, he falls down, and forgets in which direction he was just heading. When he gets up again, he takes one step in a random direction and falls again.

For the 1-dimensional random walker, there exist only two directions: back or forth. After one step, he is $x = 1 \delta$ away from his origin (the tavern, $x = 0$). After the second step, he is either two steps 'right' ($x = 2 \delta$), two steps 'left' ($x = -2 \delta$) or back at the tavern ($x = 0$). With a probability of 50%, he is back at the tavern, and in 25% of the cases he is either 2 steps to the left or right.

With increasing number of steps, n , the probability P that the sailor managed to be m steps away from the tavern can be calculated by

$$P_{n,m} = \left(\frac{1}{2}\right)^n \binom{n}{\frac{n-m}{2}} = \frac{n!}{2^n \left(\frac{n+m}{2}\right)! \left(\frac{n-m}{2}\right)!} \quad (3.3)$$

The probability distribution for 10 steps is exemplarily plotted below in Figure 3.6. The probability can be fitted by a Gaussian normal distribution.

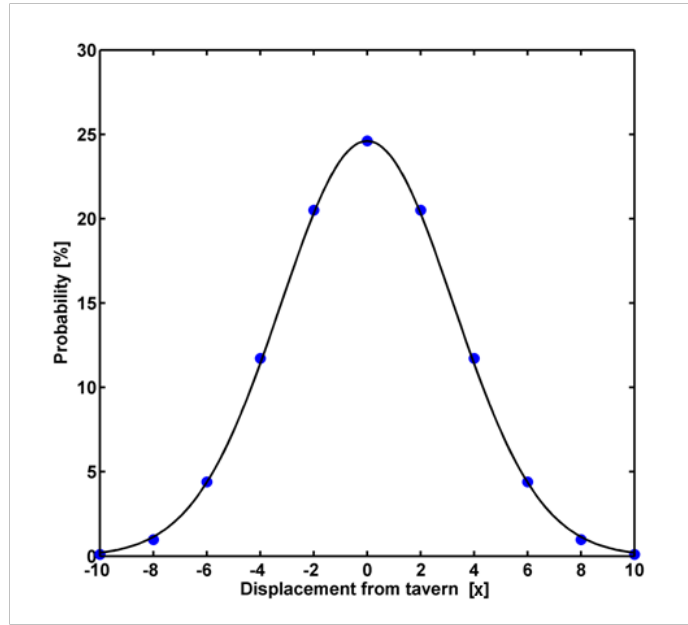


Figure 3.6: Probability density distribution for displacement after 10 steps. Black line represents a Gaussian normal distribution fit.

As illustrated by Figure 3.6, the mean displacement $\langle r \rangle$ equals zero. By squaring the mean displacement, we arrive at the mean squared displacement (MSD), which is defined by

$$MSD(\tau) \equiv \langle r^2(\tau) \rangle \quad (3.4)$$

where τ denotes the timespan in which the displacement took place. The MSD can also be seen as a representation of the area an average random walker explores during τ timesteps.

Together with equation (3.2), which describes the same phenomenon, we can derive the following relation between the MSD of a random walker and his *diffusion constant*:

$$MSD = \langle r^2(\tau) \rangle = 2n_{dim}Dt \quad (3.5)$$

While the relation in equation (3.5) holds true for model random walkers, like diffusing particles, living organisms sometimes exhibit an anomalous random walk behaviour. For the drunken sailor model, that might be a sailor that from time to time remembers that he left his purse in the tavern and therefore tries to get back until he falls again, gets up, takes three random steps and remembers again his purse...

For anomalous diffusion, equation (3.5) can be adjusted to:

$$\langle \Delta(r)^2 \rangle = 2n_{dim}K_{\alpha}\tau^{\alpha} \quad (3.6)$$

where K is the generalized diffusion constant and α is the anomalous diffusion exponent which defines the process as either *subdiffusive* ($0 < \alpha < 1$) or *superdiffusive* ($1 < \alpha \leq 2$). Subdiffusive motion i.e. would be that the sailor repeatedly goes back to the tavern, thus covering less area than he randomly would. Superdiffusive in this context would be, that he tries to head to his ship. For $\alpha = 2$, he would go straight to his ship in a ballistic motion. Here $\alpha = 1$ would denote a normal diffusion. For three sailors each with a speed of one meter per second and a α of 0.5, 1 and 2 respectively, the MSD would look like Figure 3.7.

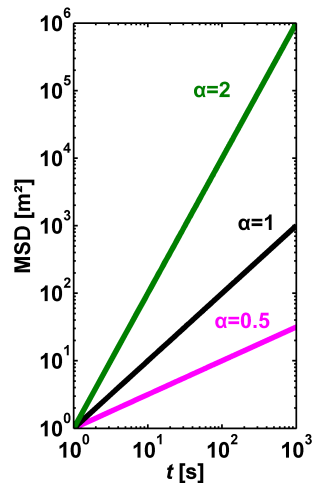


Figure 3.7: MSD of normal diffusive (black), subdiffusive (magenta) and superdiffusive / ballistic behaviour (green).

With double-logarithmic scaling, MSD plots are linear and allow for direct measure of the slope, which yields the anomalous diffusion exponent, α , and dividing the covered area by the time step yields the diffusion constant as shown in equation (3.7)

$$D = \frac{\langle r^2(\Delta\tau) \rangle}{2n_{dim}\Delta\tau} \quad (3.7)$$

One microbiological concept that is connected to the random walk model is called *chemotaxis*. A motile swimming cell might find itself in an area with low food supply. To avoid starvation, the cell moves into a random direction, hoping to find a better food supply there. After swimming a certain distance L the cell might sense an increase in food concentration. Then, the cell remains in that area, displacing itself only little in random directions. If the food supply goes down again, it will again swim the same distance L . If in the new spot, food is scarce as well, it remains only briefly there, before it again swims in a randomly chosen direction the distance L . This behaviour is called chemotaxis and depicted in Figure 3.8.

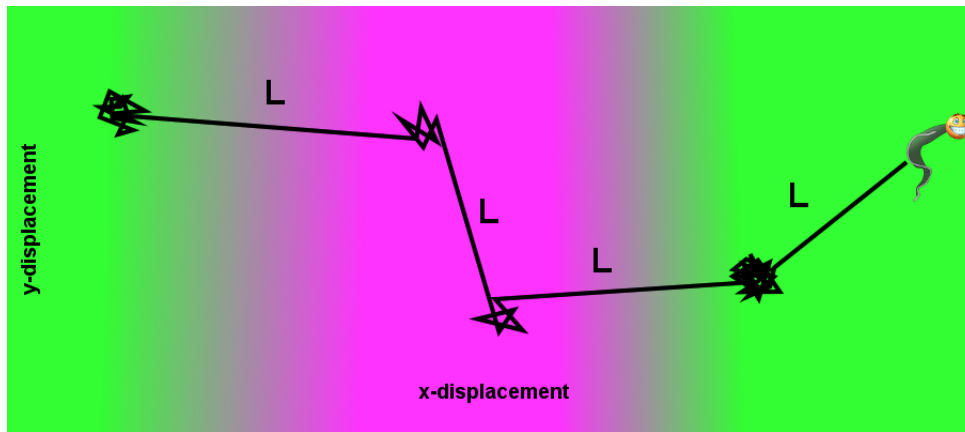


Figure 3.8: Chemotaxis shown in the trajectory of a microbial organism through an area of scarce food supply (magenta) to a space with ample nutrients (green).

To determine whether a given cell can outrun diffusion, the distance L can be compared to the diffusion constant D divided by the cell's velocity v

$$L = \frac{D}{v} \quad (3.8)$$

Equation (3.8) can be rearranged to

$$Pe = \frac{vL}{D} \quad (3.9)$$

where Pe is the Péclet number. For $Pe > 1$ the cell is better off to go and look for areas with a higher food concentration, whereas for $Pe < 1$ the cell is either too slow or stops too often to outrun the diffusion. In this case, the cell might be better off saving energy and just wait for the nutrients to diffuse towards it.

3.2 Model organisms

3.2.1 *Trypanosoma brucei brucei*

Taxonomy, life cycle and related disease

Trypanosoma brucei brucei (trypanosomes) is widely investigated as a model flagellate.^{28–32} It is a subspecies of the family of trypanosomes (Table 3.1) that causes fatal sleeping sickness in humans (Human African Trypanosomiasis, HAT),^{33–35} which is endemic in specific parts of Africa.^{34–37} Moreover, as part of their live cycle, (Figure 3.10) *T. brucei brucei* cause the Nagana disease in livestock.

Kingdom	Protista
Super-group	Excavata
Phylum	Euglenozoa
Class	Kinetoplastea
Order	Trypanosomatida
Genus	Trypanosoma
Species	<i>T. brucei</i>
Sub-species	<i>T. b. brucei</i>

Table 3.1: Taxonomy of *Trypanosoma brucei brucei*

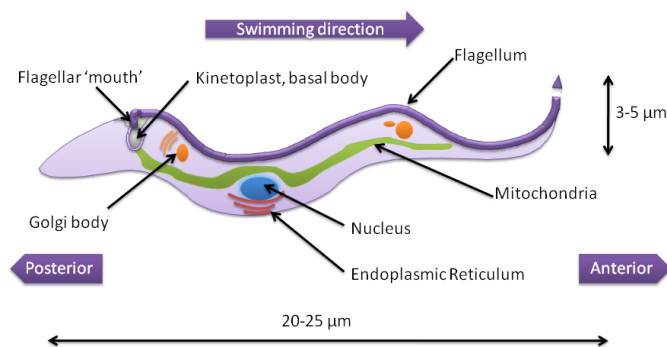


Figure 3.9: Anatomy of *Trypanosoma brucei brucei* BSF showing sizes and essential organelles. Image reprinted from Uppaluri (2011)³⁸

Course of disease

Infection of a mammalian host starts when a tsetse fly bite delivers growth-arrested metacyclic trypomastigotes to the mammalian bloodstream⁸ (Figure 3.10 a). This causes a bloodstream infection. After differentiating into proliferating slender bloodstream forms, they invade extravascular tissues and finally the central nervous system (CNS). The infection of the CNS is called the late stage or the second stage (Figure 3.10 c). When the concentration of slender trypanosomes surpasses a certain concentration in the bloodstream, the differentiation into non-proliferating stumpy forms takes place.

At this stage, a tsetse fly can take up parasites with the blood meal into the midgut. There, short stumpy forms differentiate into procyclic trypomastigotes, which multiply and establish a midgut infection. These midgut procyclic trypomastigotes migrate (**b**) through the peritrophic matrix, along the foregut to the proventriculus. From there they migrate through the mouthparts, via salivary ducts into the salivary gland, where they attach to the salivary gland epithelium (Figure 3.10 b). In the proventriculus, procyclic trypomastigotes undergo extensive restructuring, coupled to an asymmetric division, to generate one long epimastigote and one short epimastigote (Figure 3.10 a).⁸ After arriving in the salivary gland, the short epimastigote attaches to epithelial cells where it replicates before completing the life cycle via an asymmetric division. Thereby, it generates metacyclic trypomastigotes that are freely distributed in the salivary gland lumen and specialized to survive in the mammalian host. Forms that replicate via binary fission are depicted with circular arrows.

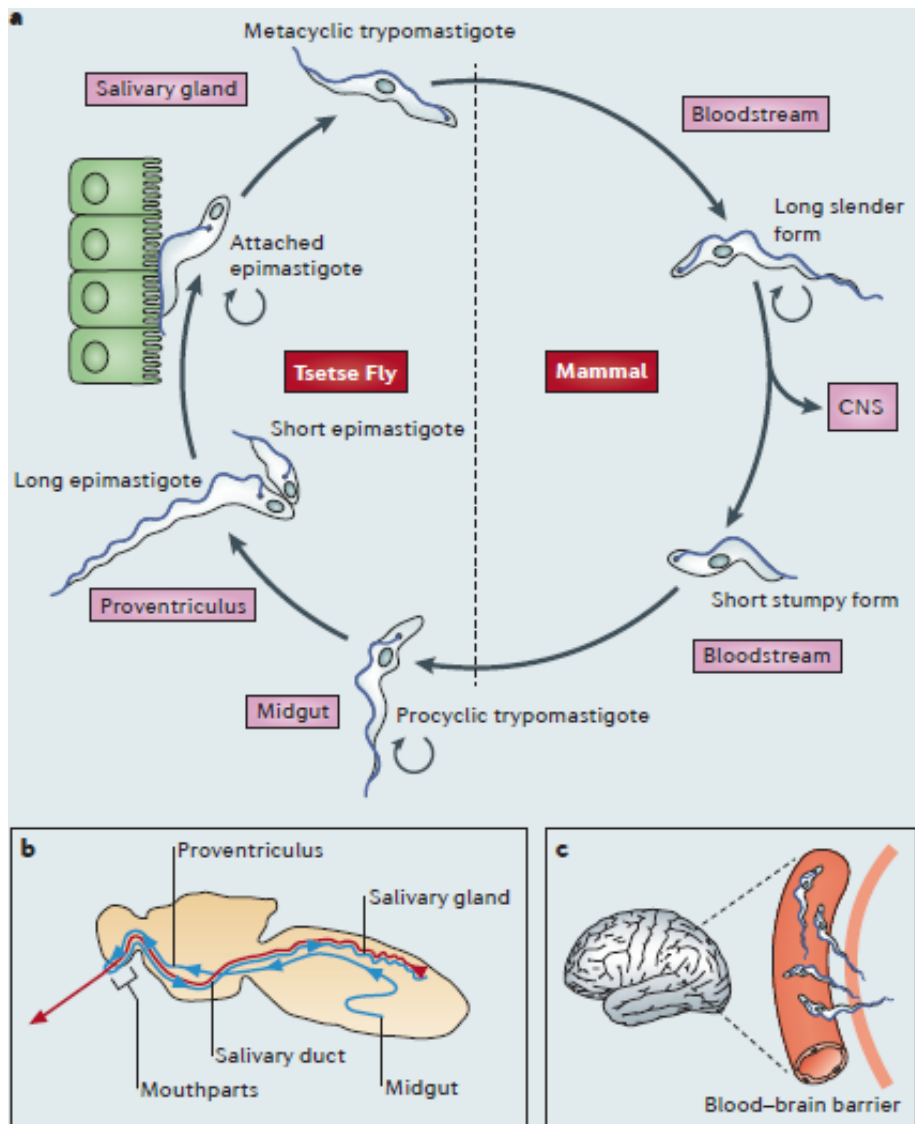


Figure 3.10: Generalized life cycle of *Trypanosoma brucei*

(a): Life cycle both in the mammalian host and in the vector.

(b): Journey through the tsetse fly, including stations that are important for the cell cycle.

(c): Trypanosomes crossing the blood brain barrier into the brain and the central nervous system (CNS). Reused and adapted from Langousis *et al.*⁸ under license of RightsLink

Sheathed flagellar propulsion

The flagellum of the trypanosomes is vital for the locomotion and viability of trypanosomes. It consists of a crystalline paraflagellar rod (PFR) a microtubular axoneme and connecting proteins³⁹. The microtubular axoneme consists of 9 doublets of microtubules that encircle a pair of singlet microtubuli⁸ known as the central pair apparatus. This central pair apparatus reaches from the basal body of the flagellum to its distal tip and does not rotate (as in similar organisms like *C. reinhardtii*) but has a fixed orientation and is vital for the beat generation. Other parts of the flagellum are important for directing, but not for generating the waves caused by the flagellar beat.⁸ The trypanosome flagellum is completely different from bacterial flagella and more complex than most other eukaryotic flagella, being equipped with a paraflagellar rod (PFR) and ciliary necklace. Additionally, it is connected to the cell body along its entire length via the flagellar attachment zone (FAZ) (Figure 3.12). *Trypanosoma brucei* is a model organism for sheathed flagellate propulsion.^{28–32} They exhibit two distinct modes of propulsion: *running* and *tumbling*.⁴⁰ In running mode, trypanosomes move persistently in one direction. In tumbling mode trypanosomes change their direction frequently without moving far (Figure 3.11). Uppaluri *et al.* (2011)⁴⁰ also discussed a third "intermediate" mode, which can be seen as a combination of running and tumbling.

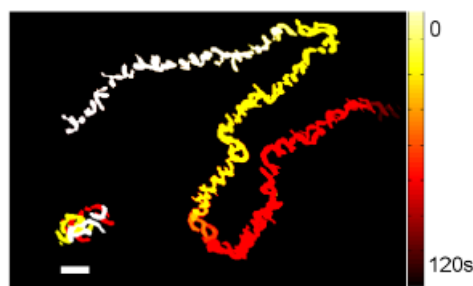


Figure 3.11: Motility modes in trypanosomes. Colour-coded time-lapse image of each one trypanosome in running (upper right) and tumbling (lower left) mode over 2 minutes. Scale bar is 20 μm . Figure reprinted from Uppaluri *et al.* 2011⁴⁰

Hydrodynamic clearing of VSG

In the blood systems of their mammalian hosts, trypanosomes are attacked by the hosts' immune systems. To evade these attacks, trypanosomes are equipped with a variant surface glycoprotein (VSG) coat.¹¹ Antibodies that bind to the VSG coat, are hydrodynamically forced into the flagellar pocket, where VSG-bound antibodies are endocytosed (Figure 3.13) and broken down within lysosomes.

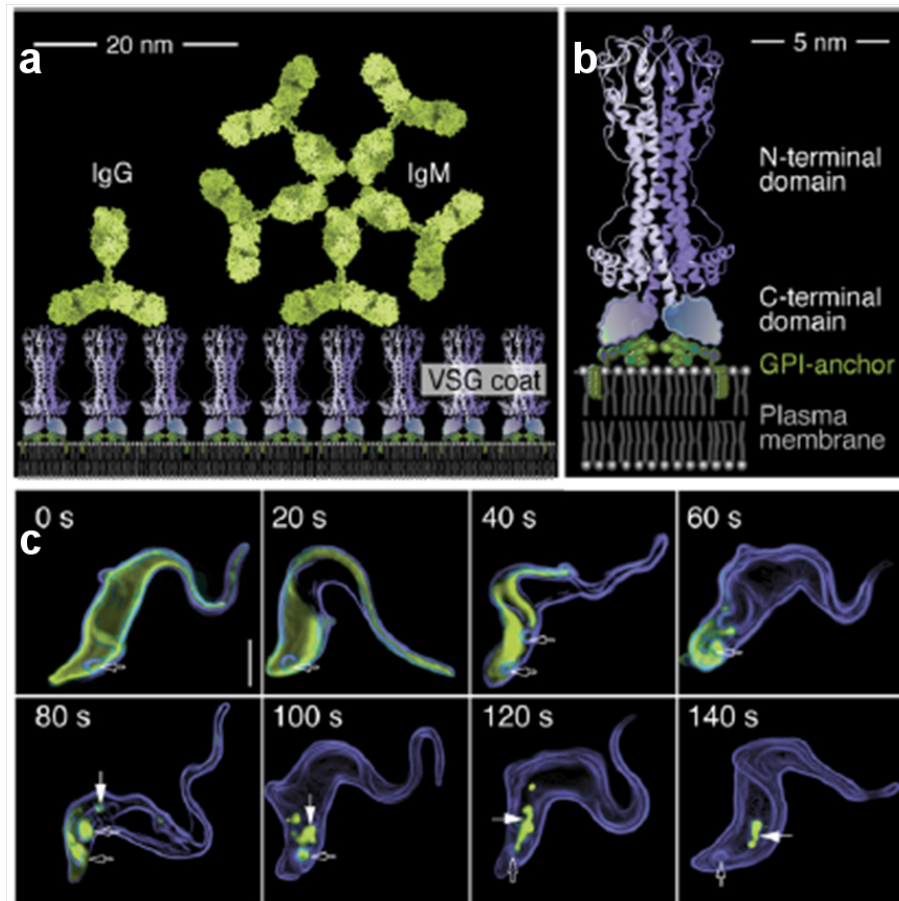


Figure 3.13: Hydrodynamic immuno-response evasion strategy of trypanosomes

(a): Stained IgG and IgM molecules bind to the VSG coat on the trypanosome's surface. (b): VSGs are homodimers that are attached to the surface by GPI anchors. (c): Hydrodynamic clearance of stained Anti-VSG antibodies (green) towards the flagellar pocket (dark arrows) where, after endocytosis, a lysosome (white arrows) is formed in which the anti-VSG antibodies are broken down. Adapted from Engstler *et al.*¹¹

3.2.2 Caulobacter crescentus

Taxonomy, live cycle and habitat

Caulobacter crescentus (caulobacter) is a gram-negative bacterium (Table 3.2), that is widely distributed in fresh water streams and lakes.

Kingdom	Bacteria
Phylum	Proteobacteria
Class	Alpha Proteobacteria
Order	Caulobacterales
Family	Caulobacteraceae
Genus	<i>Caulobacter</i>
Species	<i>C. crescentus</i>

Table 3.2: Taxonomy of *Caulobacter crescentus*.

Caulobacter is an oligotrophic bacterium, which means it can survive on a scarce supply of nutrients and exhibits a two phased live cycle (Figure 3.14).

During the first phase, the cell is a freely swimming swarmer cell (SW) equipped with several pili and one prokaryotic flagellum for propulsion. If a pilus (or multiple pili) get in contact with a solid surface, the pili are retracted and the cell adheres to the surface. Upon surface contact caulobacter starts building a holdfast by secreting adhesins (sticky polysaccharides).⁴¹ Holdfast formation also occurs in swarmer cells without surface contact after about 30 minutes.⁴¹ Once the adhering proteins for the holdfast are secreted, a stalk is assembled between the holdfast and the cell body. During the stalk assembly, the cell sheds its flagellum and becomes a immotile, stalked cell (ST). This is the second phase of caulobacter live cycle. The stalked cell subsequently undergoes asymmetric division. From the free pole, a daughter cell is produced. At the distal end of this pre-divisional cell (PD) a new flagellum appears. As the daughter cell is fully developed, a ring like contraction induces the division of the cell upon the new swarmer cell is released. Thus the live cycle of *Caulobacter crescentus* (Figure 3.14) is completed.

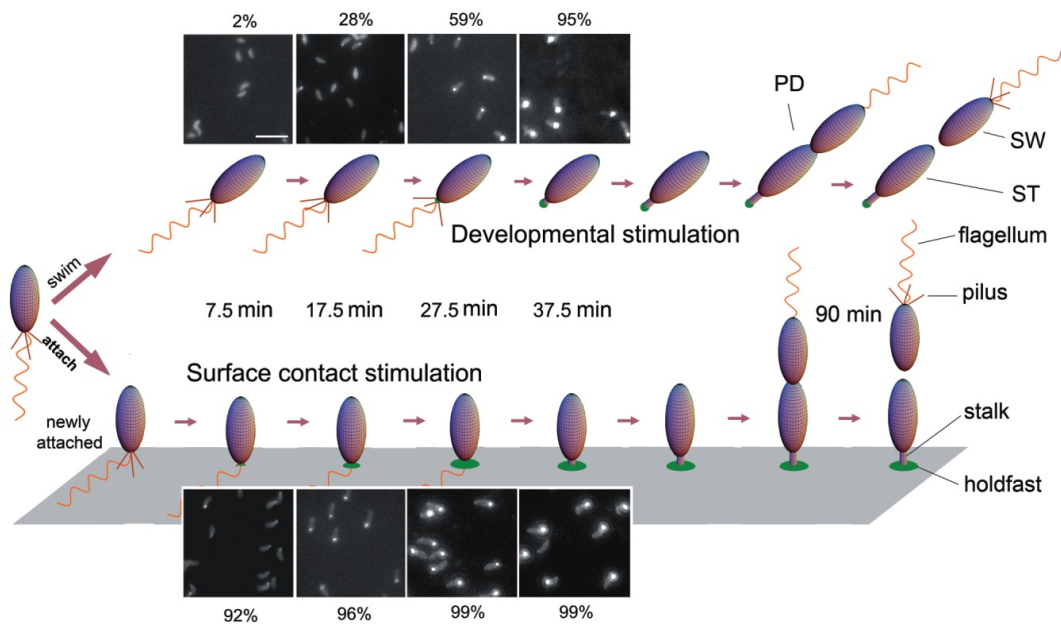


Figure 3.14: Life cycle of *Caulobacter crescentus*.

Fluorescence images of synchronized *C. crescentus* wild-type swarmer cells (top) and stalked cells (bottom). Cells are labelled with fluorescin-WGA. The numbers indicate the percentage of cells bearing a holdfast at the specified times. Image reprinted from Li *et al.* (2012)⁴¹

The gram-negative caulobacter has a bean-shaped cell body, which is enveloped by a multi-layer shell (see Figure 3.15 inset). The shell consists of S-layer of O-antigen and LPS in addition to the outer membrane, periplasm and inner membrane that shield the cytoplasm from the surrounding. Additionally, swarmer cells are equipped with pili and a prokaryotic flagellum on one pole, while stalked cells possess a stalk and a holdfast instead (Figure 3.15). Inside the stalk, diffusion barriers ensure proper nutrient supply.

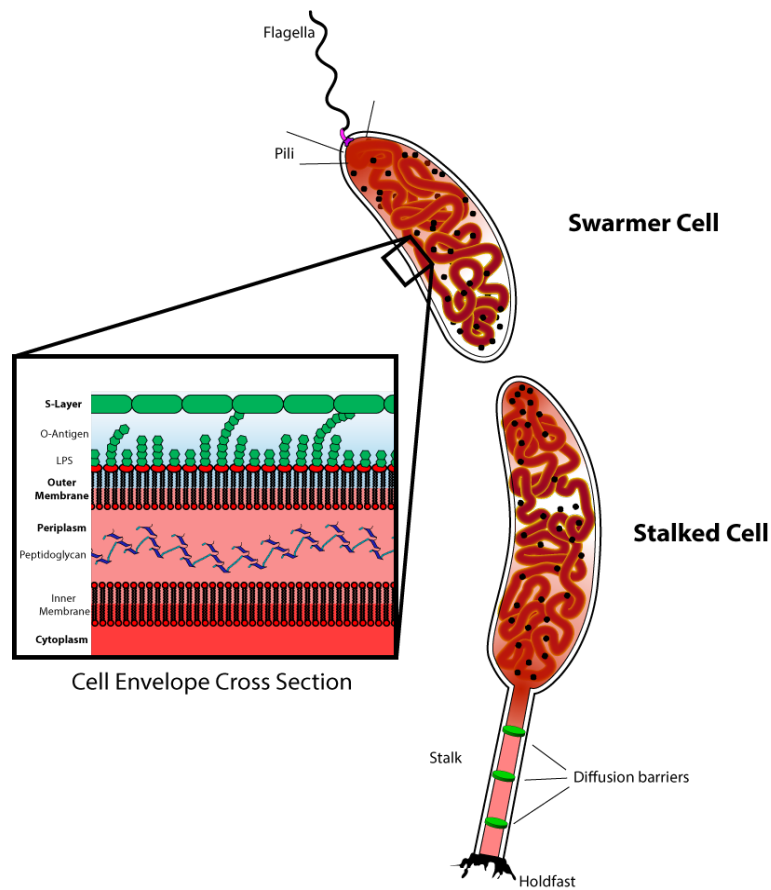


Figure 3.15: Structure of *Caulobacter crescentus*. Taken from http://en.wikipedia.org/wiki/Caulobacter_crescentus.

Due to the dimorphic life cycle (as shown in Figure 3.14) and the readily available mutants^{42–44} *caulobacter* is the main model for the bacterial cell cycle.⁴⁵

Caulobacter propulsion

Caulobacter is equipped with both pili and a prokaryotic flagellum, it propels itself in fluids by swimming using the flagellum and can crawl on surfaces short distances prior to stalk formation.⁴⁶ The motor of a *caulobacter* is reported to have a swimming torque of about $350 \text{ pN} \cdot \text{nm}$ while consuming about $1.5 \cdot 10^{-11} \text{ J}$ for swimming one meter.⁴⁶

3.3 Microfluidics

3.3.1 Definition Microfluidics

The scientific discipline investigating the behaviour and dynamics of fluids on the microscopic length scale is known as microfluidics. Microfluidics is an emergent field on the interface of engineering and physics, advancing fluid-dynamics and is already applied to chemical and biological studies. The term "microfluidic" is further used for devices that consist of channels where fluids and gasses are processed. These channels have diameters ranging from one to hundreds of micrometers. The simplest microfluidic device is a thin cylinder, which we use as a model to visualize basic concepts of microfluidics.

At first, *viscosity*. Viscosity is the property of a fluid, that offers resistance if one layer of the fluid is moved over an adjacent layer. Two layers of fluid with a distance dy and velocities v and $v + dv$ respectively. The viscosity η and the relative velocity dv cause a shear stress τ between the fluid layers.

$$\tau = \frac{F}{A} = \eta \frac{dv}{dy} \quad (3.10)$$

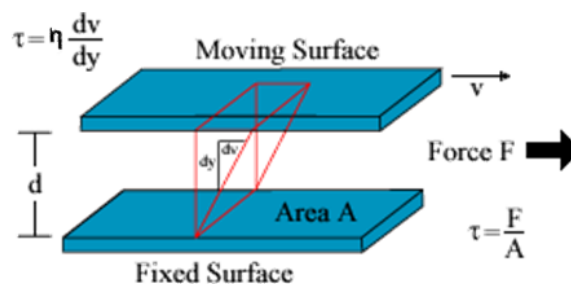


Figure 3.16: Viscosity and shear between two adjacent layers of fluid. Image taken from http://www.oocities.org/venkatej/mech/fluid_mechanics/fluid_mechanics.html

If we expand our focus from two adjacent layers to our model, the cylindrical tube, we will see that the flow inside can be either turbulent or laminar, as shown in Figure 3.17 .

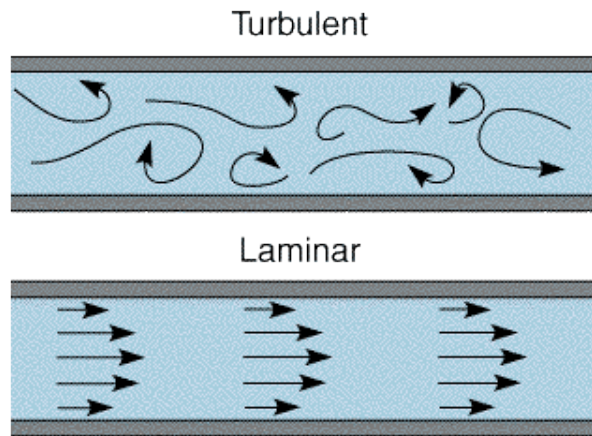


Figure 3.17: Laminar and turbulent flow inside a straight, cylindrical channel. While for turbulent flow, no time independent predictions of the flow velocity and shear can be made, laminar flow is predictable and stationary. The velocity is highest in the centre of the channel, and decreases to almost zero at the wall. Courtesy of Nial Barker.

Turbulent flow profiles change with time and are highly influenced by the geometry of the surrounding vessel. In contrast, laminar flow in a microfluidic device has at any time a parabolic velocity profile (Figure 3.18), even after flowing around obstacles. The differences in velocity of adjacent layers of fluid is the cause for shear stress, that acts upon any body that is placed across the radius of the channel.

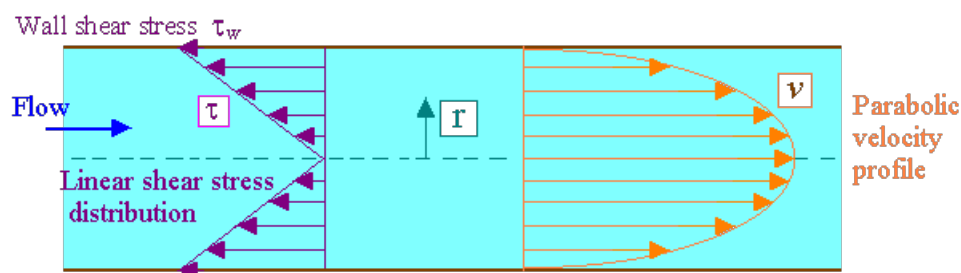


Figure 3.18: Shear stress τ and flow velocity v profile of laminar flow through a cylindrical tube of radius r . Image taken from http://www.oocities.org/venkatej/mech/fluid_mechanics/fluid_mechanics.html

The total mass transport and mass conservation that happens in a microfluidic device can be described by

$$\delta_t \rho = -\nabla \cdot (\rho v) \quad (3.11)$$

where ρ is the density of the fluid and v the velocity. For an incompressible, Newtonian liquid (like water and most buffer solutions) Equation (3.11) can be simplified to

$$\nabla \cdot v = 0 \quad (3.12)$$

All forces that are acting in this fluid system, are expressed in the Navier-Stokes equation. For the simplified case of a incompressible fluid, the Navier-Stokes equation can be expressed as

$$\rho[\partial_t \mathbf{v} + (\mathbf{v} \cdot \nabla)\mathbf{v}] = \eta \nabla^2 \mathbf{v} - \nabla p + \rho \mathbf{g} + \rho_{el} \mathbf{E} \quad (3.13)$$

where η is the fluid viscosity, p is the pressure, \mathbf{g} is the gravitational constant, ρ_{el} is the charge density and \mathbf{E} is an external electric field. While the left hand side of the term represents the inertial forces, the right hand side sums up the viscous and the applied forces.

The relation of inertial to viscous forces can be expressed by the Reynolds number Re :

$$Re \equiv \frac{\rho v l}{\eta} \quad (3.14)$$

with v as the velocity and l as the characteristic length of the system, which would be in our model approximately the internal diameter of the cylinder. For $Re \gg 1$, turbulent flows occur. At Reynolds numbers from 15-2300 flows are not linear anymore, and above 2300 flows are always turbulent⁴⁷. For Reynolds numbers below 1 flow is laminar. Since in microfluidics, both the characteristic length and the velocities are tiny, the inertial forces are feeble and thus negligible. Additionally, since neither electric nor gravitational fields influenced the observations in our experimental setups, we can neglect them as well and arrive at the linear Stokes equation,

$$0 = \eta \nabla^2 \mathbf{v} - \nabla p \quad (3.15)$$

In a microfluidic device with purely laminar flow two (or more) different fluids can interact in four ways (see Figure 3.19):

1. Through a floating interface, where two fluids are joined in one droplet that is immersed in an immiscible, third liquid.
2. Through a pinned interface, where the geometry of the device stabilizes an interface, like standing walls of water next to air.
3. Through a moving interface, where two miscible fluids are flowing alongside and solutes can diffuse freely between them.
4. Through a secondary interface in convection free environments, where all transport processes are diffusion-driven.

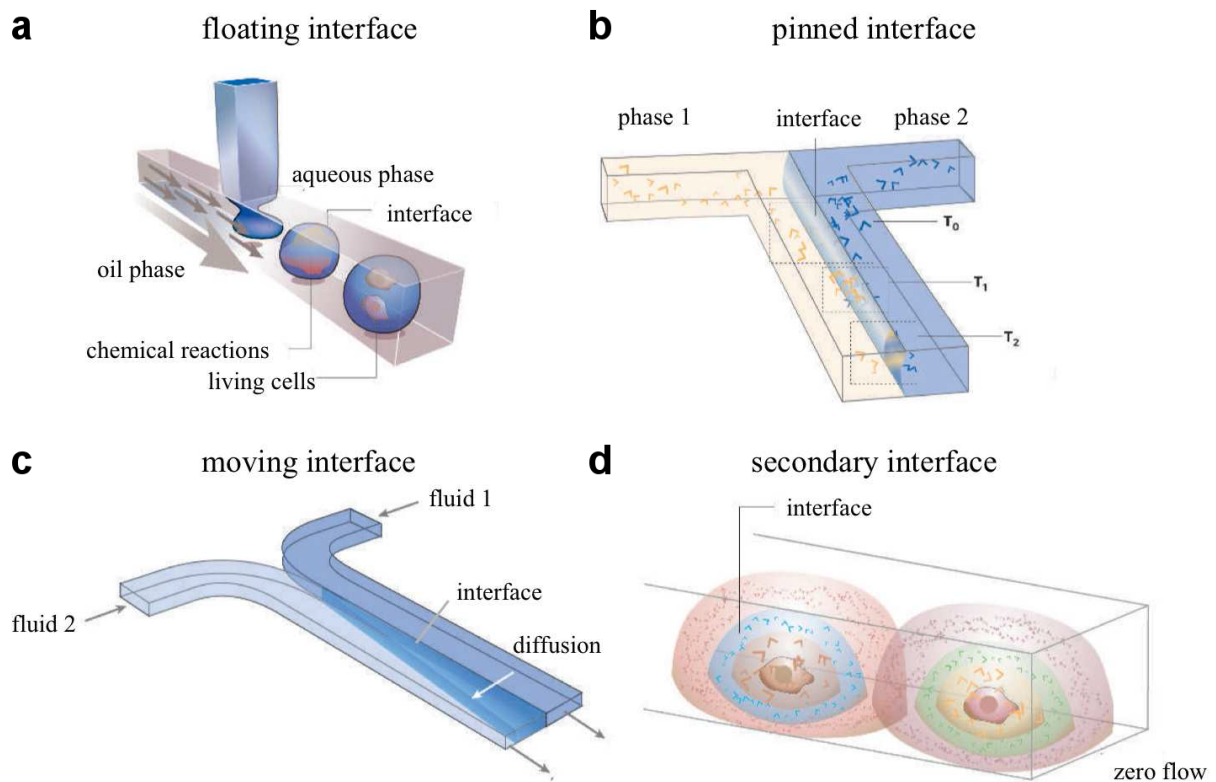


Figure 3.19: Interfaces in microfluidic devices and their functionalities:

(a): Floating interfaces between immiscible fluids produce droplets of precise shape and varying content.

(b): Pinned interfaces between immiscible liquids are created by selective surface patterning of a microchannel.

(c): Moving interfaces between miscible liquids are created under laminar flow, creating a diffusive interface with predictable geometry.

(d): Secondary interfaces arise in microscale channels due to diffusion-driven transport, which can create complex but predictable patterns (interfaces) of solutes based on the diffusivity of the solutes. Taken and adapted from Atencia *et al.*⁴⁸

All matter that is solved or immersed in one fluid can only be transported to the other fluid by crossing the interface. In all cases of laminar flow, cross-interfacial transport happens purely by diffusion. This makes the evolution of concentration gradients predictable and can be used for numerous ways. In this thesis, the diffusion in flow free environment will be of importance, which is governed by the same basic laws of diffusion, and will be discussed then.

3.4 Optical Tweezers

3.4.1 Light and matter interactions

Light is comprised of photons and can interact with matter in four ways. Light can get diffracted by crossing the interface between materials of different optical density (like e.g. glass and water), it can be deflected at such an interface and change direction, light can be reflected back to where it came from or can be absorbed (Figure 3.20).

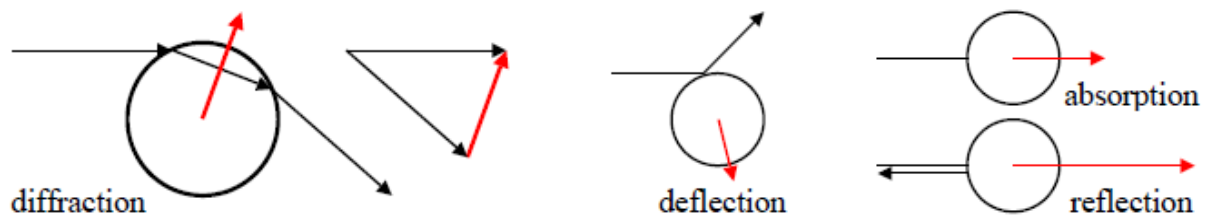


Figure 3.20: The four types of interaction of light with matter. The path of light (black arrows) is influenced by matter (black circle) and the resulting force on the object are shown (red arrows). Courtesy Eric Stellamans²

The direction of the resulting force is pointing opposite to the change in the path of light. The amplitude of the force can be calculated from momentum that is transferred during the interaction. The force F , is described by Newton's second law as

$$F = ma \tag{3.16}$$

where m is the mass and a is the acceleration the mass is subjected to. The force acting on the matter is the result of a transfer of momentum p from the photon to the matter. The momentum p of a moving matter is given by

$$p = mv \tag{3.17}$$

where v is its velocity. The relation between the force and the momentum can be stated as

$$F = \frac{p}{t} a = \frac{p}{t} \tag{3.18}$$

where t is the time duration of the interaction. So now, we could calculate the force by the momentum and the mass of the photon. Only, photons do not have rest mass, thus the classical laws do not apply to photons. But they carry an energy E , that is defined by Einstein's famous formula of mass-energy equivalence as

$$E = mc^2 \tag{3.19}$$

where m is the photons dynamic mass, the mass it has as long as it is in motion, and c , the speed of light. In combination with

$$E = h\nu \quad (3.20)$$

where h is Planck's constant ($h = 6.626 * 10^{-34}$ Js) and ν (the frequency) can be substituted by $\frac{c}{\lambda}$, where λ is the wavelength of the photon, we can rearrange Equation (3.19) to

$$m = \frac{h\nu}{c^2} \quad (3.21)$$

In combination with Equation (3.17), we obtain

$$p = mc = \frac{h\nu}{c} = \frac{h}{\lambda} \quad (3.22)$$

And finally, we can calculate the force of the light-matter interaction by combining Equations (3.18) and (3.22) to

$$F = \frac{h}{\lambda t} \quad (3.23)$$

While the interactions are extremely short lived, the forces on a single photon are practically immeasurable. Only when many photons of the same wavelength can interact at the same time with matter the force is amplified measurably. This can be achieved by using a laser or a set of filters and lamps with a high intensity.

3.4.2 Optical trap

If a laser beam is focused in one point, the forces can trap small objects in one point in space. This can be explained on the example of a transparent spherical object of high optical density that is immersed in a medium of lower optical density. While a unfocused laser beam exerts a force that pulls the object towards the centre of the beam where the intensity is highest, it also pushes the object away from the beam's origin (see Figure 3.21).

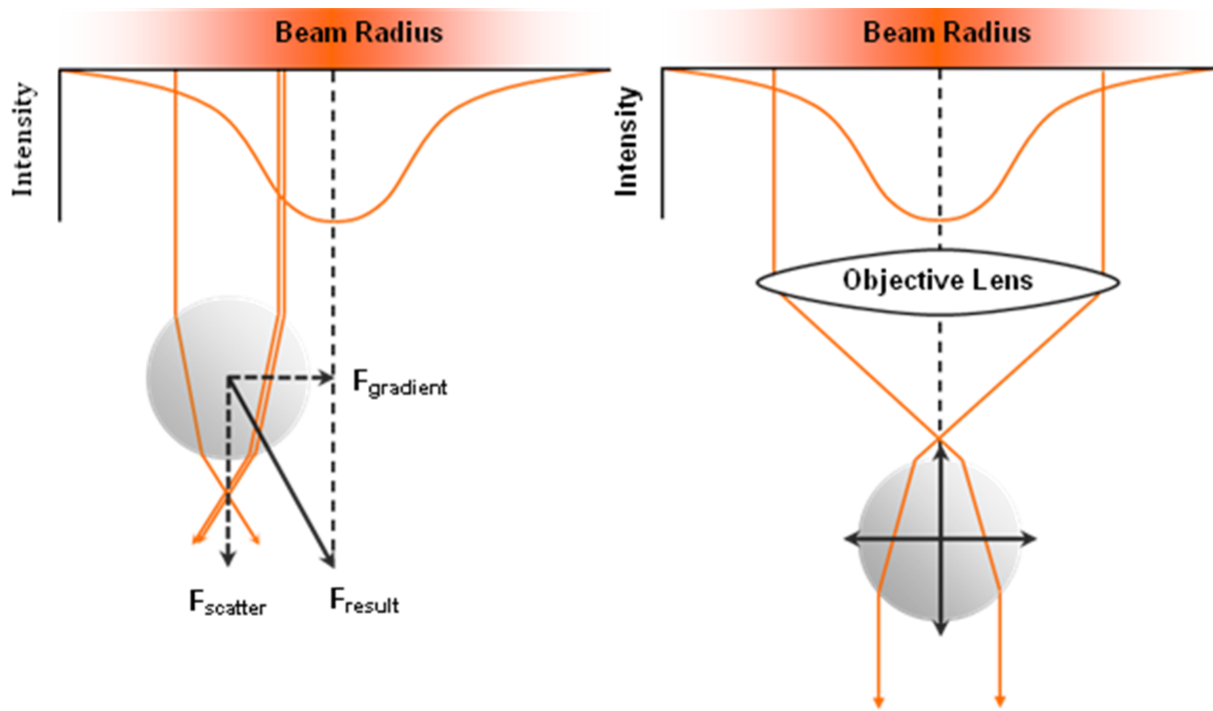


Figure 3.21: Forces on a spherical object in an unfocused vs. a focused laser beam. The focused laser beam creates one position where the object can be stably trapped. Taken and modified from Eric Stellamanns.

In contrast, a focused laser beam exhibits one point, in which all forces on the object cancel each other out. This is the position, where the object can be stably trapped. Every dislocation from this spot results in a force that pulls it back into the spot. The object even follow the focus, whenever it is moved. The application of this technique is called *optical trapping* and the instalment of a laser on a microscope (where the beam is focused onto an object on the microscopes sample stage) is called optical tweezers or optical trap (OT).

This effect and the technique has been discovered by Arthur Ashkin,^{49,50} and has since then been used amply in natural and life sciences. Not only dead, spherical objects have been trapped, but also elaborate geometrical objects have been used for molecular motors⁵¹⁻⁵³. Living cells have been optically trapped and sorted⁵⁴⁻⁵⁷. The motors of motile cells have been characterized employing optical traps.⁵⁸ OTs have further been used for investigations on single molecules⁵⁹⁻⁶² and rotating⁶³⁻⁶⁶ and holographic OTs⁶⁷⁻⁶⁹ have been developed. Yet, this is only giving a short overview of the versatility of OTs as a tool for natural sciences, life sciences and engineering.

In this thesis, all experiments were conducted using a single gradient optical trap, as described in Figure 3.21.

4 Materials and Methods

4.1 Cell Culture

Cultivating caulobacter

Caulobacter crescentus (caulobacter) strains (CB15 wild type, NA1000 wild type, CB15 Δ pilA, NA1000 Δ pilA CB15 Δ hfsA and NA1000 Δ pilA Δ flgA) were provided by the group of Prof. Urs Jenal (Biozentrum, Uni Basel, Switzerland).

Frozen *C. crescentus* were thawed and grown on plates of peptone yeast extract (PYE) with 0.2% glucose and 2% agar at 30 °C for 48 hours. Selected single colonies were transferred to 5 mL liquid PYE media, supplemented with CaCl₂ (5 mM) and incubated at 30 °C for 16-24 hours, until the optimal optical density (0.8-1.0) was reached. The optical density was measured individually, using a photo-spectrometer (Genesys6, Thermo Spectronic, WI, USA) at 660 nm. Finally, cell cultures were supplemented with hold-fast binding lectin wheat germ agglutinin (WGA), which was fluorescently labelled with Oregon Green 488 (1g/ml) and used for single cell assays.

Cultivating trypanosomes

Please note that recipes for all cell culture media and solutions for trypanosomes is provided in the Appendix A on pages 103f.

Trypanosoma brucei brucei MiTat 1.2 (trypanosomes) were a gift from the Department of Medical Parasitology and Infection Biology of the Swiss Tropical and Public Health Institute.

Trypanosomes were grown in HMI-9 cell medium at 37 °C at 5% CO₂. Populations were kept below 10⁶ cells per mL by repetitive splitting. After a maximum of 15 splittings, trypanosomes were discarded and fresh populations were defrosted.

Preparing cell and drug solutions

For experiments, 2 mL of trypanosomes in CM were centrifuged in a Heraeus Labofuge 400 R (Fischer Scientific, Switzerland) at 1400 rpm (237 xg) and washed once with 2mL of CM and once with 2 mL CM with bovine serum albumin (BSA, 5 mg/mL). The supernatant was discarded and the cells were taken up into a 1 mL syringe (Braun) in 0.7 mL of CM with BSA (5 mg/mL). This comprised the 'cell solution', which was introduced into the device. The

solution of CM and BSA was weekly prepared and stored at 37 °C and at 5% CO₂ in humid atmosphere to ascertain optimal conditions.

For the 'drug solution', the drug was dissolved in 2 mL of CM with BSA (5mg/mL) and polystyrene beads (1 µm diameter, Polysciences) solution 2 µL/mL. Suramin, as an exception, was dissolved in 2 mL of CM without BSA, for it is already known, that BSA diminishes the effect of Suramin onto trypanosomes.

Storing trypanosomes

For freezing and long-time storage, trypanosomes were grown in CM to a density of 10⁴ to 10⁶ per mL. Then a 10 mL aliquot was taken and centrifuged for 10 minutes at 1400 rpm. The supernatant was discarded, the pellet of cells was taken up into 1 mL of freezing medium (see Appendix A) in CryoTubes (VWR), which were then slowly cooled down to -80 °C in a “Mr. Frosty” (Nalgene) and finally stored either at -80 °C or in liquid nitrogen.

Thawing trypanosomes

Frozen cells were thawed in the water bath at 37 °C, re-suspended in 9 mL CM, centrifuged at 1400 rpm ($\approx 237 \times g$) and the supernatant discarded. The cell pellet was re-suspended in 1 mL of fresh cell media and split into fractions of 50-500 µL and put in 10 mL of fresh culture medium.

Preparing fixated trypanosomes

The desired amount of trypanosomes was washed twice with TDB, then taken up in 2.5% glutaraldehydic solution of TFB at RT for 2 hours. Afterwards, it was washed twice with TDB, and then re-suspend in pure water.

For on-slide-fixation a drop of this solution was air-dry on a cleaned glass-slide. For SAXS the fixed trypanosomes were taken up in pure water into a suitable glass capillary.

Disposing trypanosomes

All liquid waste containing trypanosomes was autoclaved at 121 °C for 20 minutes and were then, after cooling to RT, disposed according to federal and cantonal regulations.

4.2 Microfluidics & Soft Lithography

All devices were produced by standard soft lithography procedures. Soft lithography describes the replication of designs and structures from a mask onto a device. This happens in two steps, the generation of a master (Figure 4.1.a), and the subsequent production of a usable microfluidic device (Figure 4.1.b).

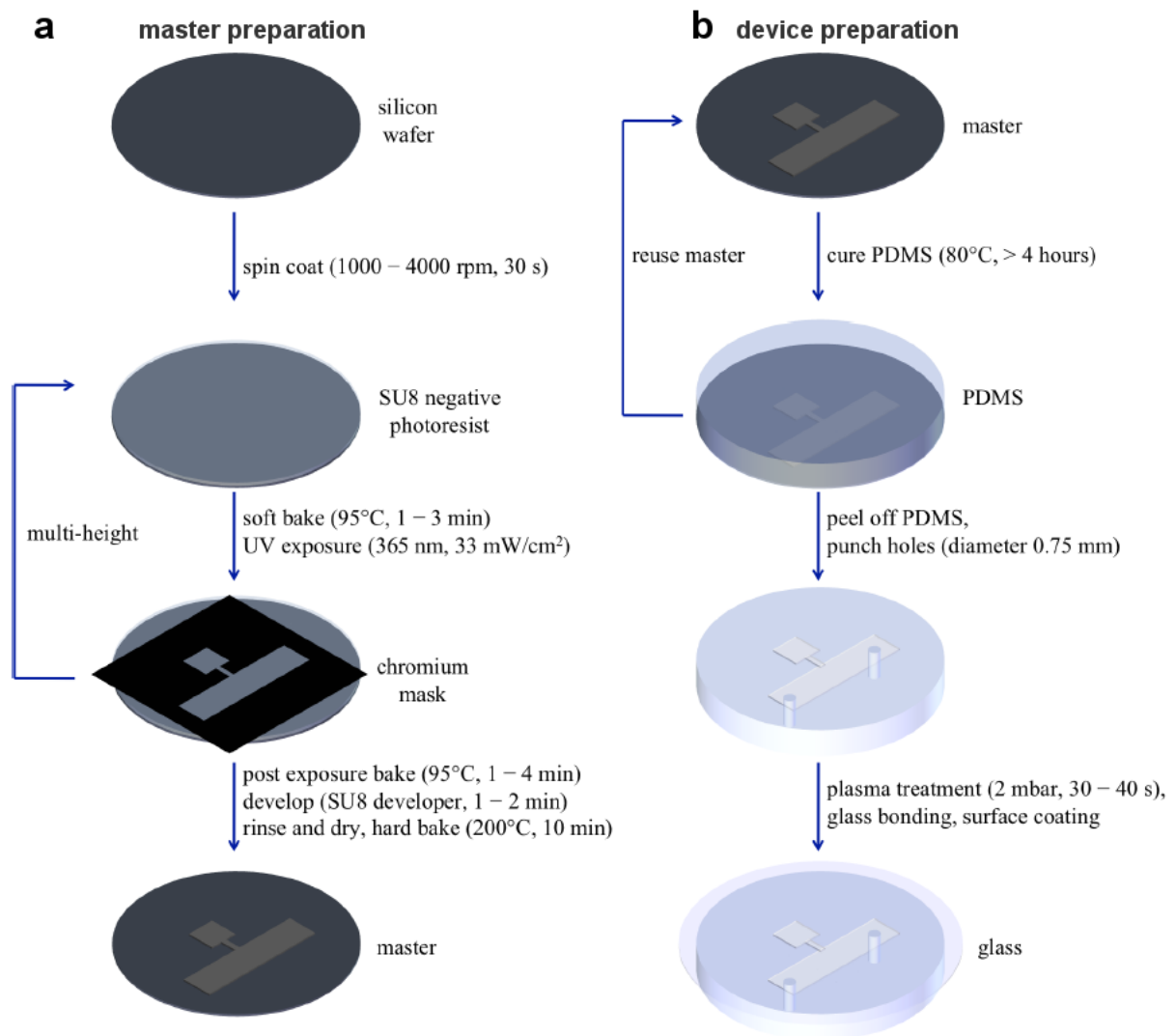


Figure 4.1: Production process of a microfluidic device. Specifications are in accordance to the supplier of the photoresist and lead to structures of about 9 μm height, when using SU8 3010 photoresist (MicroChem, USA). Image adapted from⁷⁰

(a): Preparation of the master from a silicon wafer and spin coated photoresist that is developed using a chromium mask bearing the desired design

(b): Preparation of the microfluidic device from a PDMS cast of the master that is cured and bonded with a glass cover.

4.2.1 Master preparation

The architectures of devices are designed using QCAD software (RibbonSoft, version 3.3) and manufactured as chromium masks on quartz glass (ML&C GmbH, Germany). The master, which serves as a re-usable mould for the structures of the devices, is created under cleanroom conditions (Figure 4.1). On a clean silicon waver (Si-Mat, Germany), SU8 negative photoresist (Microchem, USA) is spin-coated according to supplier specifications to obtain the desired coating thickness. The coated waver is soft baked and then the structures are written into the photoresist through the applied chromium mask (ML&C GmbH, Germany) or foil mask (JD Photo-tools, UK) by exposition to UV light (365 nm) on a MJB4 mask aligner (SUSS MicroTec AG, Germany). After exposure, the waver undergoes post-exposure baking and development in SU8 developer, where unexposed photoresist is solved off of the waver. After rinsing with propan-2-ol and drying with nitrogen the master is finished. Please note that a standard recipe for a device of 8 μm height is provided in the Appendix A on page 102.

4.2.2 Device preparation

The obtained master serves as a mould from which multiple casts can be taken (see Figure 4.1.b). Therefore, PDMS monomer and cross-linker (Sylguard 184, Dow Corning GmbH, Germany) are mixed in a mass ratio of 10:1, vigorously stirred, degassed and poured over the master. After curing the polymer by baking at 80 °C for at least 4 hours, the cast is cut and peeled from the mould. To later connect the inlets and outlets to tubing, holes are punched through the cast. To complete the device, the cast and a clean glass slide (VWR, outer diameter 50 mm) are exposed to reactive plasma of air at 2 mbar for 30 seconds in a plasma cleaner (Harris Plasma, USA), which creates highly reactive radicals on the surfaces of both glass and PDMS cast. The glass is gently pressed against the open structures of the cast. The activated surfaces then bind covalently and the device is sealed.

4.2.3 Device mounting

The finished devices were allowed at least 20 minutes to fully covalently bind and for all remaining radicals to react with ambient water and air. Then tubings (polytetrafluorethylene microtube, outer diameter 0.78 mm) were inserted into the holes and supplied with cannulas (Braun, Germany, internal diameter 0.4 mm). Afterwards, the device was mounted on a BX61 microscope (Olympus, Germany) and syringes delivered any medium and cells into the device.

4.3 Optical trapping and microscopy

The optical trap that was used for all the experiments mentioned herein consisted of a parallelized Laser beam ($\lambda = 808 \text{ nm}$, Schäfter + Kirchhoff GmbH, Germany) that was coupled into the optical pathway of an upright optical microscope (BX61, Olympus, Germany). The laser emitter was held in an in-house crafted adapter that fixed it onto an extension module for the microscope (UL2, Olympus, Germany). The extension module was fitted with a dichroic mirror (Cat.-Nr. F76-720, AHF, Germany) that reflected the laser beam into the optical pathway and towards the sample. To avoid overcasting of the optical signal by reflected laser light, the reflexion module was equipped with an additional glass filter (GPX10-30 DB5, Olympus, Germany) with a DBAR 808/940 coating.

The parallelized and collimated laser beam was focused by the objective. The focal point of the optical trap lay in the focal plane of the microscope and was calibrated to be in the centre of the field of view.

Images were recorded on a Sencicam (PCO, Germany) or a Phantom Miro 3 (Vision Research, USA).

4.3.1 Calibration of the optical trap

An object that is optically trapped in a microfluidic device mainly experiences two different forces. The stall force of the optical trap that holds the object in one position and the drag forces caused by the flow of surrounding fluid. The stall force depends on the objects geometry, the refractive indices of both the object and the surrounding fluid and on the power of the laser effective on the object. Since cells vary locally in their refractive index and geometry, calculations of the stall force can be inexact. The drag force, on the other hand can be exactly calculated (see Equation (4.1), below). Thus, the optical trap was calibrated in a setup, where both the stall force of the optical trap and the drag force of the viscous fluid were equal.

After positioning the beads in the middle of the channel with rectangular geometry, the flow velocity was increased until the drag forces of the liquid tore the sphere from the optical trap.

The drag force is the force any object experiences when moving inside a viscous fluid can be calculated by

$$F_{drag} = \gamma_{drag} \cdot v \quad (4.1)$$

with F_{drag} as drag force, γ_{drag} as the drag force coefficient and v the velocity of the object relative to the fluid.

The drag force coefficient depends on the geometry of the object and the viscosity of the surrounding fluid and is given for a spherical object as

$$\gamma_{drag} = 6\pi\eta r \quad (4.2)$$

where η is the viscosity of the fluid and v the speed of the fluid relative to the spherical object. Thus, the drag force can be calculated by:

$$F_{drag} = 6\pi\eta r \cdot v \quad (4.3)$$

As long as the force of the optical trap is stronger than the drag force, the bead is held inside the optical trap. At a point, where the drag force equals the optical force, the tiniest additional forces (like from Brownian motion) will push the spherical object from the optical trap.

In order to calibrate the optical trap, polystyrene beads of $1 \mu\text{m}$ diameter (Polybead® Microspheres, Cat.-Nr. 07310-15, Polysciences, Germany) have been optically trapped in the middle of a microfluidic channel of $8 \mu\text{m}$ height and $40 \mu\text{m}$ width. Then a flow has been slowly ramped up using syringe pumps (neMESYS, Cetoni, Germany). When the particle left the trap, the flow velocity was measured by recording images with a set exposure time. During this time, the particle travelled a certain way Δx . By multiplying the displacement Δx with the exposure time, the flow velocity was obtained (Figure 4.2).

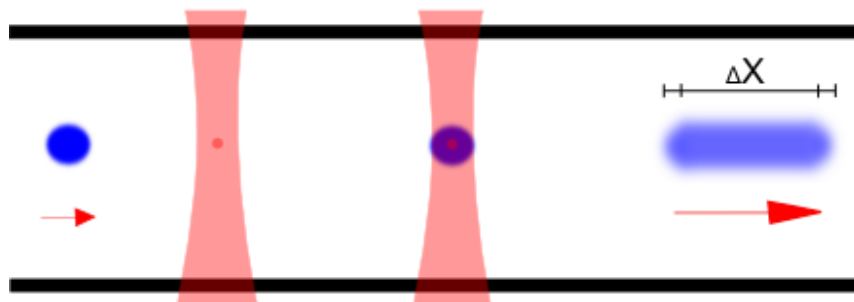


Figure 4.2: Experimental setup for optical trap force calibration: The polystyrene bead (blue) was trapped at the focal point of the optical trap (red dot). With increasing flow velocity (red arrows) the beads were pulled from the optical trap. This was recorded at long exposure times resulting in blurred beads on the recorded images. By multiplying the displacement (Δx , which equals the length of the blurred beads minus their diameter) with the exposition time of one image the flow velocities were calculated. Image is a courtesy of Benjamin Banusch.

This measurement was repeated several times at different laser powers show that there is a linear relationship between the laser power P and the velocity v at which the beads leave the optical trap. In combination with equation (4.3) and taking into account that η of the surrounding fluid (aqueous solution at RT) was $0.001 \text{ Pa} \cdot \text{s}$, we found that each Watt in laser power corresponds to 35.7 pN of stall force (Figure 4.3).

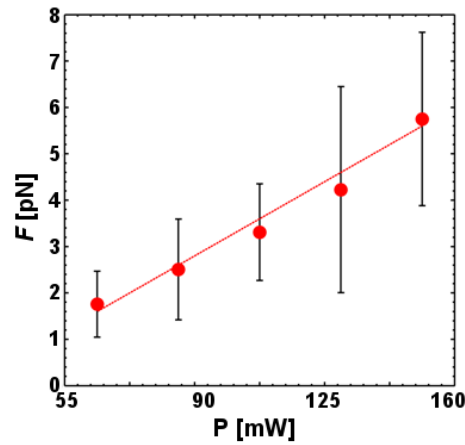


Figure 4.3: Drag force plotted over the laser power of the optical trap. The red circles show the averaged forces that were exerted by the optical trap at the given lasing currents. According to the linear fit (red dashed line) the stall force increases by 35.7 pico-Newton per Watt.

4.3.2 Image recording and analysis

Images were recorded on a Miro 3 (Phantom) and a Sensicam (PCO) respectively.

The images were analysed using ImageJ (version 1.48g, Wayne Rasband, National Institutes of Health, USA) and MATLAB (R2011a and R2013b, The MathWorks Inc.). All MATLAB scripts used herein are self-written and can be found under section 12.1 on page 102ff.)

Tracking

Trajectories of trypanosomes were recorded using the "Manual Tracking" plug-in for Fiji⁷¹. For trajectories of optically trapped trypanosomes, the position of the flagellar tip was recorded. For experiments investigating the drug impact of chemicals on trypanosomes, the position of the flagellar pocket was followed, and all other experiments were based on the centre of mass-measurements of the motile trypanosomes.

Polystyrene spheres of 1 μm diameter (Polybead® Microspheres, Cat.-Nr. 07310-15, Polysciences, Germany) were used for the particle image velocimetry. The same polystyrene spheres were also used to measure flow rates inside channels and micro chambers and to optically distinguish translucent fluids inside the device like culture medium and drug solutions.

Aligning of Stacks (Registration)

To obtain the trajectories, series of images have been recorded. Due to vibrations within the microscope-stage-complex, these images were not entirely aligned over each other. This misalignment was mended using the StackReg plugin⁷² for Fiji.

Plot Profile

Plot profiles give the grey value (= brightness) of an image along a line that is manually drawn over the image. It is an inherent feature of the Fiji software.⁷¹

CFD Simulations:

For the CFD simulations we used the CFD module from the software COMSOL 4.3a. The microfluidic device was modelled in 3D using 54,167 finite elements. At first, the stationary laminar flow was calculated, whereas in a second step the time dependent material transport of the diluted species were calculated by using the beforehand obtained stationary flow fields.

RESULTS I:

OPTICAL TRAPPING OF LIVING CELLS

5 Optical trapping of bacteria on the example of *C. crescentus*

5.1 Introduction

Optical tweezers and microfluidics have already been employed for the sorting and stretching of cells, as well as for the measurement of forces, elasticity, and cell stiffness of unicellular organisms.^{53,55,73} The advantage of the combination between microfluidics and optical traps is the possibility for touch-less administration and measurement of miniscule forces. Yet, for a reliable quantification of the measured force, any optical trap has to be calibrated depending on the respective organism under study. The optical trap exerts stall forces onto a trapped object which can be assessed by pushing the trapped object out of the trap, using the drag force of the surrounding, moving medium (see 5.2.2 Assessing the trap parameters for the force calculations).

The forces exerted by optical traps can be used to move, manipulate and study cells, such as *Caulobacter crescentus*. During their live cycle, caulobacter undergo metamorphosis from freely swimming swarmer cells to stalked cells, which have the ability to firmly attach to a surface via holdfast induction. The surface adhesion is a key point for the formation of a biofilm,¹³ The process of surface adhesion in caulobacter is divided in three steps. At first, pili attach to the surface which are then retracted in order to pull the entire cell towards the surface whereby the flagellum bearing cell pole touches the surface. At this pole, holdfast is either pre-existing or produced to increase the attachment, and the flagellum is ejected. Finally, a stalk is formed between the holdfast and the cell body^{41,45}. The holdfast has already been analysed in respect to its composition and elastic properties⁷⁴ and its formation in stalked⁴¹ and swarmer cells¹². The formation of a biofilm has also been studied over days for various wild-types and mutants¹³.

Using an optical trap calibrated for caulobacter, we aim to directly measure the forces generated by a swimming caulobacter, to induce surface adhesion and to analyse the surface attachment process for caulobacter on the single-cell level. By including mutants lacking either pili (CB Δ pilA, NA1000 Δ pilA), holdfast (CB Δ hfsA) or both pili and flagellum (NA1000 Δ pilA Δ flgA), we aim to investigate their role during induced surface attachment.

Additionally the forces generated by the swimming caulobacter as well as the motility within and outside of the optical confinement were assessed.

5.2 Materials and methods

5.2.1 Device design

The device was designed in order to create a no-flow condition within the experimental micro chambers. The device consisted of one main channel (height $8\ \mu\text{m}$, width $40\ \mu\text{m}$) between an inlet and an outlet with adjacent square micro chambers ($100\ \mu\text{m}$ by $200\ \mu\text{m}$) protruding from the main channel via narrow connecting channels (length: $10\ \mu\text{m}$, width $6\ \mu\text{m}$).

5.2.2 Assessing the trap parameters for the force calculations

The force of the optical trap was measured on immotile caulobacter swarmer cells at variable laser strengths in order to know at which power the laser exerts which force. After positioning the cell in the middle of a main channel with a rectangular geometry (height: $8\ \mu\text{m}$, width $40\ \mu\text{m}$), the flow velocity was linearly increased using syringe pumps (neMESYS, Cetoni, Germany) until the drag forces of the liquid flow tore the cell out the optical trap. Flow velocity at the moment of escape from the trap, was assessed using images recorded with high exposure time (about 100 ms). When cells were leaving the trap, they left a trace on the image. The length of this trace minus the cell radius corresponds to the displacement of the cell by Δx (Figure 5.1). Dividing the displacement Δx by the exposure time results in the flow velocity.

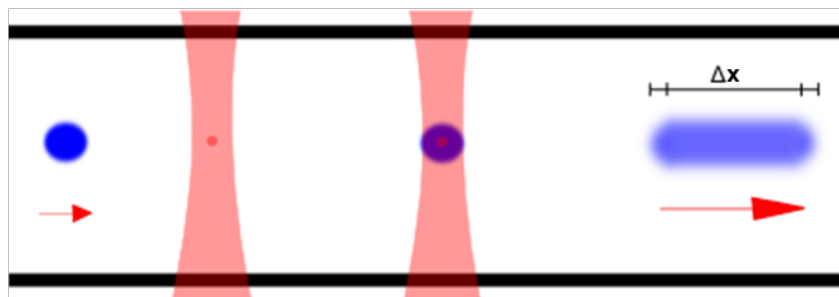


Figure 5.1: Experimental setup for the force calibration of the optical trap: the particle or cell (blue) was trapped at the focal point of the optical trap (red dot). With increasing flow velocity (red arrows) the beads were pulled from the optical trap. This was recorded at long exposure times resulting in blurred traces on the recorded images. By dividing the displacement Δx by the exposition time of one image the flow velocities were calculated. Image by courtesy of Benjamin Banusch.

From the obtained velocities, the drag force can then be calculated by

$$F_{drag} = \gamma_{drag} \cdot v \quad (5.1)$$

whereby F_{drag} is the drag force, γ_{drag} is the drag coefficient and v is velocity of the object relative to the fluid.

The drag coefficient is a function of the viscosity of the surrounding fluid and the size and shape of the object. The shape of a caulobacter can be approximated by a prolate ellipsoid (Figure 5.2) with a width of $2a$ and a length of $2b$.⁴⁶ The thin flagellum at the posterior pole of the immotile cell can be neglected for the purpose of this calculation. It was assumed that an immotile flagellum would align with the flow, thus experiencing little to no drag force.

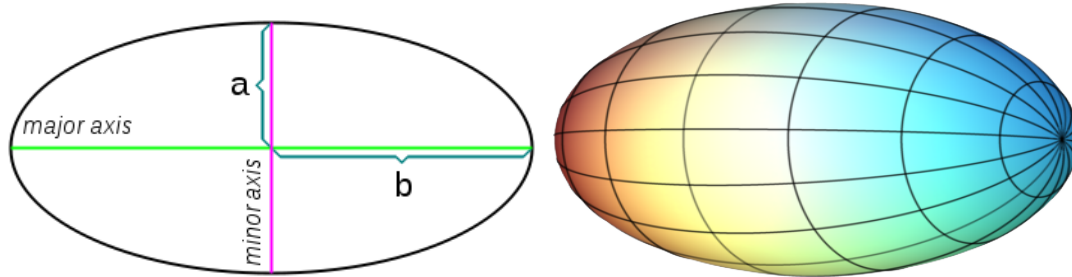


Figure 5.2: A prolate ellipsoid can be created by rotating an ellipsis of length $2b$ and width $2a$ along the major axis (green). Image by courtesy of User Amit6 (modifications by James B Watson) and Sam Derbyshire respectively, taken from wikicomons, http://en.wikipedia.org/wiki/Prolate_spheroid (2014-08-17)

Using the equation for the translational drag coefficient of such prolate ellipsoids of:⁷⁵

$$\gamma_{trans}^{\parallel} = 6\pi\eta a \cdot \frac{\frac{4}{3}(\beta^2 - 1)}{\frac{(2\beta^2 - 1)}{\sqrt{\beta^2 - 1}} \ln[\beta + \sqrt{\beta^2 - 1}] - \beta} \quad (5.2)$$

as well as the lengths of $b = 0.8 \mu\text{m}$, and $a = 0.25 \mu\text{m}$ for *Caulobacter crescentus*⁴⁶, a drag coefficient of $\gamma_{trans}^{\parallel} = 5.46 \cdot 10^{-9} \frac{\text{N}\cdot\text{s}}{\text{m}}$ can be computed for *C. crescentus*.

However, it has to be considered that a prolate ellipsoid within the beam of a strong optical trap will always aligns perpendicular to the flow (see Figure 5.3), whereas it will align parallel to the flow when outside of the trap. Thus the drag coefficient within the trap has to be calculated differently.

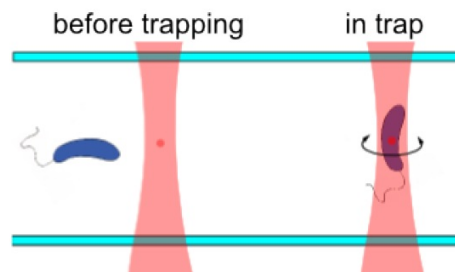


Figure 5.3: Orientation of a swarmer cell before and during optical trapping. Inside the optical trap the swarmer cell aligns itself along the propagation of the beam. Image by courtesy of Benjamin Banusch.

The drag coefficient for prolate ellipsoids aligned perpendicular to the flow is given by:⁷⁵

$$\gamma_{trans}^{\perp} = 6\pi\eta a \cdot \frac{\frac{8}{3}(\beta^2 - 1)}{\frac{(2\beta^2 - 3)}{\sqrt{(\beta^2 - 1)}} \cdot \ln[\beta + \sqrt{(\beta^2 - 1)}] + \beta} \quad (5.3)$$

Whereby $\beta = \frac{b}{a}$.

Thus, for $b = 0.8 \mu\text{m}$ and $a = 0.25 \mu\text{m}$, the translational drag coefficient for trapped *C. crescentus* equals $\gamma_{trans}^{\perp} = 8.46 \cdot 10^{-9} \frac{\text{Ns}}{\text{m}}$.

Another formula to approximate the drag coefficient $\gamma_{trans}^{Li} = 6\pi\eta a \left[1 - \frac{1}{5} \left(1 - \frac{b}{a}\right)\right]^{46}$ was used for an experiment-based mean value of the drag coefficient of $\gamma_{trans}^{Li} = 6.8 \cdot 10^{-9} \frac{\text{Ns}}{\text{m}}$ whenever calculate 2-dimensional diffusion regardless of cell orientation was assessed.

5.2.3 Assessment of photo-toxicity

During our experiments, we found that caulobacter suffered a decrease in motility when optically trapped. This loss of motility can be classified as *photo-toxicity*. In order to quantify the photo-toxic effect of the trap on *C. crescentus*, motile swarmer cells in buffer were put into a flow-free environment. Subsequently a time series experiment was performed in which *C. crescentus* were trapped with a laser power of 95 mW for increasing amounts of time from 2 to 22 seconds. Motility of *C. crescentus* was recorded at a rate of 120 fps during the entire experiment and velocity before and after optical trapping was compared. The highest velocity within a 10 second frame before and after trapping was used as the respective *top speed in the frame*. Through division of the top speed v_e (after release) by the top speed v_a (before trapping), the loss of motility was calculated as the total loss in top speed.

5.2.4 Measuring escape probability and force

In a medium with a viscosity of $10^{-3} \text{ Pa}\cdot\text{s}$, Caulobacter were optically trapped under flow free conditions using laser powers of 62.5, 85, 107.5, 130, and 151.5 mW respectively. When a trapped caulobacter left the optical confinement within 10 seconds, it was defined to have managed an *escape*. The escape probability within 10 seconds after trapping as a function of the laser power was then determined and used to compute the average force generated by motile caulobacter swimming in a liquid medium. Power measurements in the results are reported as the power emitted by the laser diode. The power emitted by the diode then has to be multiplied with 0.121 in order to calculate the power at the trapping site.²

5.2.5 Induction of holdfast formation

Under no-flow conditions, different caulobacter mutants and wild-type were caught in the optical trap, pushed to the PDMS bottom of our microfluidic device as quickly as possible (Figure 5.4) and immediately released from the optical trap thereafter. This process was recorded at a rate of 10 fps. Laser power and exposure times were kept to a minimum in order to reduce photo toxicity.

To verify holdfast existence, cells were labelled with fluorescent WGA lectin.

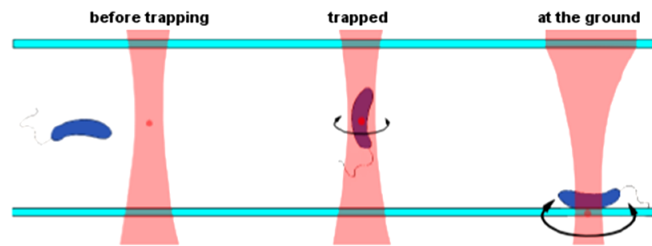


Figure 5.4: Experimental setup of induced holdfast formation with side-on surface contact for one caulobacter. Image by courtesy of Benjamin Bausch.

5.3 Results

5.3.1 Optical trap calibration for caulobacter

As described before, the optical trap was calibrated by trapping immotile caulobacter cells and measuring the drag forces of the medium used to subsequently push them dead cells out of the trap. The recorded flow velocities for cells escaping the trap show a linear correlation to the laser powers of the optical trap thus enabling us to know the stall forces in relation to the power of the laser.

The following calibration parameters for forces exerted on caulobacter by the optical trap have been found

Between laser powers of 85 mW to 151.5 mW, the velocities for caulobacter escaping the optical trap can be calculated by: $v_{escape} = (3 \cdot P - 21) \cdot 10^{-3} \text{m/s}$, where P is the power of the laser in Watt (Figure 5.5).

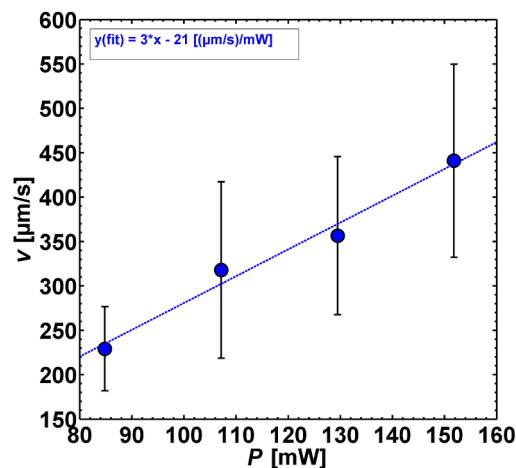


Figure 5.5: Calibration curve for caulobacter escape velocities over laser current of the optical trap. The fit (blue dashed line) shows a linear dependence of the flow velocity to the current with a slope of $3 \frac{\mu\text{m}}{\text{s}\cdot\text{mW}}$.

For the interval of 85 mW to 151.5 mW, the stall force of the optical trap on caulobacter can be calculated by $F_{stall} = (26 \cdot P - 180) \cdot 10^{-12} \text{N}$, where P is the power of the laser in Watt (Figure 5.6). It can be assumed that the stall force of the optical trap equals the drag force of the surrounding flow at the moment when the caulobacter is pushed out of the trap.

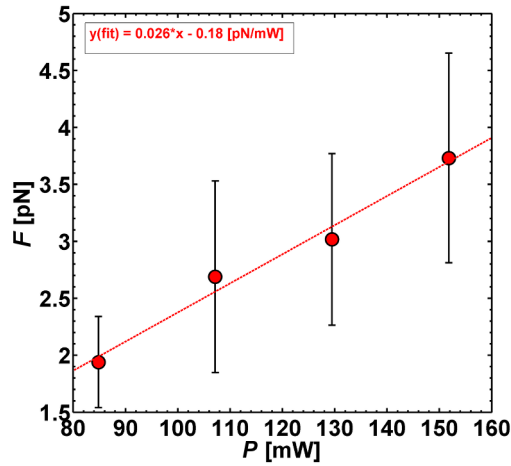


Figure 5.6: Stall force exerted upon caulobacter by viscous drag in the optical trap versus the laser current needed to trap caulobacter perpendicularly to the flow velocity. The fit (red dashed line) shows a linear relation between the laser power and the corresponding drag force with a slope of 26 pN/W.

5.3.2 Photo-toxicity

While the velocity of swarmer cells before trapping was on average $60 \mu\text{m/s} \pm 8.30 \mu\text{m/s}$, the velocity after trapping dropped rapidly depending on the exposure time to the laser (Figure 5.7). Caulobacter trapped for 2-5 seconds lost about 50% of their top speed, whereas a trapping for 5-10 seconds resulted in a top speed loss of circa 75%. Cells that were released after 10-22 seconds, reached velocities of only $5-8 \mu\text{m/s}$ which corresponds to a top speed loss of approximately 90%.

The reduction of top speed by 90% of the pre-trapping velocity, however, seems to indicate a plateau in the motility loss. The same range of motility reduction was observed in all cells trapped for 10 seconds or longer. The remaining velocity after trapping is nevertheless still higher than the velocity of an immotile caulobacter only moved by diffusion (Figure 5.7). This diffusion can be approximated using the Stokes-Einstein-equation:

$$D = \frac{k_B T}{\gamma} \quad (5.4)$$

Thereby, a caulobacter with a drag coefficient of $\gamma_{trans}^{Li} = 6.8 \cdot 10^{-9} \frac{\text{N s}}{\text{m}}$ at RT, has a diffusion constant equal to $D = 5.95 \cdot 10^{-13} \frac{\text{m}^2}{\text{s}} = 0.595 \frac{\mu\text{m}^2}{\text{s}}$ whereas its diffusion velocity v_{caulo}^{diff} as calculated using the Einstein-Smoluchowski equation, $t_{\Delta r} = \frac{\Delta r^2}{6D}$ (5.5), amounts to: $v_{caulo}^{diff} = \frac{\Delta r}{t_{\Delta r}} = 1.89 \frac{\mu\text{m}}{\text{s}}$

The thus calculated diffusion velocity $v_{caulo}^{diff} = 1.89 \frac{\mu\text{m}}{\text{s}}$ for immotile caulobacter is indeed lower than the average velocity of the formerly trapped caulobacter which amounts to a minimum of $4.4 \frac{\mu\text{m}}{\text{s}}$.

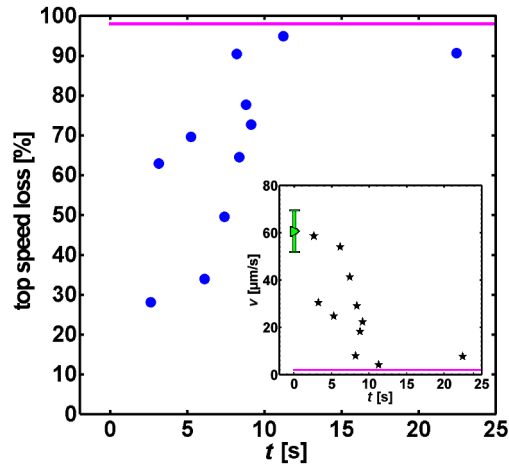


Figure 5.7: Decrease of velocity of caulobacter due to optical trapping.

The blue dots show the swimming speed after trapping in relation to the swimming speed before trapping versus the time spent in the optical trap. Each dot denotes one caulobacter.

The average top speed before trapping (green) and the velocities measured for individual caulobacter after release (black stars) are shown in the inset. The velocity of a diffusing caulobacter is shown as a reference (magenta line).

This indicates that caulobacter trapped for up to 22 seconds in an optical trap with a wavelength of $\lambda=808$ nm and a power of 95 mW, are partially incapacitated yet not killed. Nevertheless, this rapidly occurring photo-toxic effect, drastically reduces the viability of motile caulobacter and has to be taken into account when handling caulobacter with an optical trap.

5.3.3 Forces generated by caulobacter

When trapped with optical tweezers, caulobacter can generate forces through the flagellar motion. If these forces are strong enough, they can overcome the stall forces of the trap itself and enable the caulobacter to escape.

For stall forces up to 1.8 pN, all caulobacter cells managed to escape within 10 seconds, while at stall forces of 3.4 pN and more, none of the caulobacter cells escaped. In the regime between 1.8 pN and 3.4 pN, however a fast, near linear decrease in escape probability can be observed. The 10-second escape probability of caulobacter reached 50% with a stall force of 2.6 pN (Figure 5.8). Since the force needed to escape equals the stall force of the trap, it can be concluded that 2.6 pN is the average maximum force F_{max} caulobacter generates in optical confinement.

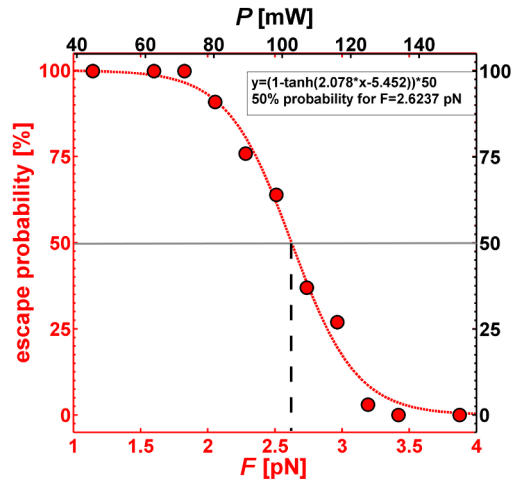


Figure 5.8: Escape probability for caulobacter over the stall force of the optical trap including the conversion to the laser power (upper x -axis).

In contrast, the force generated by caulobacter swimming freely in the same medium can be calculated by

$$F_{prop} = \gamma_{trans}^{\parallel} v_{prop} \quad (5.6)$$

Outside the optical trap, caulobacter reach an averaged top speed of about $60 \mu\text{m/s}$. Thus, the average propulsion force would be $F_{prop} = 3.28 \cdot 10^{-13} \text{ N} = 0.328 \text{ pN}$ for motile caulobacter

There is one order of magnitude between the average propulsion force F_{prop} of free-swimming caulobacter and the average maximum force F_{max} of trapped caulobacter. This shows that in a liquid surrounding with a viscosity of $10^{-3} \text{ Pa}\cdot\text{s}$, a force of 0.328 pN is all that is needed to drive this unicellular flagellated prokaryote forward. However, if need be, caulobacter is able to generate much higher forces with their flagellar movement. A fact that would indeed be useful when faced with the higher drag forces caused by flowing water in their natural habitat. A force of 2.6 pN would enable caulobacter to counter flow velocities of up to 0.3 mm/s in a medium with a viscosity of $10^{-3} \text{ Pa}\cdot\text{s}$, such as water. Furthermore, our findings on the phototoxic effect of laser beams on caulobacter have to be taken into account as well. It seems conceivable that the force measured in our experimental setup is reduced through phototoxic incapacitation of the caulobacter and that the real F_{max} could indeed be even higher.

5.3.4 Motility of caulobacter in the optical trap

When caulobacter swarmer cells are trapped with optical tweezers, they align with the laser beam as discussed before. However, during this optical confinement they also exhibit a rotational movement around their longitudinal axis and thus around the axis of the laser beam. The bean-like form of the caulobacter accounts for the darker colour-value on one side of the cell body that can always be seen when recording images or videos of trapped caulobacter (Figure 5.9). This difference in colour allows us to trace the position of a certain point on the caulobacter thus enabling us to compute the rotational frequency of caulobacter around its axis. The frequency of this rotation was around 50 Hz, a finding that is in line with the works of Liu (2009)⁵⁸.

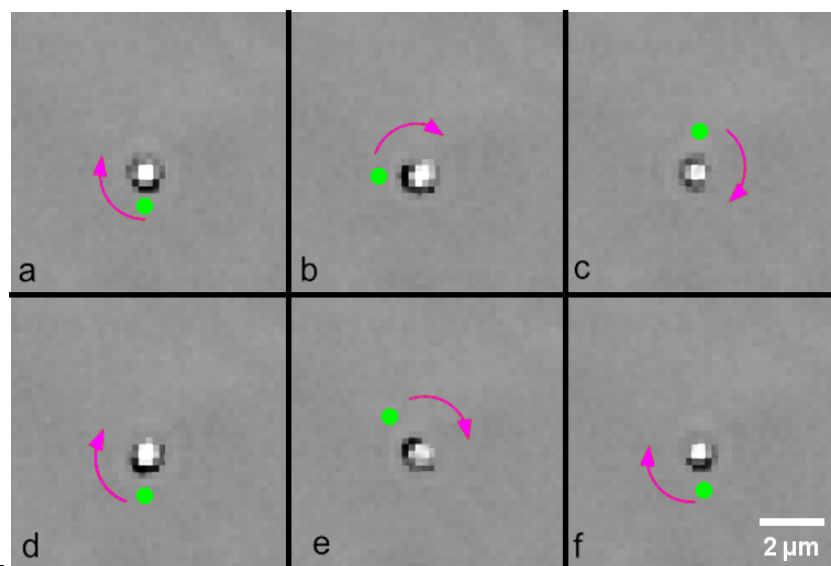


Figure 5.9: Rotation of an optically trapped caulobacter. Due to the bean-like structure of the caulobacter, the rotation (magenta arrow) can be seen by the darker spot (marked with green dot), caused by the curved protrusion. The time lapse between two images is 0.06 s. Image by courtesy of Benjamin Bausch.

Free-swimming caulobacter outside of the optical trap likewise rotate around their longitudinal axis. Indeed, the frequency with which free-swimming caulobacter rotate around their axis is, with 50 Hz⁴⁶, the same as for caulobacter in the trap. The similarity in the rotation frequency between confined and free-swimming caulobacter indicates that optical confinement does not generally influence the propulsion of caulobacter. However, after some time in optical confinement, movement can be hampered by photo-toxicity as discussed before, leading to a rapid decrease in the rotational frequency over time with our setup.

5.3.5 Mechanically induced surface adhesion

After having analysed the movement and generated forces of caulobacter, we next tried to induce the metamorphosis from swarmer cells to stalked cells with the help of optical tweezers. During this metamorphosis, motile cells shed their flagellum and adhere to a suitable surface with their flagellar pole by the formation of a holdfast. Since chromosome replication and cell division can only take place in stalked cells, this metamorphosis is key for the progression of the cell cycle and the proliferation of the caulobacter⁴¹. Holdfast formation and subsequent cell differentiation is induced by surface contact.

By optically trapping and lowering caulobacter to the PDMS bottom of the device, we aimed to introduce holdfast formation as an indicator for imminent or completed cell differentiation from swarmer cells to stalked cells.

Since the flagellar pole, as the adhering side of an optically trapped caulobacter, can either face towards the ground or away from it, the chances of inducing holdfast formation is at maximum 50% or lower, depending on the escape probability of caulobacter from the trap.

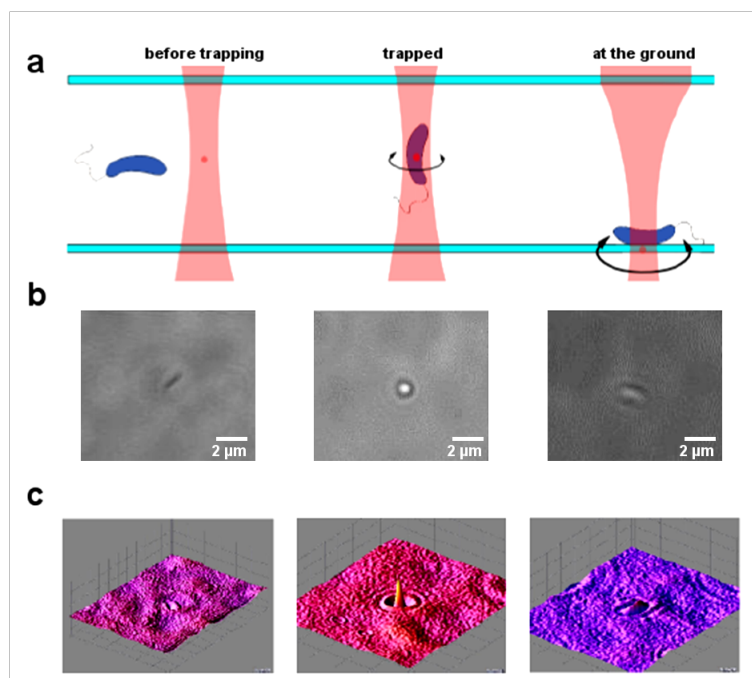


Figure 5.10: Experimental setup of induced holdfast formation with side-on surface contact for one caulobacter.

(a): Schematic representation, (b): micrographs and (c): false-coloured 3D-images based on the grey values of (b). Image by courtesy of Benjamin Banusch.

Indeed, formation of holdfast could be induced by simply bringing the caulobacter into contact with the surface as seen in Figure 5.11. Once attached to the surface, the stalked cell may sway and change its orientation, for example upon collision with a swarmer cell, but remains attached to the same position on the PDMS surface. In case the flagellum faced upward when the cell was brought into contact with the surface, the optical trap could also induce side-on surface contact (Figure 5.10).

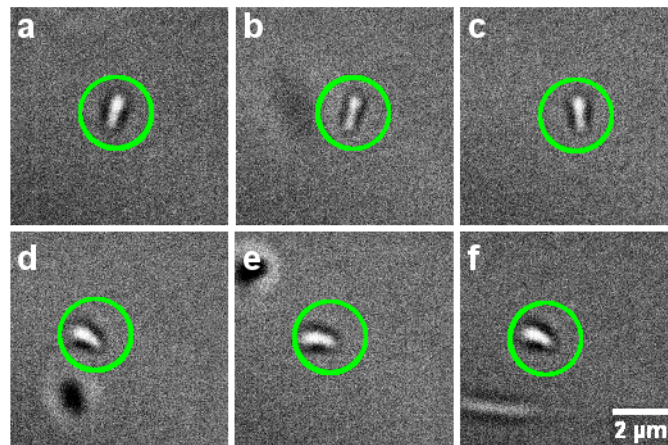


Figure 5.11: Caulobacter stalked cell after forcefully induced holdfast formation (green circle). Time-lapse between two images is 20 s.

To better understand the determinants of holdfast formation, the experiment was repeated with mutants lacking either pili (CB15 Δ pilA, NA1000 Δ pilA), holdfast (CB15 Δ hfsA), or pili and flagellum simultaneously (NA1000 Δ pilA Δ flgA).

Mutants lacking pili were found to still be capable of holdfast formation, although the percentage of successful attachment was only 30% in CB15 Δ pilA and 5% in NA1000 Δ pilA mutants. Nevertheless, since holdfast formation was still induced in pili-negative mutants in a rather high number of cases, we deduce that pili are not strictly essential for holdfast formation, but nevertheless important to initiate surface attachment (Figure 5.12). Moreover, NA1000 Δ pilA Δ flgA mutants, expressing neither pili nor flagellum also exhibited surface attachment through holdfast formation in rates comparable to CB15 Δ pilA indicating that neither pili nor the flagellum is necessary for holdfast induction.

However, the holdfast negative CB15 Δ hfsA mutants showed a surface adhesion rate of only 10% and this attachment was also weaker in comparison to wild-type cells as could be seen by the easy relocation of such attached cells using the optical trap. We assume that this adhesion of the CB15 Δ hfsA to the surface is mediated by pili, which is a precursor for the holdfast induction that can, however, not take place in a holdfast-negative mutant.

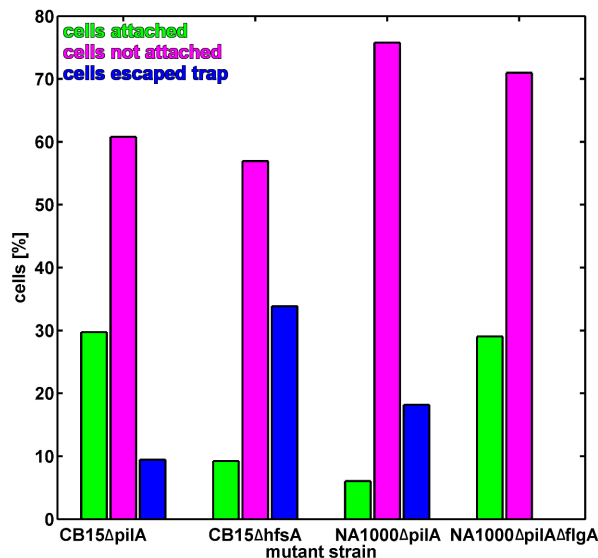


Figure 5.12: Attachment rates for caulobacter mutant strains. For each mutant, the percentage of attached cells (green), non-attached cells (magenta) and cells that escaped the trap (blue) are given.

In addition to the holdfast attachment, other, unspecific forms of attachment could be observed in CB15ΔpilA and NA1000ΔpilA mutants. Some mutant cells seemed to have attached to the surface with a long filament. This attachment was, however, not as rigid as the attachment with holdfast. With the help of the optical trap, the cells could be moved around the attachment point in a radius of about 8 μm . After release from the optical trap, these cells were drawn back towards their attachment point in a spring like motion. And even when not moved around with the optical tweezers, the cells exhibited random movement in a radius of about 2 μm around the attachment point. Some of these filament-attached cells even started rotating in circles with radii of 1-4 μm . For this kind of attachment, fluorescence tests for holdfasts were negative. Since pili were missing and holdfast was not formed, the attachment has to be achieved by other means. Stalks as the next possible suspect, are, however, only formed after holdfast has been induced. This leaves the flagellum as the only possible filament for attachment to the surface, unless some other, yet unknown filament-like structure is being expressed by the Caulobacter in absence of pili and holdfast. Indeed, the rotational radii of thus attached caulobacter, which are slightly shorter than the length of the caulobacter flagellum⁴⁶, seems to hint into this direction. To know for sure, the flagellum should be fluorescence labelled. It is an interesting observation that no cases of flagellum-adhesion was observed in wild-type cells, therefore it should be checked whether pili-adhesin expression might be relocated onto the flagellum in absence of pili.

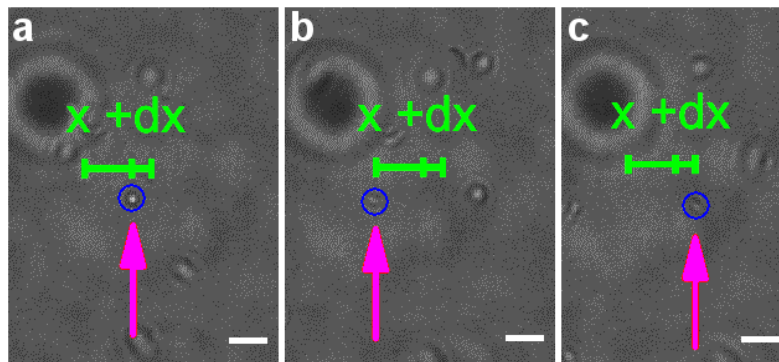


Figure 5.13: Filamentous attachment of $\Delta pilA$ mutants

(a): The attached cell (blue circle) at its attachment point.

(b): The attached cell (blue circle) can be displaced by about $8 \mu\text{m}$ (green x) using the optical trap.

(c): After release from the optical trap, the filament pulls the cell (blue circle) back towards the attachment point in a spring-like fashion. Then, the cell shows random walking in a radius of about $2 \mu\text{m}$ around the attachment point (green dx). Scale bar is $5 \mu\text{m}$. Image by courtesy of Benjamin Banusch.

Yet another, unspecific form of attachment was found in CB15 wild-type and NA1000 $\Delta hfsA$ mutants. Attached cells exhibited a tumbling or elliptical rotational motion, with a radius of less than $1 \mu\text{m}$ around their attachment point. This is most likely explained by the attachment of pili to the surface when holdfast was not (yet) induced. The tumbling motion in this unspecific adhesion most likely arose because the beating flagellum was not shed since no holdfast could be formed. In CB15 wild-type cells, which were unable to form holdfast attachment at this specific moment, this form of attachment probably occurs due to a side-on surface contact, in which pili attach but cannot bring the holdfast bearing pole in contact to the surface.

5.4 Conclusions

Optical traps can be calibrated and used as a tool to quantify forces generated by motile unicellular organisms, like *Caulobacter crescentus*. However, optical traps, like any form of high intensity light, can induce photo damage and even render cells incapacitated within seconds, depending on the wavelength and power of the optical trap. This has to be taken into account and assessed when working with living cells.

Using an optical trap, we were able to induce holdfast formation by bringing the caulobacter into close contact with the surface. Using pili-lacking mutant strains, we could even demonstrate other forms of surface attachment not frequently displayed by wild-type caulobacter. In mutants that did not express holdfast but still attached to the surface with pili, we observed a tumbling motion and elliptic rotation, which indicates that even after surface contact has been established by the pili, the flagellum was not shed. A possible explanation for this could be that the shedding of the caulobacter flagellum would only happen after holdfast formation, and was independent of pili-surface-contact. Further research is warranted in order to shed more light on this mechanism.

Filament mediated attachment was also observed in pili-negative mutants but could never be observed in pili-positive wild-type caulobacter. The reason for this is unclear and one can only speculate which side-effect of the pili inhibition causes the flagellum, usually responsible for displacement of the caulobacter, to suddenly act as an anchor for surface adherence.

6 Optical trapping of protozoa, e.g. *Trypanosoma brucei brucei*^a

6.1 Introduction

Trypanosoma brucei brucei, a widely used model organism, exhibits mainly two distinct swimming modes, a random-walk-like movement called *tumbling*, and a ballistic motion, also called *persistent* motion.^{2,40} The propulsion of trypanosomes requires beating of the sheathed eukaryotic flagellum alongside the body which wiggles in helical waves and pushes the trypanosome forward.⁷⁶ In addition to the directed movement, the cell body rotates approximately 60° around its major axis during each beat of the flagellum,⁷⁷ The forces it thereby generates deform the shape of the cell body^{2,78}. In this work we present a model to characterize and quantify the torque and power of the trypanosome flagellar movement.

6.2 Methods

Optical tweezers with a wavelength of $\lambda = 808$ nm and a power of 10-27 mW were employed to dislocate and manipulate *Trypanosoma brucei brucei* (trypanosomes) in its wild-type bloodstream form (BSF) in spatial confinement.

Moving trypanosomes were optically trapped and the trajectories of trapped trypanosomes was recorded using a Phantom Miro 3 high-speed camera (Vision Research, USA) at 150 fps. The position of the flagellar tip was than traced in each frame using the manual tracking plugin for Fiji. The obtained trajectories were plotted and analysed using MATLAB software.

The laser power mentioned denotes the power of the laser at the trapping point.

Power spectra of the trajectories were obtained by determining the Fourier transform of the temporal autocorrelation functions of the flagellar tip displacement.

^a Parts of this chapter have been published in: Stellamanns, E., Uppaluri, S., Hochstetter, A., Heddergott, N., Engstler, M. & Pfohl, T. Optical trapping reveals propulsion forces, power generation and motility efficiency of the unicellular parasites *Trypanosoma brucei brucei*. *Sci. Rep.* **4**, 6515:1–6515–7 (2014).⁷⁸

6.3 Results

6.3.1 Optical trapping of trypanosomes

While optically trapped, trypanosome vitality remains unaffected over long periods of time. Trypanosomes survive up to 60 minutes inside optical traps, rendering possible photo-toxicity negligible for trapping times of less than 15 minutes.⁷⁸ A time span of 15 minutes is by far enough to study trypanosomal motility, as this exceeds the longest reported movement patterns in trypanosome motility by two orders of magnitude.⁴⁰

Within the optical trap, only a small part of the trypanosome is actually optically confined in the focus of the trap (see Figure 6.1a). Thus trypanosomes remain fully mobile, whereas their movement is limited. The location of this trapping point varies between persistent swimmer and tumbling walkers. The main trapping point for persistent trypanosomes coincides with the kinetoplast, around the flagellar pocket. This is consistent with the fact that the optical trap would react to the relative high refractive index of DNA, which is the primary component of the kinetoplast⁷⁸. For tumbling trypanosomes, the trapping points show a broader distribution over the posterior half of the cell body (Figure 6.1b).

Trypanosomes in optical confinement exhibit two forms of motion. They either rotate around the focus of the optical trap or twist and turn irregularly. Trypanosomes that twist and writhe irregularly when inside an optical confinement are tumbling when outside the optical trap,⁴⁰ whereas Trypanosomes characterized as persistent walker⁴⁰ outside the trap exhibit periodic motility patterns and rotation when trapped.

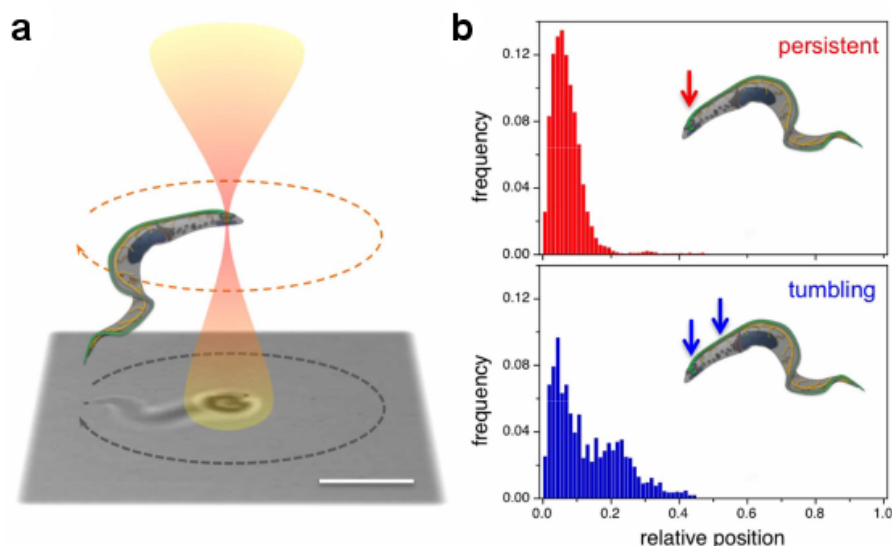


Figure 6.1: Optical trapping of trypanosomes

(a): Schematic representation of the setup for optically trapping motile trypanosomes. Within the optical trap, the motility is limited, whereas the mobility is unaffected.

(b): Histograms of trapping loci of persistent walker and tumbling cells versus the position from the posterior end relative to their contour length. Main trapping loci (arrows) are at the posterior end close to the flagellar pocket and internal structures around the nucleus. Adapted from Stellamanns *et al.*⁷⁸

The periodic rotation of the trypanosome cell body is overlaid by a zigzagging movement pattern of the flagellar tip. The frequency of the rotation around the trapping point, f_{Ω} , amounts to about 1.5 Hz (Figure 6.2)

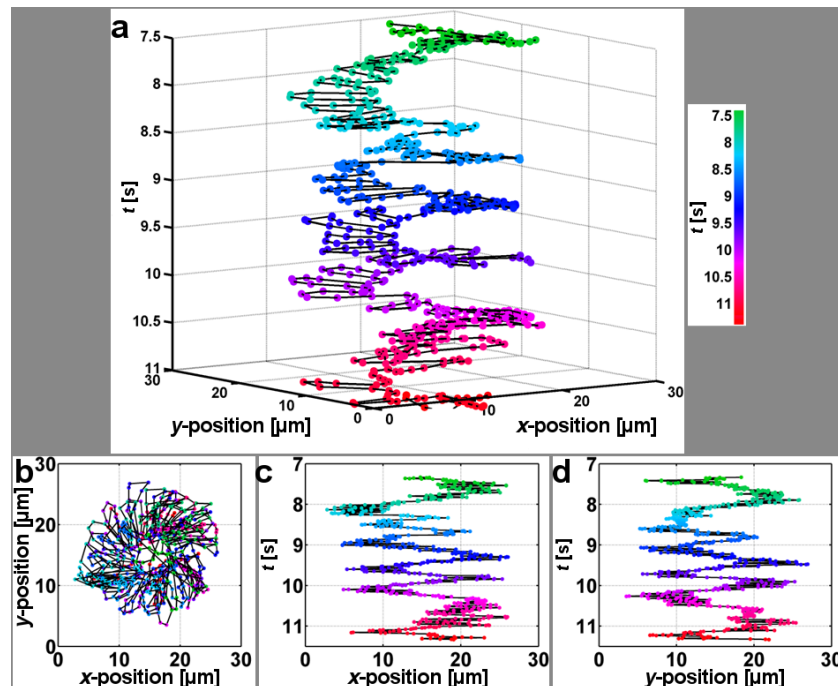


Figure 6.2: 2-D-time-trajectory of the flagellar tip of an optically trapped trypanosome
 (a): The x- and y-position of the flagellar tip is shown versus time. The colours represent time points (colour bar).
 (b-d): 2-D-projections of the flagellar tip's trajectory in the x-y-plane (b), the x-t-plane (c), and the y-t-plane (d).

The power spectrum of a trapped, rotating trypanosome, exhibits two main peaks, corresponding to the frequencies $f_{\Omega} \sim 1.5$ Hz and $f_{\omega} \sim 15$ Hz (Figure 6.3). The frequency f_{ω} represents the beating of the flagellum, whereas $f_{\Omega} \sim 1.5$ Hz is the earlier mentioned rotational frequency.

The frequency of 15 Hz for the flagellar beat is consistent with the reported flagellar beat frequency for freely swimming trypanosomes⁷⁷, which serves to demonstrate that optical confinement did indeed not alter the cell's mobility.

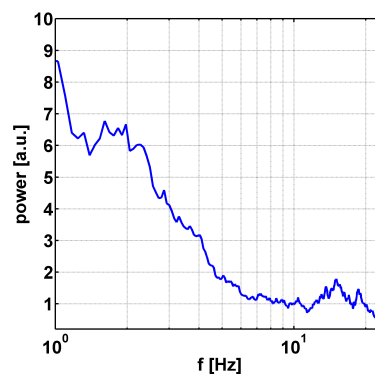


Figure 6.3: Power spectrum of the displacement of the trypanosomes' flagellar tip. The two peaks denote re-occurring frequencies in the trypanosome motion, here $f_{\Omega} = 1.5$ Hz and $f_{\omega} = 15$ Hz.

6.3.2 Dissipative energy of trypanosomes

As mentioned before, propulsion of persistently walking trypanosomes results in a continuous rotational movement inside the optical trap. The energy in this system is dissipated by friction between the trypanosomes and the surrounding fluid. Thus, the flagellar beats and rotations enable us to assess the work and power of persistently swimming trypanosomes.

To estimate the dissipated energy, we employed the following model: The rotation of the trypanosome around the centre of the optical trap is approximated by a rotating rod and the beating tip is described by a small rod with a combination of rotational and translational motion (Figure 6.4). The energy dissipated by one full body rotation of 2π is

$$W_B = 4\pi^2 \xi_{rB} f \Omega \quad (6.1)$$

and the generated power equals

$$P_B = 4\pi^2 \xi_{rB} f \Omega^2 \quad (6.2)$$

with ξ_{rB} as the friction coefficient for the rotating body. The friction coefficient ξ_{rB} of a rotating rod of length L_B and diameter $2r$ is given by

$$\xi_{rB} = \frac{4}{3} \frac{\pi \eta L_B^3}{\ln(L_B/2r) + \Gamma_{rB}} \quad (6.3)$$

with Γ_{rB} as the end correction factor.⁷⁹ The motion of a beat with the flagellar tip is approximated by a small rod of length l and diameter $2a$, performing a rotation of about π and a subsequent translation of approximately one tip length l in centrifugal direction.

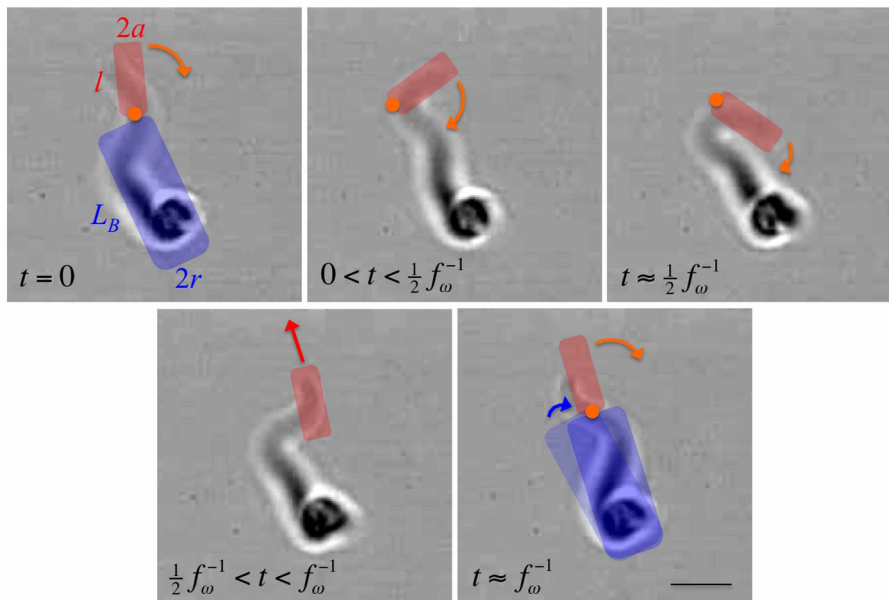


Figure 6.4: Picture sequence of a flagellar beat of an optically trapped trypanosome.

A sketch of the used rotating and beating rod model is overlaid. Scale bar represents $5 \mu\text{m}$ ⁷⁸. Image reprinted from Stellamanns *et al.* (2014)⁷⁸.

The time intervals of the rotation and translational steps were almost equal with the beat time $t \approx \frac{1}{2}t_{beat} = \frac{1}{2}f_{\omega}^{-1}$. The energy corresponding to one flagellar beat equals the sum of the energy for the rotation of about π and the translation of the tip by l with a velocity $v_t = l \cdot 2f_{\omega}$:

$$W_{beat}^l = W_{beat}^r + W_{beat}^t = 2f_{\omega}(2\pi^2\xi_{rl} + l^2\xi_{tp}^l) \quad (6.4)$$

For rotating the friction coefficient rod is $\xi_{rl} = \frac{4}{3} \frac{\pi\eta l^3}{\ln(l/2a) + \Gamma_l}$ and the parallel translational friction coefficient equals $\xi_{tp}^l = \frac{2\pi\eta l}{\ln(l/2a) + \Gamma_l}$ with the end correction factor Γ_l . The power generated by the flagellar is given by

$$P_{beat} = 2f_{\omega}^2(2\pi^2\xi_{rl} + l^2\xi_{tp}^l) \quad (6.5)$$

From the recorded trajectories, we can visually estimate the lengths of both the trypanosome cell body and the flagellar tip, according to our model. The length of a rotating trypanosome, is the sum of the cell body and the flagellar tip and defines the radius of the recorded trajectory. The trajectory exhibits also an *inner radius*, where no flagellar tip can reach. The ring between the inner radius and the outer radius shows the range in which the flagellar tip can be located. Thus, by subtracting the inner radius from the outer radius, we arrive at twice the length of the flagellum, $2l$. The length of the cell body can then be obtained by subtracting the length of the flagellar tip l from the outer radius (Figure 6.5). From this visual inspection, we obtain a length of the cell body of $L_B = 8 \mu\text{m}$, and for the flagellar tip $l = 2.5 \mu\text{m}$.

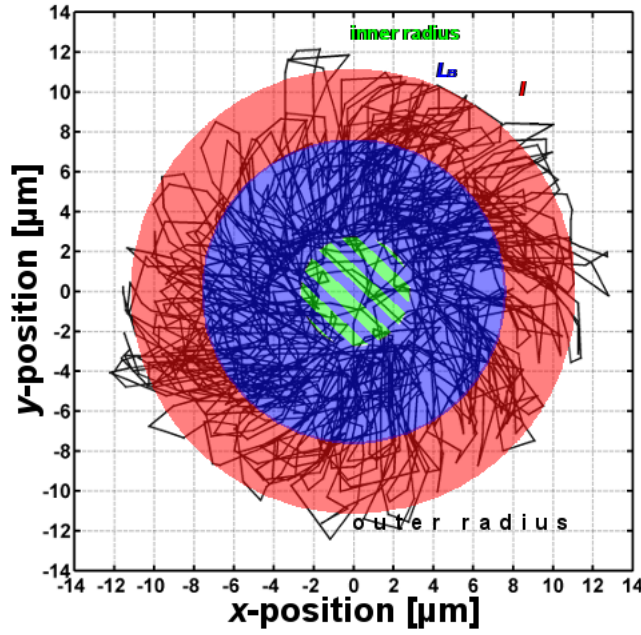


Figure 6.5: Visual model to estimate the lengths of cell body and flagellar tip.

The trajectory of the flagellar tip positions of an optically trapped trypanosome (black) is overlaid with markers for the cell body length (L_B , blue) and the flagellar tip (l , red). The green area denotes the inner radius, where the flagellar tip does not reach to.

The power which a rotating and persistently walking cell generates is the sum of the power generated by both the cell body and the flagellar tip, $P_B + P_{beat} = P$. Since $2\pi^2\xi_{rl} \gg l^2\xi_{tp}^l$, the power calculation can be simplified to $P \propto f_\Omega^2\xi_{rB} + f_\omega^2\xi_{rl}$. The torque of the trypanosome propulsion can be approximated by the torque of a flagellar beat $T \approx 2\pi f_\omega \xi_{rl}$.

Using our experimental values, we calculate $\xi_{rB} = 1.9 \cdot 10^{-18} \text{ kg} \cdot \text{m}^2/\text{s}$, $\xi_{rl} = 5.8 \cdot 10^{-20} \text{ kg} \cdot \text{m}^2/\text{s}$ and $\xi_{tp}^l = 1.4 \cdot 10^{-8} \text{ kg}/\text{s}$ for a persistent walker cell. The torque of the flagellar motor thus equals $T = 5.5 \cdot 10^{-18} \text{ N} \cdot \text{m}$. The energies that are dissipated during one body rotation are $W_B = 1.1 \cdot 10^{-16} \text{ J}$ and $W_{beat}^l = 3.7 \cdot 10^{-17} \text{ J}$ for one stroke of the flagellar tip. The power of a beat and a rotation are $P_{beat}^l = 5.6 \cdot 10^{-16} \text{ W}$ and $P_B = 1.6 \cdot 10^{-16} \text{ W}$, respectively, and sum up to a total power generation of $P = 7.2 \cdot 10^{-16} \text{ W}$. These findings are in good agreement with measurements we published previously.⁷⁸ The ratio of the power needed for the rotation and the power generated P_B/P may be used to measure the motility efficiency. We found that only one sixth to one quarter of the power generated ($P_B/P = 0.15 - 0.25$) is actually needed to rotate the body. This rather low power efficiency might be explained by the fact, that the motility mechanism of trypanosomes also serves other reasons apart from self-propulsion. The removal of antibodies attached to VSGs to evade the immune responses of their hosts is one well known example for such another use.¹¹

6.4 Conclusions

Combining microfluidics and optical trapping, we were able to stably trap trypanosomes and analyse their motility inside the optical confinement. By introducing a motility model for rotating trypanosomes, we determined the dissipated energy, power generation, torque and propulsion efficiency of trypanosomes. On the basis of the low propulsion efficiency, we suggest that the motility mechanism of trypanosomes is not only used for propulsion, but also essential in surviving the immune responses of their mammalian hosts.

The presented methodology to study motility patterns and dissipated energy of trypanosomes may also be applicable to other species of trypanosomes, e.g. *Trypanosoma cruzi* or other unicellular organisms.

RESULTS II:

MICROFLUIDICS APPLIED ON CELL STUDIES

7 Hydrodynamic impact of trypanosomes on their environment

7.1 Introduction

Unicellular organisms developed multiple swimming strategies. According to Ishikawa (2009)²⁰ these swimming strategies can be classified by the flows generated around the swimmer. A cell that pulls itself through the surrounding fluid and presses the fluid aside is called a *puller*. Whereas, a cell that attracts the surrounding fluid from the side and subsequently pushes it behind the moving body is classified as a *pusher* (Figure 7.1)

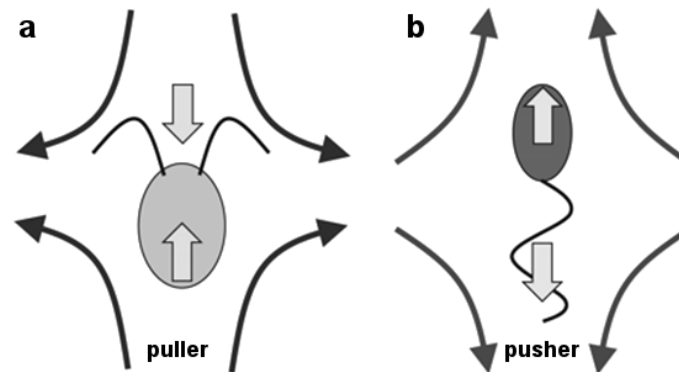


Figure 7.1: Hydrodynamic classification of motile cells. Black bent arrows illustrate flows in the surrounding fluid, straight grey arrows show net movement of the bodies and flagella respectively.

(a): A puller pushes the surrounding fluid sideways while it pulls itself forward.

(b): A pusher pushes the fluid backwards in swimming direction. Image reprinted from Ishikawa (2009)²⁰.

Such hydrodynamic flow fields are analysed using particle image velocimetry (PIV), where the displacement of particles over time is used to reveal flows in the surrounding fluid. This technique has been widely used within the field of microfluidics for the last 15 years⁸⁰.

Trypanosoma brucei brucei is a model flagellate, that has been known and studied for over 160 years.⁸¹ In terms of trypanosome motility, it has been shown by Heddergott *et al.* (2012) that persistently swimming trypanosomes propel themselves with flagellar beats from the tip to the base whereby each beat of the flagellum rotates a trypanosome 60° around their major axis. However, the question whether trypanosomes are to be classified as pusher or puller among the unicellular swimmers, remains open. We therefore aim to describe the hydrodynamic flow field around the trypanosome cell body in order to classify them into one of the two swimmer types.

7.2 Methods

The flow field around swimming trypanosomes was analysed in a quasi-2-dimensional environment by introducing polystyrene spheres of 1 μm diameter (Polybead® Microspheres, Cat.-Nr. 07310-15, Polysciences, Germany) into a quadratic chamber (62.5 μm x 62.5 μm x 2 μm) containing culture medium and polybeads solution (2% solids in water) in equal aliquots.

The subsequently generated flow field around the trypanosomes was thus visualized and analysed using particle image velocimetry (PIV).

Videos of the movement for the PIV analysis were recorded at 120 fps.

The data analysis of the obtained frames was performed using PIVLab for Matlab⁸².

7.3 Results

Swimming trypanosomes generated a hydrodynamic flow field extending up to 5 μm around themselves. Within the predominant flow field, polystyrene particles travelled from the anterior end, along the trypanosome body to the posterior end and beyond. A second flow field attracts particles from the environment around the trypanosome's mid-section towards the cell body and further to the posterior end (Figure 7.2). The interplay of these two flows generates vortices in the vicinity of the flagellar tip as well as between the midsection and the posterior end. These vortices vary in intensity during one flagellar beat, but the direction of the flow is not reversed. The velocity of the flow ranges between $0.4 \cdot 10^{-5} \text{m/s}$ around the midsection, and up to 10^{-4}m/s around the flagellar tip and posterior end of the trypanosome (Figure 7.3). As described by Ishikawa (2009) this flow field is characteristic for a pushing locomotion by a unicellular flagellated organism²⁰.

During a time-lapse of 58 ms, where the flagellar beat travels from the flagellar tip to the flagellar pocket, the trypanosome moves about one micrometer in the direction of the flagellar tip. These flagellar beats did not induce any abrupt changes in the flow field surrounding the trypanosome, even when several beats were performed consecutively with a frequency of around 17 Hz.

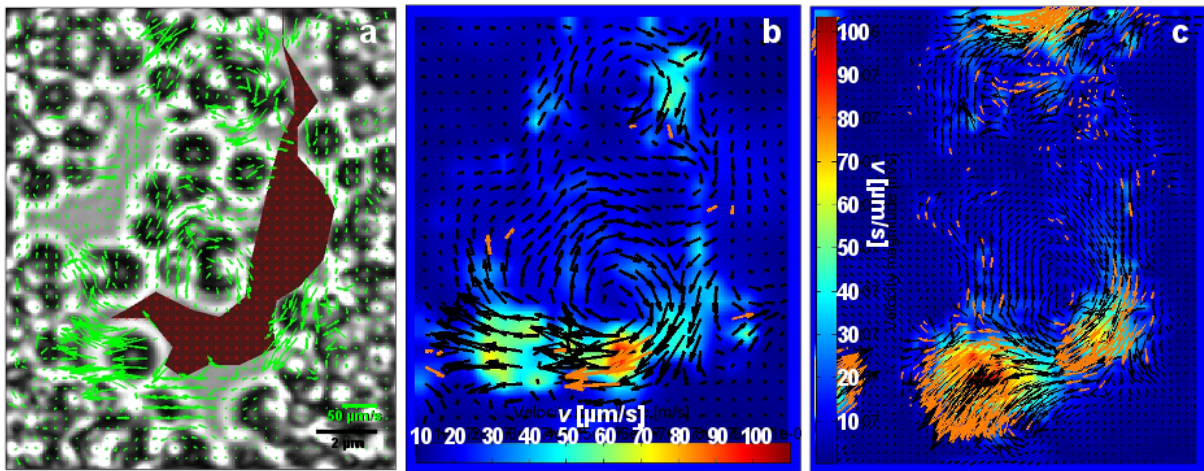


Figure 7.2: Hydrodynamic flow field around a swimming trypanosome.

(a): Micrograph showing the trypanosome (brown) surrounded by beads and the flow field during one flagellar beat.

(b): Velocity map of the averaged vectors generated during one flagellar beat, (average over 6 frames, total time lapse 58 ms)

(c): Velocity map in one frame (9 ms).

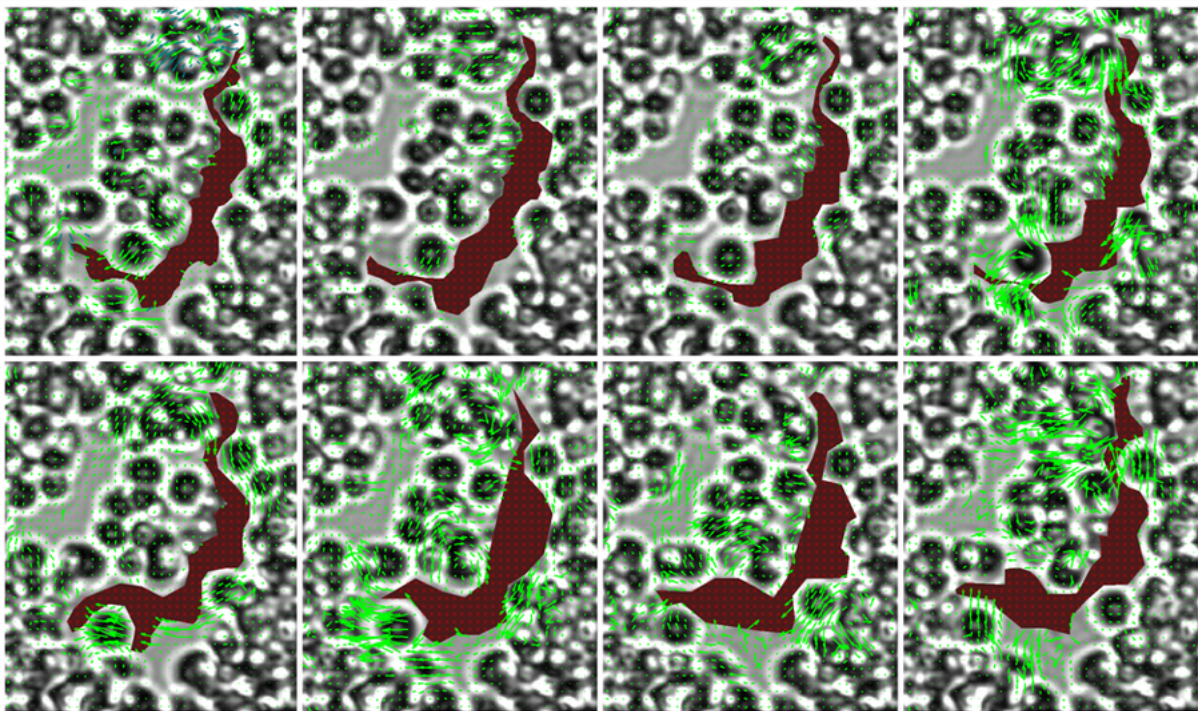


Figure 7.3: Flow field around a trypanosome during one flagellar beat. Time-lapse is 58 ms.

Based on our results, we were able to classify trypanosomes as *pusher*, which generate a hydrodynamic flow-field attracting the surrounding fluid from the sides (perpendicular to the direction of motion) and pushing it backwards in direction of motion. The knowledge that trypanosomes are *pushers* helps to better understand other findings, such as the highly effective

hydrodynamic surface clearance of trypanosomes, which is assisted by the force of the flow field pushing the VCGs in the direction of the flagellar pocket as discussed in an earlier chapter.

The fact that no changes in the surrounding flow field of trypanosomes are induced by the flagellar beat, disproves the elsewhere proposed kink-based propulsion of trypanosomes⁸³. Indeed, the continuity in the flow field in our experiment, supports the motility model of trypanosomes as proposed by Heddergott *et al.* (2012)⁷⁷. Additionally the fact that we found almost no trypanosomes exhibiting tumbling motion in our setup, is in line with the finding of Heddergott *et al.* (2012) that trypanosomes in a crowded environment exhibit mostly directed motion.⁷⁷

7.4 Conclusion

With the help of a straightforward experiment, we could not only classify trypanosomes as *pusher*, but also show that the hydrodynamic field around them extends up to 5 μm away from the cell body, wherein surrounding particles are accelerated to velocities of up to 100 $\mu\text{m/s}$. The knowledge about the flow field generated by trypanosomes and their classification as *pusher* sheds new light on the complex way in which trypanosomes move about in their crowded environment.

8 Hydrodynamic manipulation of Trypanosomes

8.1 Introduction

In the field of microfluidics, geometry of micro chambers and connecting channels can be used to sort self-propelling cells. Generally, the microfluidic environment does not favour one swimming direction over another as can be seen by the homogeneous distribution of cell-position over time in the device.

However by employing specific structures that favour cell migration in one direction over the other – so called ratchets – it is possible to concentrate motile cells in a predefined space.⁸⁴

The directional migration within the device as well as cell concentration can thus be altered and controlled. There are several possibilities to achieve this, either by funnel-like structures that guide motile cells in one direction while inhibiting passage in the other direction⁸⁵, or by asymmetric constrictions in the chamber shape itself⁸⁶ (see Figure 8.1).

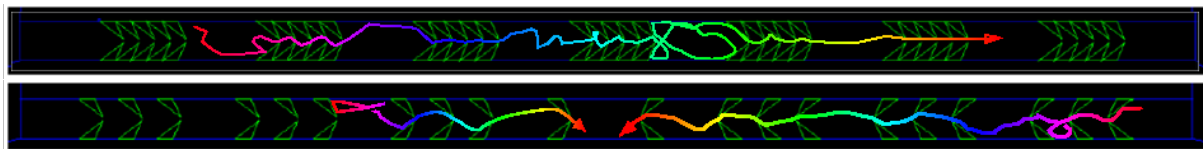


Figure 8.1: Two sample structures designed to induce self-concentrating of motile cells to the left (top) and in the middle (bottom) respectively. Multicoloured arrows show sample paths directed by the ratchets in the sorting channels over time.

In these ratchets, the flow velocities must be kept at a minimum, so cell concentration is only driven by self-propulsion. This no-flow condition can be established in chambers adjacent to the main flow channel.

Indeed, such ratchets have already been used to concentrate bacteria in a device and sort them according to their size, deformability or motility^{84–88}.

In the light of these findings, we explore the possibility to develop a device design which would enable us to separate *Trypanosoma brucei* spp. from a matrix of immotile cells such as red and white blood cells without external manipulation. Within such a device, the active propulsion of the trypanosomes itself would lead to their concentration in a predefined position, whereas immotile cells would diffuse randomly through the whole device without any concentration (Figure 8.2).

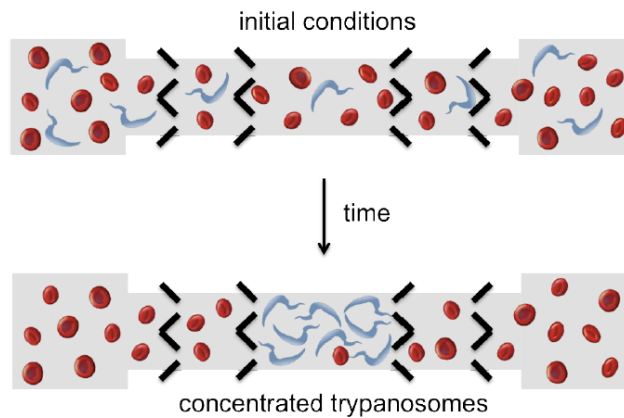


Figure 8.2: Ratchets to concentrate trypanosomes in blood.

The capability to concentrate trypanosomes from a sufficient amount of blood or spinal liquor would be highly useful as a diagnostic approach for trypanosome infection.

To date, diagnosis of *Trypanosoma brucei* spp. in humans remains inefficient.⁸⁹ However, in the fight against this neglected tropical disease, new improved diagnostic approaches are needed which should be cheap while, at the same time, easy to use even in resource-poor settings by untrained personnel.⁸⁹ A hand-held microfluidic device enabling passive cell-sorting and concentration without external manipulation would, when produced in large quantities, fulfil these requirements.

8.2 Methods

8.2.1 Influence of device geometry and flow on the confinement of trypanosomes

With the help of optical tweezers, trypanosomes were placed inside different devices comprised of a combination of the following parameters:

- Chamber geometry: round ($\text{Ø}30\ \mu\text{m} \times 8\ \mu\text{m}$) vs. squared ($37.5\ \mu\text{m} \times 37.5\ \mu\text{m} \times 8\ \mu\text{m}$)
- Connecting-channel size: narrow ($5\ \mu\text{m} \times 6\ \mu\text{m} \times 8\ \mu\text{m}$) vs. broad ($10\ \mu\text{m} \times 6\ \mu\text{m} \times 8\ \mu\text{m}$)

Additionally, flow velocity in the main channel was varied between $< 1\ \mu\text{m/s}$ and $\geq 10\ \text{mm/s}$.

The resulting flow-profiles inside the chambers were computed for both types of connecting channel with the computational fluid dynamics (CFD) module from the software COMSOL multiphysics (version 4.3a).

Upon release from the optical tweezers, trajectories in the confinement were recorded at a frame rate of 10-15 fps and analysed for movement patterns within the specific geometry/channel size/flow combination.

Likewise, dwelling time until escape from the chamber was measured for a maximum time of 8 minutes. The retain probabilities were calculated and fitted to an exponential decay function according to the equation

$$P_{\text{retain}} = 100\% \cdot (e^{-t/\tau}) \quad (8.1)$$

where the detainment time τ equals the time elapsed until the probability of detainment decreases by a factor of e .

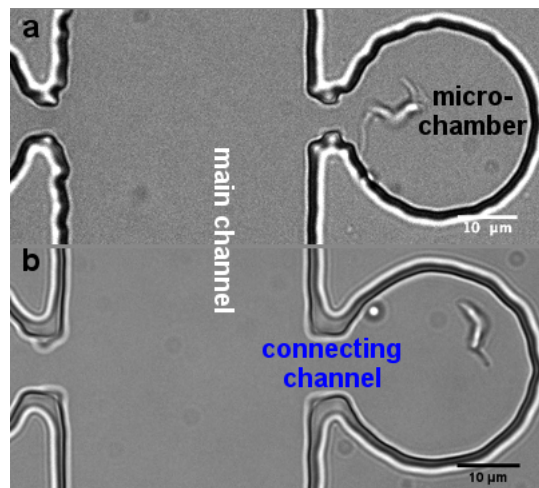


Figure 8.3: Experimental setup: Trypanosomes are put in circular micro chambers with $30\ \mu\text{m}$ diameter and the time is recorded till trypanosomes escape. The discriminating parameter is the width of the connecting channel of either $5\ \mu\text{m}$ (a) or $10\ \mu\text{m}$ (b).

By exposing trypanosomes in the micro chambers to various flows, we investigated if the presence of flow has any measurable impact on trypanosome escape times.

8.2.2 Ratchet design for the passive concentration of trypanosomes

A first parallel-ratchet device was created where four neighbouring channels connected an inlet with an outlet. Within each of these channels, triangular constrictions or funnels were designed and strategically placed in order to assess their capability to retain trypanosomes in the middle of the channel (Figure 8.4).

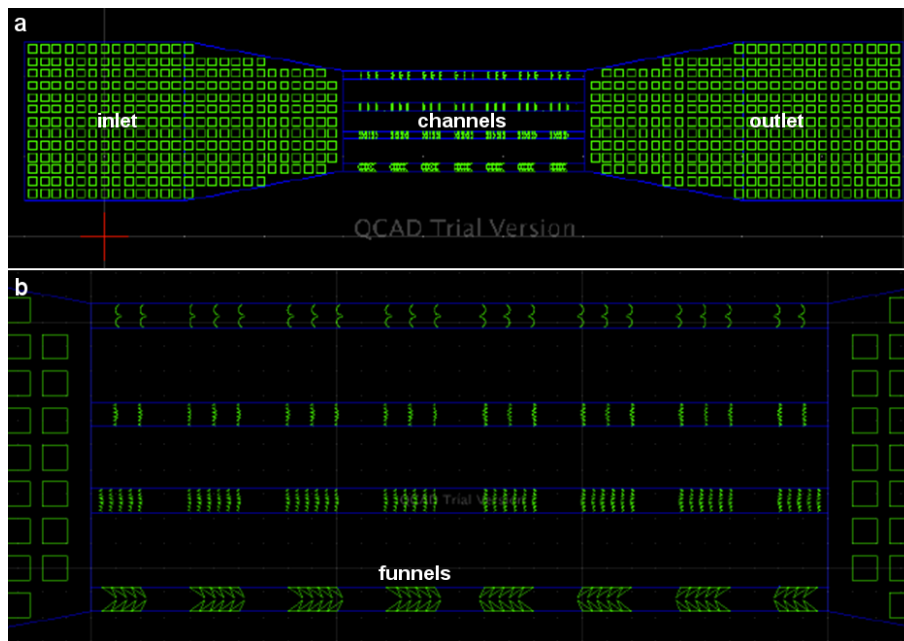


Figure 8.4: General layout for sorting devices

(a): Four channels - each filled with a different kind of obstacles - are connecting inlet and outlet of the device.

(b): Close-up on the channels reveals the thinness of the structures. By courtesy of Hermeto Gerber.

Additionally, an orthogonal-ratchet device was designed where sorting structures were placed perpendicular to the flow in order to easily control the flow condition within the sorting channels. This flow control was achieved by directing a flow through two parallel channels connecting two inlets and outlets (Figure 8.5).

Now to control the cross-flow through the sorting structures, the pressure difference between both main channels has to be controllable. This was achieved by bringing together the two main channels before and after each sorting structure (Figure 8.6, green).

When guiding fluid simultaneously from both inlets to both outlets, a no-flow condition can be achieved inside the ratchet structures. However, by increasing the flow rate through one inlet while keeping the other inlet's flow rate constant, a *cross-flow* through the ratchet structures can be induced, with which trapped cells can be flushed out of the structure again.

The sorting structures themselves consisted of so called *arrow heads* (Figure 8.6, white) as well as a structure called the *gear-wheel concentrator* (Figure 8.6, magenta). Consecutive arrow heads build a linear ratchet that governs motile cells in the direction of the pointed tip. The gear-wheel on the other hand, is designed to re-direct swimming motile cells towards the centre of the concentrator, by making use of its gear-wheel- or circular-saw blade shape.



Figure 8.5: Layout of the improved device design, featuring two inlets (green, left) and two outlets (green, right) connected by two symmetric, interconnected main channels. The sorting channels are run perpendicular to the main channels (up-down).

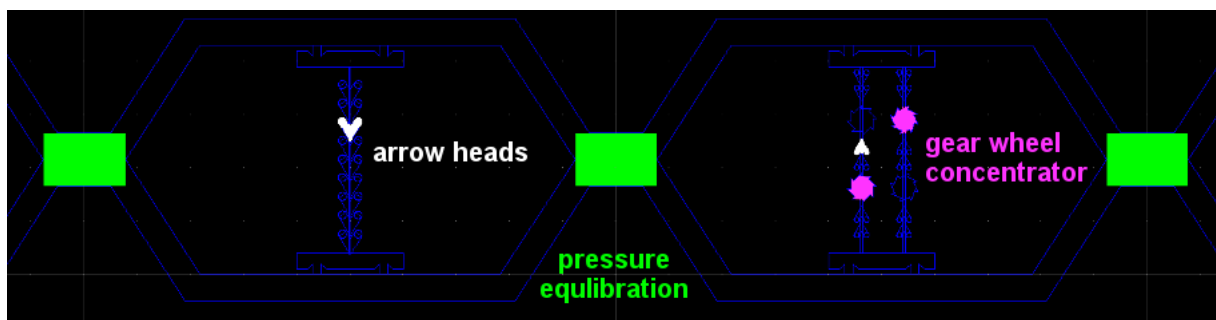


Figure 8.6: Close-up of the design featuring arrow heads (white) to direct motile cells, gear-wheel concentrators (magenta) to store motile cells and pressure equilibration junctions (green) to avoid unwanted cross-flow.

8.3 Results

8.3.1 Influence of device geometry and flow on the confinement of trypanosomes

The width of the connecting channel decisively influences the propagation of flow from the main channel into the micro chambers.

For narrow connecting channels ($5 \mu\text{m} \times 6 \mu\text{m} \times 8 \mu\text{m}$), the reduction in flow velocity from the main channel to the chamber was reduced by 5 orders of magnitude, whereas broader connecting channels ($10 \mu\text{m} \times 6 \mu\text{m} \times 8 \mu\text{m}$) reduced the flow velocities by about 3 orders of magnitude (Figure 8.7).

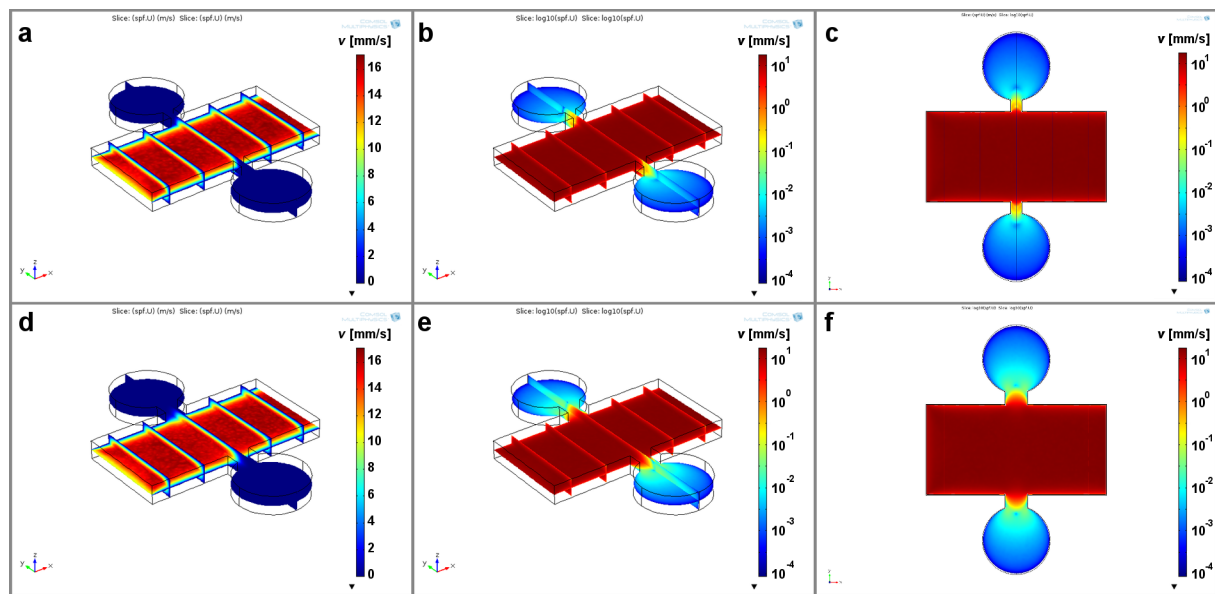


Figure 8.7: CFD calculations of flow velocities in devices with a height of $8 \mu\text{m}$, consisting of circular chambers (diameter: $30 \mu\text{m}$) alongside a main channel (width: $40 \mu\text{m}$)

(a-c): Connecting channel size 5 by $6 \mu\text{m}$, (d-f): Connecting channel size 10 by $6 \mu\text{m}$. The images show the relative flow velocities on linear scale (a,d) and on logarithmic scale (b,c,e,f). The flow fields are also shown in top view for the central height of the device (c,f).

Under no-flow conditions, round micro chambers with broad connecting channels retained about 25% of all cells within the time span of 8 minutes, whereas with strong flows in the main channel, only 10% of cells were retained within 8 minutes.

In contrast, in round-chamber devices with narrow connecting channels almost 60% of all cells remained inside the chamber during the 8 minute time span when there was no flow in the main channel. However, like for broad connecting channels, a strong flow in the main channel of chambers with narrow connecting channels, lead to a mere 10% retention of cells during 8 minutes (Figure 8.8).

Within the square-chamber set up, none of the observed trypanosomes was able to escape the confinement within the time span of 8 minutes.

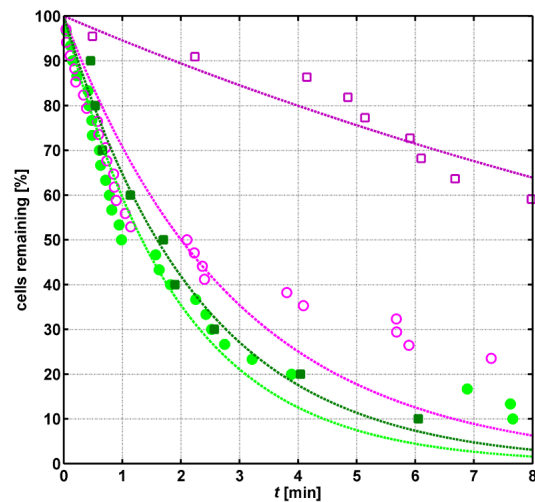


Figure 8.8: Remaining cells over time, fitted with exponential decay curves. Narrow connecting channels (squares) retain cells longer than broad connecting channels (circles). In the presence of flow (filled green markers) trypanosomes escape from faster than in the absence of flow (open magenta markers). While narrow connecting channels increase the detainment of cells, the presence of flow is decreases detainment time drastically.

For circular chambers and in the presence of a strong flow in the main channel the detainment time τ is about 125 s for both narrow and broad connecting channels. Conversely, under a no-flow condition, it ranged from 173 s for broad connecting channels, to 1072 s for narrow connecting channels (Table 8.1)

Details on the calculated detainment time τ of trypanosomes for each experimental combination, can be seen in Table 8.1.

Upon analysing the recorded trajectories, we observed that trypanosomes placed into the middle of the chamber swim into a general direction until they hit the wall of the micro chamber. After having hit the wall, the trypanosomes continue moving forwards alongside the wall in either direction (Figure 8.11).

chamber geometry	connecting channel size	flow	detainment time τ
Round	tight	no flow	1072 s
Round	tight	flow	138 s
Round	wide	no flow	173 s
Round	wide	flow	116 s
Square	tight	no flow	∞
Square	tight	flow	∞
Square	wide	no flow	∞
Square	wide	flow	∞

Table 8.1: Detainment times for trypanosomes depending on chamber shape, presence of flow and the size of the connecting channel between chamber and main channel.

8.3.2 Detaining and concentrating trypanosomes

In neither of the parallel channels any form of trypanosome enrichment could be observed. Upon further investigation we noted that some trypanosomes were swimming right through the ratchet structures and thus avoided the intended directional guiding (Figure 8.9). We assume that these structures, especially the very fine ones, did not properly bind to the glass surface of the device. This in turn enabled the trypanosomes to circumvent the directional determination of the ratchet.

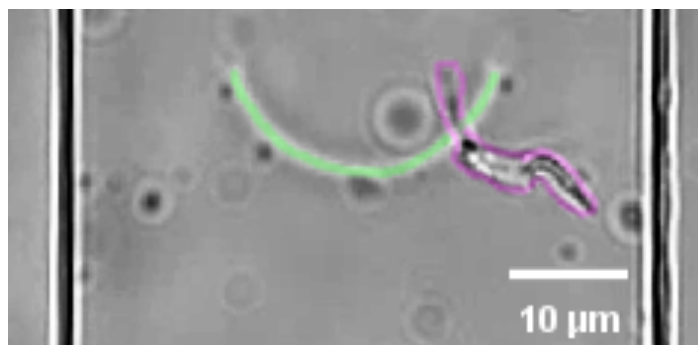


Figure 8.9: One trypanosome (magenta) swimming through a sorting structure (green).

Additionally, it was not possible to achieve a no-flow condition in the parallel-ratchet devices. Due to the design, all fluids in the device flow through the ratchets and can potentially move trypanosomes out of the channel again. Even the tiniest pressure difference between inlet and outlet is enough to create a flow inside the ratchets, dragging motile cells along and overrunning their own propulsion.

In the orthogonal-ratchet device with arrow heads and gear-wheel contractors however, it was possible to force trypanosomes to swim towards a predefined space and remain there as long as flow conditions stay the same. With this design we were able to keep motile trypanosomes confined for more than 4 minutes. Upon inducing a cross-flow through the ratchets, we could then remove the trypanosomes again from the ratchet (Figure 8.10).

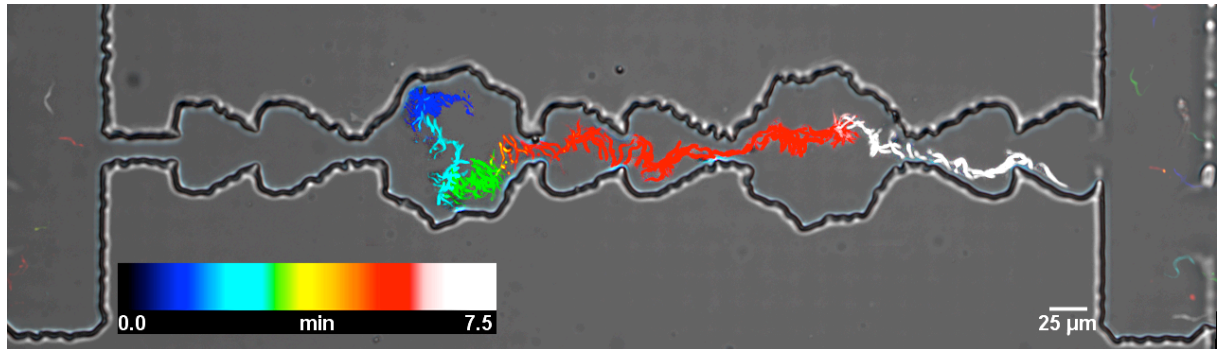


Figure 8.10: Trypanosomes can be stored (blue - green $t = 0 - 4$ min) in the new devices and pushed out again upon inducing a flow ($t > 4$ min).

8.4 Discussion

We observed that trypanosomes manage to escape quicker from micro chambers when there is a strong flow in the main channel that propagates into the micro chambers. However, with this experimental setup we cannot deduct whether the trypanosomes are able to sense flows and adapt their taxis accordingly, or whether they are merely guided out of the micro chambers by the flow field. Both explanations seem conceivable. Indeed, the shear forces that arise from the circular flow inside the micro chambers could cause the unsymmetrical trypanosome body to align along the velocity gradient of the flow during its locomotion. Such a self-alignment in shear forces has been reported for trypanosomes swimming inside a Poiseuille flow ($v_{max} = 1.6$ mm/s within straight channels⁹⁰). This alignment along the velocity gradient would then cause the trypanosome to predominantly dwell in places where they have a higher probability to be guided out of the chamber by the flow.

In terms of the influence of chamber geometry on the escape probability of trypanosomes, we found that square chambers were much more likely to retain trypanosomes over a time span of 8 minutes. These findings are probably explained by simple geometrical factors. Starting in the centre of a micro chamber, a directionally swimming trypanosome will hit the wall of the micro chamber at some point. From there it continues persistently moving forward by gliding alongside the wall of the chamber in either direction. Circular walls will eventually lead the trypanosome to the exit of the micro chamber. In squared chambers, however, trypanosomes will most likely hit a corner instead. Constituting an obstacle, the orthogonal wall in the corner will likely cause the trypanosome to change direction. Furthermore, even when a trypanosome in a square chamber swims along the wall toward the exit, the right-angled nature of the connecting channel would make it very difficult for the trypanosome to actually detect the exit because it approaches the channel in a very shallow angle (see Figure 8.11, right).

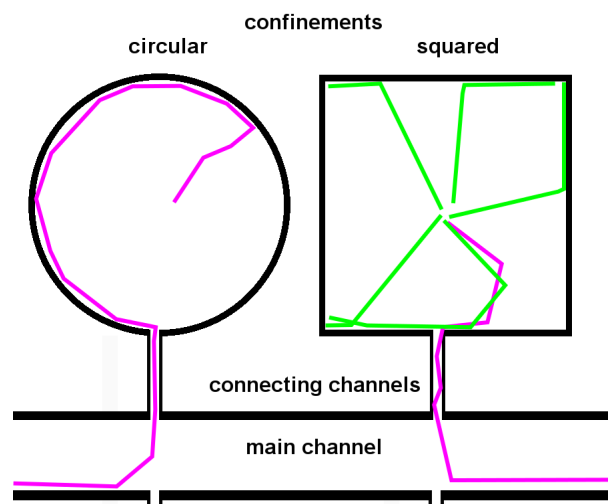


Figure 8.11: Sample trajectories for persistently swimming cells depending on confinement geometry. Trajectories leading out of confinement (magenta) are outnumbered in squared confinements by trajectories retaining the cells in confinement (green).

These findings about the geometrical determinants of detainment chambers can be considered as one factor when designing devices with which motile cells can be captured. Another factor would be the employment of suitable ratchet structures. Indeed we could show that it was possible to passively guide trypanosomes into a wanted direction and trap them at a predefined space with the help of arrow-head and gear-wheel ratchets. Our attempt to create ratchet channels parallel to the flow within the device, served to show that care has to be taken when designing very fine PDMS structures, as it may be difficult to sufficiently attach these structures to the glass surface of the device.

Nevertheless, through this prove of principle, we show that it is indeed possible to create a device with which living trypanosomes can be caught and concentrated. Further research is warranted in order to transform these findings into a usable diagnostic tool for African Trypanosomiasis, apt for cheap production and easy use in resource-poor settings.

8.5 Conclusion

We could show that trypanosomes react to flow and their motility can be manipulated by shaping their environment accordingly, which enables control over trypanosomes that does not require optical traps or other external manipulation with magnetic or electric fields. Thus, concentrating trypanosomes from blood seems feasible and might help to improve diagnosis of this neglected, yet fatal pathogen in developing countries.

9 Microfluidics-based single cell analysis to study drug-dependent motility changes in trypanosomes^b

9.1 Introduction

The discovery of drugs that are effective in the battle against rapidly adapting pathogens requires concerted efforts with respect to developing improved screening assays and understanding of the mode of action of drugs on the target cell. To economize these efforts, pharmaceutical research increasingly employs cell culture assays that bridge the gap between molecular and animal drug testing.⁴ In many instances, analysis of whole cells allows for more accurate predictions of drug responses than molecular assays because the complex molecular interactions and the cellular compartments that significantly influence the host's reaction to a drug are retained.⁴ Cell culture-based drug discovery commonly involves cell chips, high throughput screenings, and cell viability assays using fluorescence or luminescent transgenic target organisms.^{4,91–93} Often, these assay systems are unable to distinguish between drugs that kill the target cells (cytotoxicals) and drugs that merely inhibit cell growth (cytostatics).⁹⁴

In recent years, microfluidics has emerged as a powerful tool for the discovery of drugs, as well as for elucidating their effects on cells, cell secretions, and signaling pathways.^{4,95–97} Moreover, microfluidics has proven useful for exploring individual cells in a heterogeneous population.⁹⁵ The range of applications in single cell analysis is increased manifold by combining microfluidics with optical tweezers that allow the manipulation of cells by miniscule forces without touching.^{98,55} Examples include the sorting of motile cells⁵⁷ and the characterization of cell motility⁹⁹, but also specific placing of cells into defined environments.^{57,100,101}

In single cell assays, the effects of environmental parameters are frequently assessed through analyzing cell lysates.^{95,102,103} However, this type of endpoint analysis excludes further investigations of downstream effects. On the other hand, physical or biophysical properties of living cells so far are very rarely used as readout. The few published examples include monitoring bioelectrical impedance¹⁰⁴ in response to drug treatment or migratory behavior.⁹⁷ Highly motile cells or pathogenic unicellular organisms have not yet been studied by single cell assays.

Trypanosoma brucei, a unicellular organism belonging to the genus of trypanosomes, is one of the most rapidly adapting pathogens.^{28–32} The subspecies *T. brucei brucei* is endemic in sub-Saharan Africa where it causes Nagana disease in livestock¹⁰⁵, whereas *T. brucei rhodesiense* and *T. brucei*

^b This chapter is currently being submitted in collaboration with Stellamanns, E., Deshpande, S., Uppaluri, S., Engstler, M., & Pfohl, T.
Please note that supplementary information can be found on the CD-ROM.

gambiense are responsible for the acute and chronic form of the fatal sleeping sickness in humans (Human African Trypanosomiasis, HAT), respectively.^{33–37}

Trypanosomes are extensively studied model flagellates.^{11,31,106} The flagellum is structurally different from bacterial flagella and more complex than most other eukaryotic flagella.³⁹ Nonetheless, it is essential for locomotion and viability. Moreover, the flagellum is key to evading the immune response of the infected mammalian host.¹¹

Present screening procedures for trypanocidal compounds involve either *in vitro* assays that take several hours^{93,94,107} or *in vivo* experiments that are based on establishing mutant trypanosomes that take weeks¹⁰⁸ and therefore, are even more time-consuming.

Here, we introduce a real-time motility analysis system that is based on a straightforward microfluidic device in combination with time-resolved microscopy and optical tweezers. In the device, the concentration of drugs and chemicals is diffusion-controlled and can be changed gradually, while simultaneously observing single cells. This setup allows us to physically characterize and quantify how drugs and chemicals affect trypanosome motility. Specifically, we quantify drug-induced reversible paralysis and irreversible chemical fixation of trypanosomes in a dose-dependent manner.

9.2 Results

9.2.1 Design and function of drug testing device

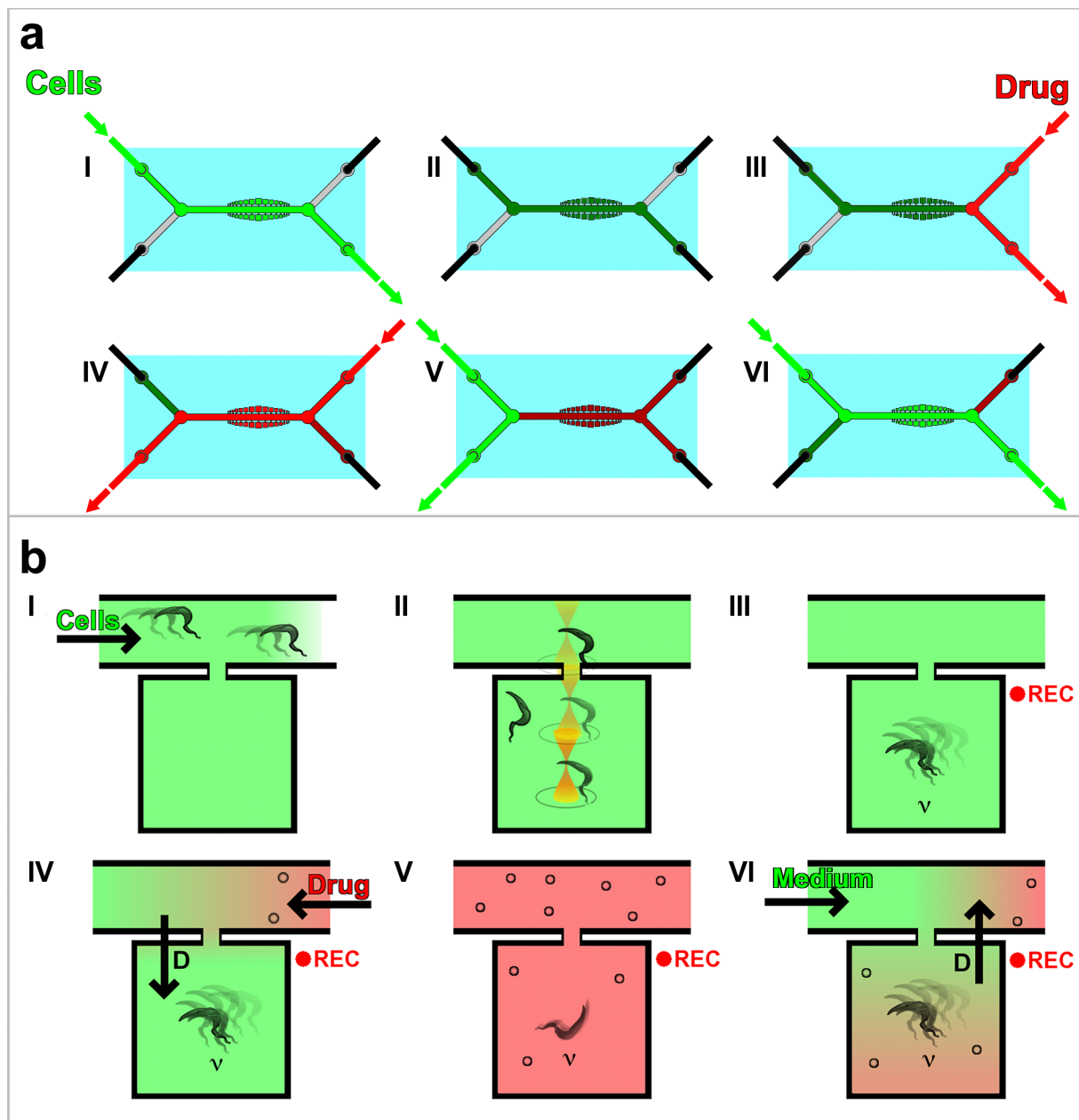


Figure 9.1: Schematic representation of the experimental design at the level of (a) the device and (b) the micro chamber (a,b): The device consists of micro chambers along a main channel that connects the cell side with the drug side. Both sides have an inlet and an outlet at the end of the respective Y-split. Panels (I-VI) illustrate individual operational steps in (a) and the resulting relative concentrations of solutions in (b). (I) Channels and micro chambers are filled with culture medium, (II) in the absence of applied flow, individual cells are trapped by optical tweezers and moved into a micro chamber. (III) Cell movements in a drug-free confinement are recorded while the drug side is flushed with drug-containing solution (Drug) to remove culture medium. (IV) Drug is pumped through the main channel and drug molecules diffuse into the chambers while cell movements are recorded. (V) At maximum drug concentration, the cell side is flushed with culture medium. (VI) Culture medium is pumped from the inlet on the cell-side through the main channel and recording can be stopped.

Our experimental setup for single cell analysis combines microfluidics with time-resolved microscopy and optical tweezers. The essential microfluidic device is a structured PDMS mold covalently bound to a glass slide. The structure inside the PDMS consists of one main channel (width: 40 μm , height: 9 μm). The main channel is linked to adjacent square micro chambers by connecting channels (width: 4 μm , length: 12 μm) and ends on both sides in a Y-fork (Figure 9.1a).

The dimensions of the connecting channels shield the chambers from the high flow velocities of the main channel and thus, only diffusion-driven material transport into the chambers occurs (supporting information S1).¹⁰⁹

Both inlets are attached to controlled micro liter syringe pumps via Teflon tubing. The outlets can be opened and closed individually, while the device rests on the stage of a microscope.

9.2.2 Device operation

At the beginning of an experiment, the device is flushed with culture medium from the cell inlet to the outlet on the opposite side (step I). When all chambers are filled with medium, the flow is stopped. Using optical tweezers, individual trypanosomes are trapped, moved through the connecting channel into the micro chambers and then released (step II).⁹⁸ Once the desired number of cells occupies the chambers, cell motility is recorded in a series of images at about 10 frames per second (step III). Subsequently, the culture medium on the drug side of the device is replaced with drug solution. By opening the outlet on the cell side, the drug solution flows from the drug inlet through the main channel (step IV). To trace the flow of incoming drug solution, polystyrene spheres (1 μm diameter) are added to the drug solution. A flow velocity of $v_{main} \approx 2 \text{ mm/s}$ is applied to reduce the time delay between the drug arriving at the first and at the last chamber to less than 0.5 s. While the drug diffuses into the micro chambers, the flow in the main channel is maintained for the drug concentration to stay constant (step IV). Image recording is continued beyond maximum drug concentration in the chambers (step V) or if applicable, until the drug is completely washed out by pumping drug-free culture medium through the device (step VI).

9.2.3 Drug diffusion

Changes in the concentration of drugs and chemicals in the main channel that result from the advective flow as well as those in the micro chambers are calculated employing computational

fluid dynamics (CFD) simulations. We used the CFD module from the software COMSOL multiphysics version 4.3a to calculate the evolution of concentration gradients in the microfluidic device. CFD simulations of the distribution of a drug with a diffusion coefficient of $D_{drug} = 5.7 \cdot 10^{-10} \text{ m}^2/\text{s}$ are shown in supplementary video S1 and S2 and Figure S1. The chosen diffusion coefficient is representative for a small molecule, such as 2-deoxy-D-glucose (2DG), glutaraldehyde (GA) and the drug suramin, all of which have been used in our experiments.

9.2.4 Microfluidics single cell motility analysis with glutaraldehyde

We tested the feasibility of single cell analysis in microfluidic devices by exposing confined trypanosomes to GA, which is widely used to fix cells for microscopy.^{110,111} GA was diluted with culture medium (final concentration 1M) in this control experiment to maintain maximal similarity with subsequent experiments. Following the procedure described above, GA solution was administered from the drug side. The effects of GA on trypanosome motility were recorded with a frame rate of 10 Hz before and during the inflow of GA.

Based on sequential images, we determined the center of mass trajectories of the trypanosomes

(Figure 9.2) and calculated their velocity, $v(t) = \frac{\sqrt{(r(t+\Delta t) - r(t))^2}}{\Delta t}$, where r is the position, t is the time and Δt is the interval between two consecutive images. Furthermore, the mean square displacement of the trajectories, $MSD \equiv \langle r(\tau)^2 \rangle = \langle (r(t + \tau) - r(t))^2 \rangle^c$, where τ is the time interval, was computed. MSD is a common measure for cellular motion⁹⁸ and can be interpreted as the space which is covered over time. In two dimensions, the time dependence of the MSD can be described by the following equation: $\langle r(\tau)^2 \rangle = 4 \cdot M_\alpha \cdot \tau^\alpha$, where α is the scaling exponent and M_α the motility coefficient.⁴⁰ For $\alpha > 1$, the motion is super-diffusive, for $\alpha < 1$ sub-diffusive and for $\alpha = 1$ diffusive or random walk-like.^{40,112}

Figure 9.2 shows the color-coded time-lapse trajectories of two confined trypanosomes over six minutes in culture medium (Figure 9.2a,b) and after GA inflow (Figure 9.2c; see also supplementary video S3). At the onset of the experiment, when the device is filled with culture medium, trypanosomes in micro chambers were highly motile (Figure 9.2b). Exposure to GA led to a rapid fixation of trypanosomes (Figure 9.2c). Velocity analyses revealed that their initial velocity of about $3.5 \mu\text{m/s}$ (green) decreased within 1 second to almost zero (Figure 9.2d,e and supplementary video S3) after contact with GA (magenta). The MSD of trypanosomes moving in a micro chamber for 500 s prior to fixation (green) and after fixation (magenta) are shown in

^c Please note that, the MATLAB script used to calculate MSDs can be found in the Appendix A on page 105.

Figure 9.2f. The MSD of motile cells show that trypanosome motility is a random walk ($\alpha \approx 1$). At much longer time scales, the confinement by the micro chamber walls drives the MSD into a plateau.

Conversely, GA-fixed trypanosomes exhibited Brownian rather than self-propelled motion. This difference results in a downshifting of the MSD of fixed cells by about two orders of magnitude.

The fixation process was – as expected – irreversible since the trypanosomes did not regain motility after the GA drug solution in the device had been replaced by culture medium (Figure 9.2c).

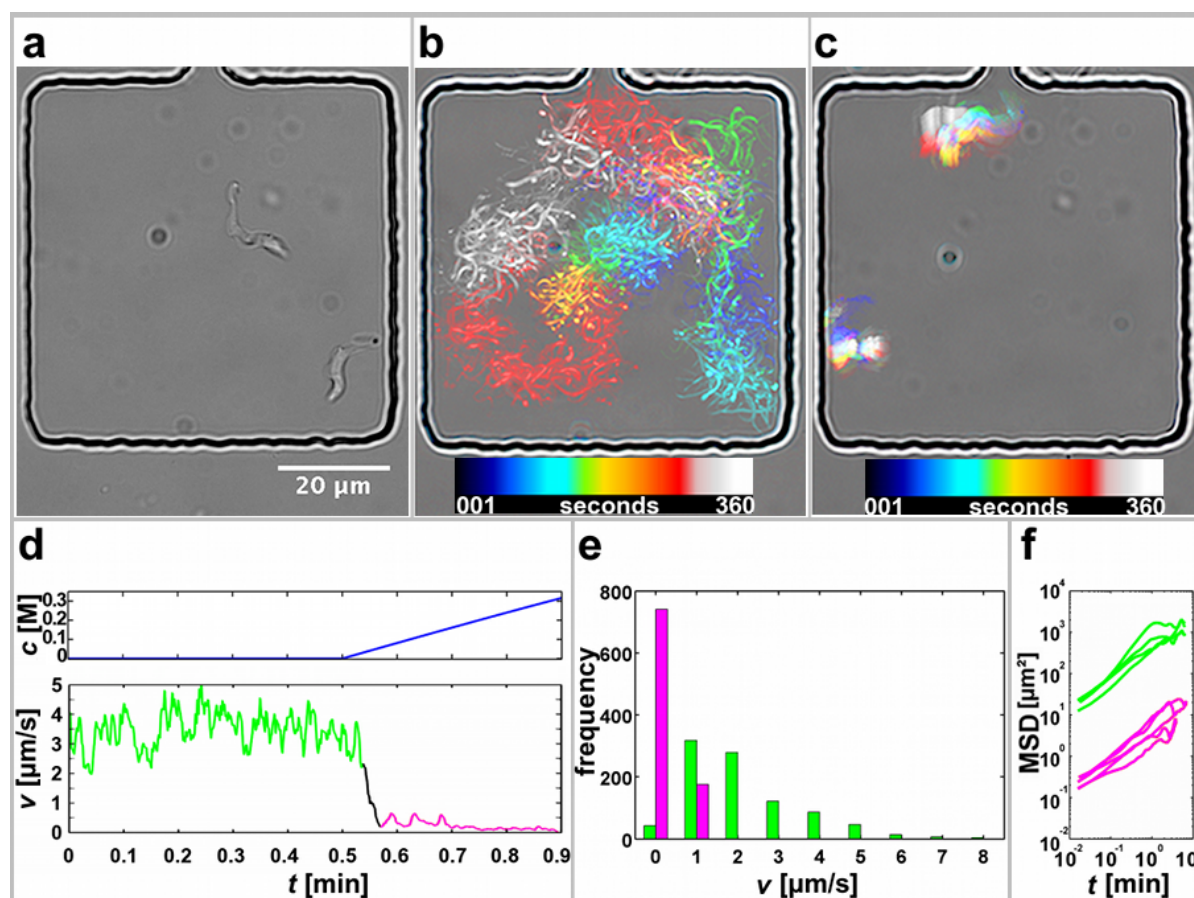


Figure 9.2: In situ cell fixation

(a) Bright-field micrograph of two trypanosomes confined to a micro chamber. (b) Overlaid colour-coded time-lapse trajectories of trypanosomes over 6 min in culture medium. (c) Time-lapse trajectories over 6 min after the addition of GA. (d) Velocity vs. time plot of a trypanosome before (green), during (black) and after (magenta) fixation with GA. (e) Velocity histogram of several trypanosomes before (green) and after (magenta) fixation with GA. (f) MSD of several trypanosomes in confinement before (green) and after GA fixation (magenta).

9.2.5 Microfluidics testing of 2DG on trypanosome motility

2DG is a glucose analogue that has previously been used to investigate trypanosome metabolism and motility.^{28,98,113,114} For our experiments, a small number of trypanosomes were placed in the

medium-filled micro chambers by optical tweezers and then the flow of a 2DG solution from the drug side into the main channel was initiated at concentrations ranging from 4 mM to 1.05 M. 2DG rapidly diffused into the micro chambers until it reached the concentration as in the main channel (supplementary video S1 and Figure S1). After cells were exposed for several minutes to the respective 2DG maximum concentration, drug-free was flushed in from the cell inlet (Figure 9.1, step VI) thereby decreasing the 2DG concentration in the micro chambers to zero (supplementary video S2). The motion of trypanosomes before, during and after exposure to 2DG was recorded at about 10 frames per second and the trajectories determined Figure 9.3a illustrates how the velocity $v(t)$ changes over time while the concentration of 2DG increased gradually for 5 minutes to 2.5 M and then was reduced again to zero. Trypanosome motility gradually decreased with the inflow of 2DG. After approximately 4 minutes of 2DG inflow, motility suddenly ended. Correspondingly, beyond this critical concentration $v(t)$ was virtually zero (supplementary video S4). However, if the 2DG concentration was reduced by flushing the device with culture medium (step VI), trypanosomes started to move again at a nearly constant $v(t)$ (supplementary video S5). It was even possible to repetitively paralyze and re-activate the same trypanosomes. The histogram of $v(t)$ and MSD for several trypanosomes before, during and after paralyzing are shown in Figure 9.3b and Figure 9.3c. All MSD exhibit a mean slope of $\alpha \approx 1$. In comparison to motile cells, the MSD of paralyzed cells were downshifted by about two orders of magnitude, thus resembling those of trypanosomes fixed by GA.

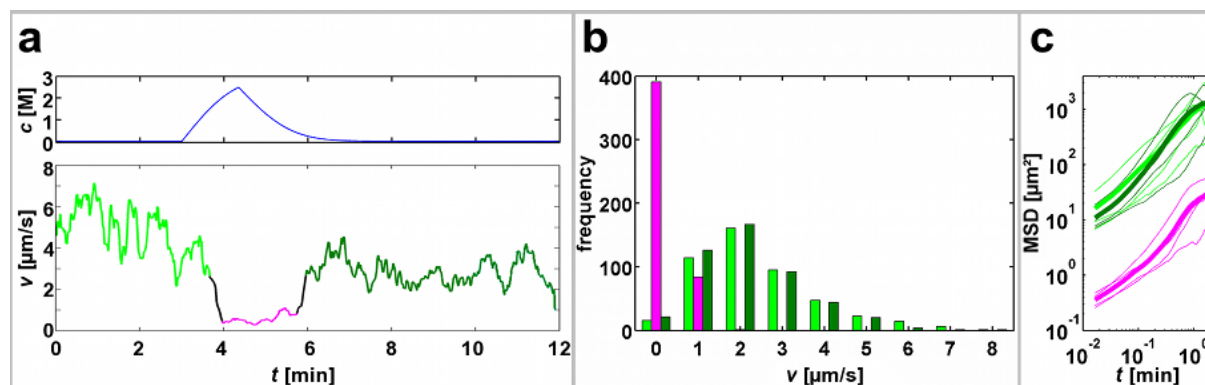


Figure 9.3: Reversible paralyzing of trypanosomes with 2DG

(a) Concentration of 2DG in the chamber (top) with representative velocity vs. time plot of an individual trypanosome (bottom). At $t = 3$ min, 2DG started diffusing into the micro chamber and the cell velocity decreased (green). After the 2DG concentration reached the critical value (here around 4 min), the trypanosome was completely paralyzed (magenta). In response to the inflow of culture medium, 2DG diffused out of the chamber. After approximately 6 min, the concentration of 2DG was below the critical value and the trypanosome regained mobility (dark green).

(b) Histogram of the velocities of several trypanosomes before (green) and above the critical value (magenta) of 2DG was reached, as well as after 2DG concentration fell below the critical value (dark green).

(c) MSD of trypanosomes at corresponding 2DG concentrations.

From the simulations of the evolution of the 2DG concentrations in the micro chambers applied to the corresponding motility analysis, we calculated at what concentration 2DG paralyzes the trypanosomes. The percentage of trypanosomes found to be paralyzed at specific concentrations is plotted in Figure 9.4. Full paralysis in trypanosomes occurred at 2DG concentrations of 400 mM and higher. At around 515 mM, 50% of the trypanosomes were paralyzed, resulting in the paralyzing dosage, $PD_{50} = 515$ mM. This paralyzing dosage of 515 mM has been confirmed by experiments with steady concentrations of 2DG.

Moreover, our method allowed for the direct observation of the evolution of the paralyzing effect on trypanosomes. With increasing dosage of 2DG, the trypanosomes moved slower, and at concentrations close to PD_{50} , the flagellum was still moving whereas the cell body was immobilized (supplementary videos S4 & S5).

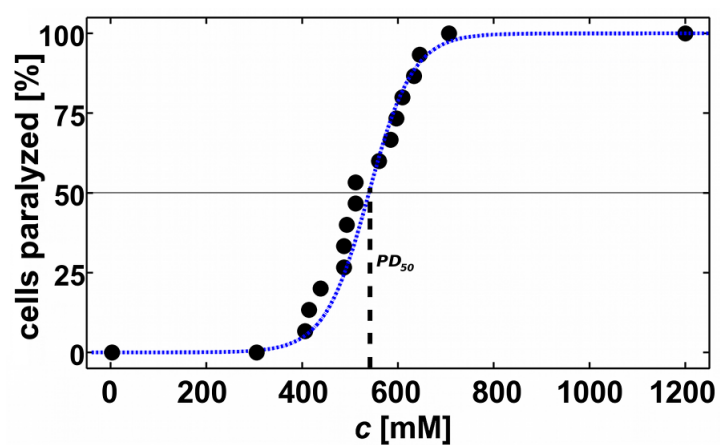


Figure 9.4: Paralyzing dosage PD_{50}

Percentage of trypanosomes paralyzed vs. concentration of 2DG. PD_{50} denotes the concentration of 2DG at which 50% of trypanosomes are paralyzed.

9.2.6 Impact of low dosages of 2DG on trypanosomes motility

We examined the effects of 2DG on trypanosome motility at concentrations more than two orders of magnitude lower than PD_{50} . For these low concentrations the recorded videos showed no obvious impact on trypanosome motility. But an increase of 2DG correlated with a downshift of MSD curves even at low concentrations (Figure 9.5a).

For a more quantitative description of the impact of 2DG on the motility of trypanosomes we used a simple hydrodynamic model. Whereas paralyzed cells exclusively exhibited Brownian motion, the motile cells at different 2DG concentrations were characterized by a random walk ($\alpha \approx 1$). Using the Stokes-Einstein relation, the motility coefficient of paralyzed cells, M_{para} , can be related to the thermal energy, $k_B T$. The friction factor of a paralyzed trypanosome, ξ_{para} , is

linked to its diffusion coefficient, D_{para} , by $M_{para} = \frac{\langle r(\tau)^2 \rangle_{para}}{4\tau} = D_{para} = \frac{k_B T}{\xi_{para}}$. By analogy, the motility coefficient of the motile, randomly walking cells ($\alpha = 1$), $M_{motile} \approx M_{\alpha=1} = \frac{\langle r(\tau)^2 \rangle_{motile}}{4\tau}$, can be described as $M_{motile} \cong \frac{\tilde{\epsilon} k_B T}{\xi_{motile}}$, using a virtual temperature, $\tilde{\epsilon} T$, or an apparent motility energy, $\tilde{\epsilon} k_B T$, where $\tilde{\epsilon}$ is a dimensionless factor. Taking into account that the friction factors of motile and paralyzed cells are almost identical, $\xi_{para} \approx \xi_{motile}$, the motility factor, $\tilde{\epsilon}$, can be obtained by $\tilde{\epsilon} \cong \frac{M_{motile}}{M_{para}} = \frac{\langle r(\tau)^2 \rangle_{motile}}{\langle r(\tau)^2 \rangle_{para}}$. The motility factor $\tilde{\epsilon}(c)$ in dependence of the 2DG concentration, which is a coarse estimate of the motility energy in multiple of $k_B T$, is presented in Figure 9.5b. A motile trypanosome in culture medium utilizes a motility energy that is approximately 130 times greater than the thermal energy. The motility factor $\tilde{\epsilon}(c)$ shows a strong, exponential-like decay with increasing concentration of 2DG (0 - 400 mM). However, for $\tilde{\epsilon}(c) \gg 1$, the trypanosomes were still motile. At 400 to 680 mM 2DG, the trypanosomes became paralyzed with a $PD_{50} = 515$ mM (Figure 9.4). For a motility factor $\tilde{\epsilon}(c) = 1$ the motility energy of a trypanosome equals the thermal energy, $k_B T$. Thus, propulsion is arrested and only Brownian motion occurs.

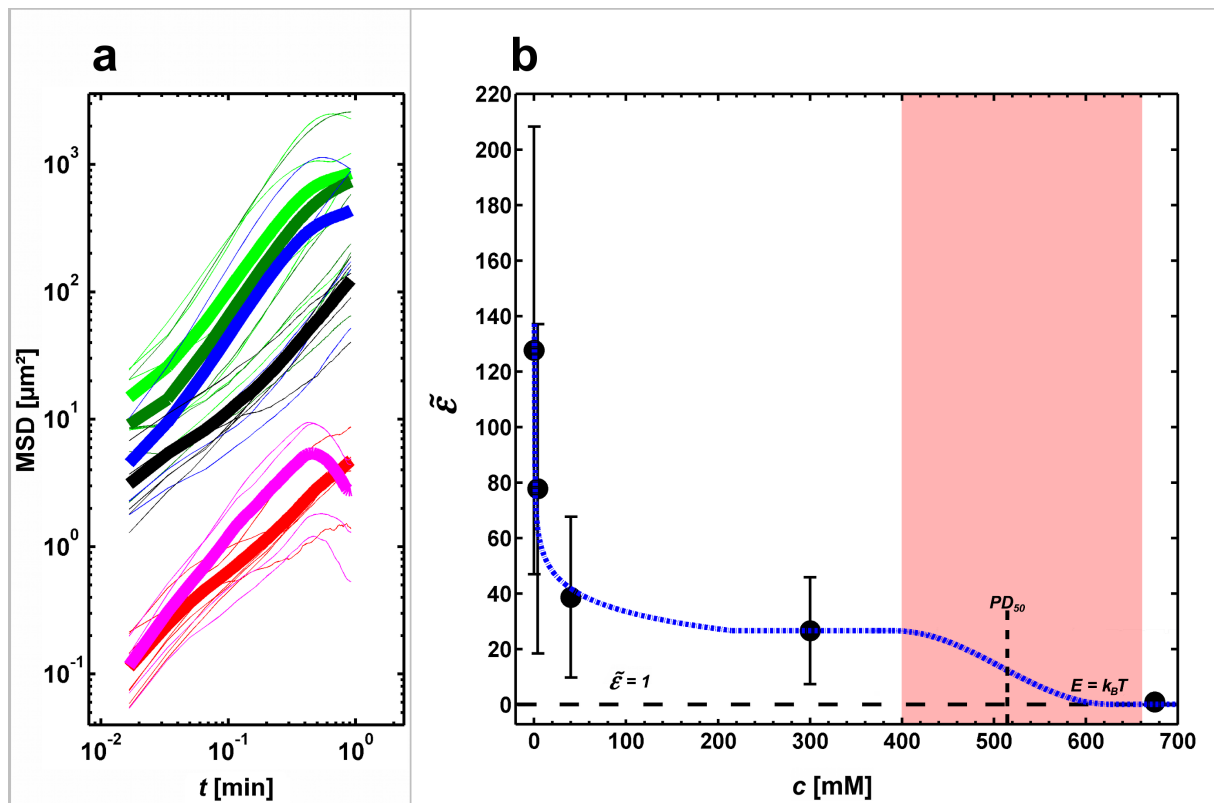


Figure 9.5 Analysis of the impact of 2DG on trypanosome propulsion

(a) MSD of trypanosomes in identical chambers but at different concentrations of 2DG in the medium (bright green: drug-free culture medium, dark green: $c_{2DG} = 4$ mM, blue: $c_{2DG} = 40$ mM black: $c_{2DG} = 300$ mM, magenta: fixed with GA, red: paralyzed; $c_{2DG} = 700$ mM). Thin lines are MSD of individual cells, bold lines are averages of a number of cells at the same 2DG concentration.

(b) The motility factor $\tilde{\epsilon}$ plotted against the concentration of 2DG in the medium. The dashed black line represents a motility factor $\tilde{\epsilon} = 1$, which means that the propulsion energy of a trypanosome equals the thermal energy, $k_B T$. The area shaded in red corresponds to the concentration range shown in Figure 9.4. Dashed blue line serves as a guide to the eye.

9.2.7 Single cell analysis with suramin

Suramin was introduced almost a century ago, and despite its severe side effects, still is the drug of choice in treating early stages of Eastern African sleeping sickness in humans.^{115–117} The route of entry into the trypanosomes as well as the mode of action remain enigmatic. Suramin presumably associates with different serum proteins in the bloodstream, e.g. low-density lipoproteins (LDL).^{117,118} It has been proposed that suramin's trypanocidal activity arises from its by interference with endocytic uptake of LDL.¹¹⁸ While it has been indicated, that suramin might inhibit several enzymes and receptors promiscuously¹¹⁷, a more recent study suggests that suramin undergoes receptor-mediated endocytosis to the lysosome where it escapes to the cytoplasm and may inhibit cellular processes¹¹⁹.

To gain a better understanding on the effects of suramin, we tested the response of trypanosomes to the drug in our single cell analysis. Similar to 2DG, suramin induced a paralysis of confined cells at a critical concentration of $PD_{50} = 123$ mM, (Figure 9.6a). Moreover, when the drug was flushed out of the device by culture medium, paralyzed trypanosomes regained motility.

We quantitatively assessed the impact of suramin on the motility of trypanosomes on the basis of MSDs that largely exhibit a mean slope of $\alpha \approx 1$ (Figure 9.6c). At a concentration of 3.5 mM suramin, which is significantly below PD_{50} , the motility factor $\tilde{\epsilon}$ was reduced to about one third as compared to trypanosomes in a drug-free environment. Between 35 mM and 80 mM suramin, a steady state with $\tilde{\epsilon}(c) \approx 35$ was reached, while between 80 and 170 mM, paralysis resulted in $\tilde{\epsilon}(c)$ of 1 (Figure 9.6d).

Besides the reversible reduction in cell motility, suramin exhibited trypanocidal effects. At dosages above 35 mM, trypanosomes were found to start rupturing and disintegrating after about 6 minutes of exposure to suramin (supplementary video S6). The percentage of trypanosomes that disintegrated at the end of a time lapse of 14 min increases with the concentration of suramin at steady state (Figure 9.6b).

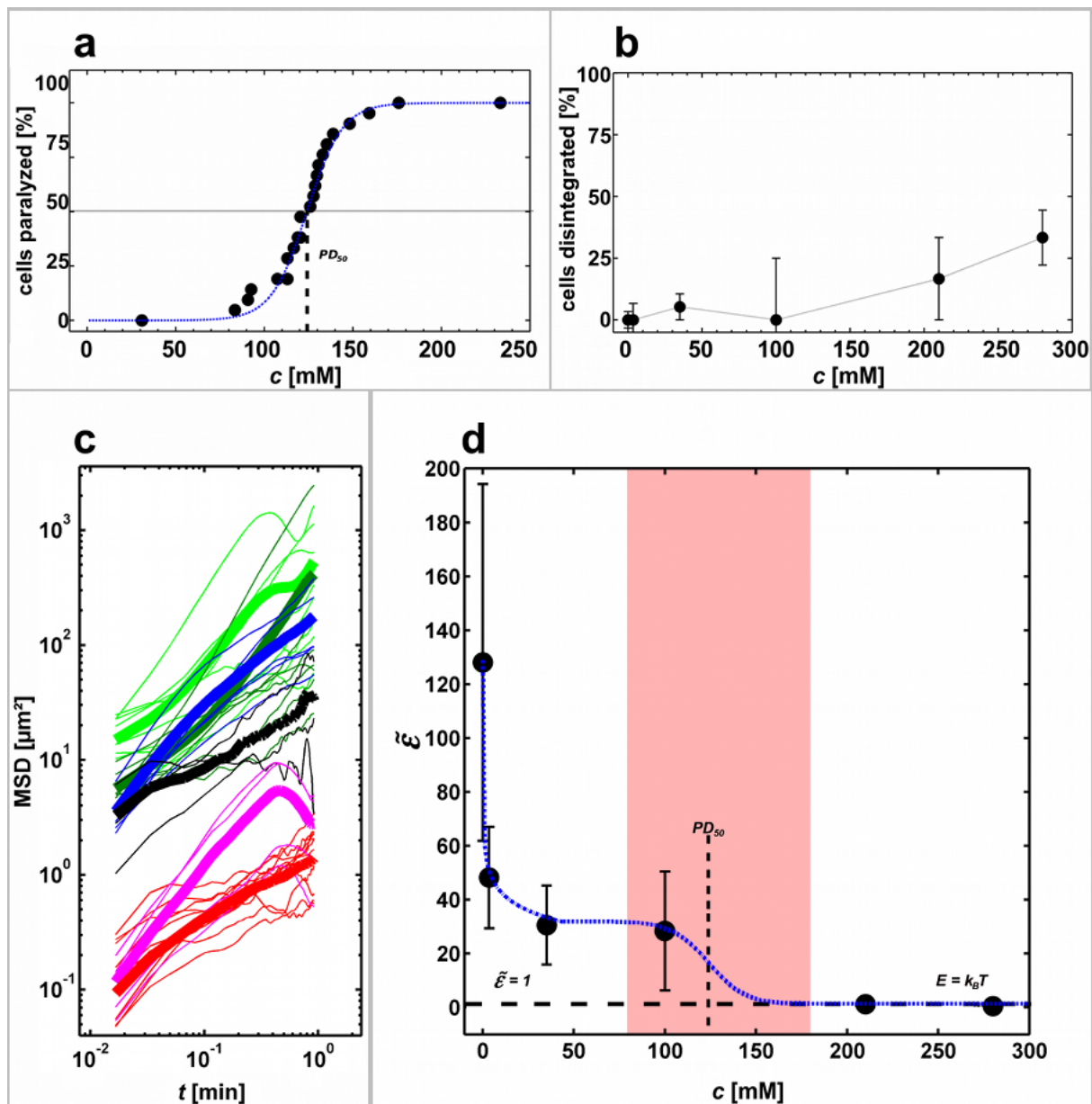


Figure 9.6: Quantitative analysis of the impact of suramin on trypanosome propulsion and disintegration

(a) Concentration dependent paralysis by suramin. PD_{50} denotes the concentration of suramin at which 50% of trypanosomes are paralyzed (123 mM).

(b) Disintegration of trypanosomes in response to different suramin concentrations.

(c) MSD of confined trypanosomes over time (bright green: drug free medium, dark green: $c_{\text{suramin}} = 3.5$ mM, blue: $c_{\text{suramin}} = 35$ mM, black: $c_{\text{suramin}} = 100$ mM, magenta: fixed with GA, red: paralyzed; $c_{\text{suramin}} = 210 - 280$ mM). Thin lines represent MSD of individual cells, bold lines are averages at the respective suramin concentrations.

(d) The motility factor $\tilde{\epsilon}$ at different concentrations of suramin in the micro chamber. The dashed black line represents $\tilde{\epsilon} = 1$, which indicates that the propulsion energy of a trypanosome equals the thermal energy, $k_B T$. The red area represents the concentration range shown specified in Figure 9.6a. Dashed blue line serves as a guide to the eye.

9.3 Discussion

The quantitative assessment of reversible and irreversible paralysis of trypanosomes shows that microfluidics in combination with microscopy is a versatile tool for single cell analysis and pharmaceutical testing. Our straightforward microfluidic-based method allows not only for an *in situ* analysis of single cells in defined, gradually changeable environments but also for a rapid evaluation of the impact of chemicals and drugs by analysing cell motility. Moreover, this approach eradicates the error of concentration inhomogeneity that arises from adding drug solutions drop-wise into a cell-laden well, that can lead to false results in commonly used micro-assays.

The rapid fixation of trypanosomes with GA represents an excellent model for a highly cytotoxic drug. We found that exposure to GA immediately and irreversibly ended active motion. This is most likely a result of cross-linking proteins involved in flagellum-dependent parasite motility, e.g. dynein¹²⁰. In contrast, paralysis of trypanosomes was reversible when trypanosomes were exposed to respective concentrations of 2DG, which is a competitive inhibitor of glycolysis¹¹⁴. Based on the precise and rapid control of drug concentrations in the confinements, we were able to determine the dosage at which 50% of the trypanosomes are paralyzed (PD₅₀). Furthermore, our data reveal an impact of 2DG on the motility of the cells at doses that are significantly lower than PD₅₀.

We introduced a simple random walk model to derive the propulsion energy from cell trajectories. According to this model, we noted a reduction of propulsion energy with increasing concentration of 2DG. This finding is consistent with the decrease in cell motility and with reports of 2DG as inhibitor of glycolysis in *Trypanosoma brucei* bloodstream forms. It is conceivable, that the resulting depletion of ATP might cause a decrease in flagellar motor activity and thereby reduce cell motility and hence vitality.

As the cytotoxicity-free, microfluidics-based single cell analysis revealed effects of 2DG at concentrations significantly lower than those used in common drug testing systems and had a much faster assessment than regularly used assays,^{92,94} we examined the response of trypanosomes to suramin, which is still the most commonly used drug in early-stage Trypanosomiasis. Our data show that suramin and 2DG have comparable effects with respect to cell motility, which is likely due to suramin blocking endocytosis in trypanosomes. Unlike 2DG, suramin also caused individual trypanosomes to rupture and disintegrate after exposure to concentrations of 35 mM and higher. Interestingly, the suramin-triggered disintegration occurred even after suramin removal, indicating that suramin either accumulates in trypanosomes or irreversibly alters cell regulations. The cytotoxic effect of suramin suggests that the suramin might

affect cellular mechanisms that ultimately result in cell lysis in addition to the inhibition of glycolysis, also exhibited by 2DG.

The concentration of suramin in a human patient, treated for Trypanosomiasis can accumulate to about 0.1 mM¹¹⁶ (based on the current chemotherapy¹⁰⁵, a volume of distribution V_D of 31-46 litres and a terminal half-life of 50 days). The dosages investigated herein are much higher but show the impact of suramin onto trypanosomes within minutes instead of weeks. From the drastic reduction of motility at low suramin dosages, a reduction in trypanosome propulsion energy of 10-25% at 0.1 mM seems plausible and might result in reduced immune evasion, and thus explain the therapeutic effect of suramin.

9.4 Conclusion

While we characterized our microfluidics-based method with established drugs and chemicals that affect *Trypanosoma brucei brucei*, the system lends itself to numerous adaptations, like finding and characterizing new drugs against trypanosomes or any other pathogenic cell. Further versatility can be easily accomplished by integrating additional methodologies, such as screening for mutants or fluorescence imaging – live as well as after fixation. Moreover, by applying our device to human cells and to pathogens simultaneously, effective drug doses could be determined in a single experiment.

10 Discussion

This doctoral thesis provides new insight into the motility of both prokaryotic (on the example of *Caulobacter crescentus*) and eukaryotic (on the example of *Trypanosoma brucei brucei*) flagellated single-cell organisms, as well as on the methodology with which they can be manipulated physically and chemically.

Even after over 160 years of research, some aspects of trypanosomal motility are still unknown. However, their way of locomotion is key in understanding how trypanosomes manage to evade the host immune system, how their pathogenicity is explained and why there is no inoculation against trypanosomes.

Trypanosomes that performed a directed motion before optical trapping, entered into a rotational movement with an average rotation frequency of 1.5 Hz during trapping. This rotational movement was overlaid by a zigzagging oscillation of 15 Hz caused by the beating of the flagellum. Similar beat frequencies of 15 and 18 Hz, respectively were also reported for untrapped, free swimming trypanosomes by Stellamanns *et al.* (2014)⁷⁸ and Heddergott *et al.* (2012)⁷⁷. This similarity in beat frequency, shows that optical confinement does not alter the flagellar beat of trypanosomes. It can therefore be assumed that the force generated by the flagellar movement will be the same for both trapped and free swimming trypanosomes. Thus we can conclude that the torque of $5.5 \cdot 10^{-18} \text{ N} \cdot \text{m}$, the energy, and power of $3.7 \cdot 10^{-17} \text{ J}$ and $5.6 \cdot 10^{-16} \text{ W}$ respectively, corresponds to the torque, power, and energy actually generated by a freely swimming trypanosome in the same liquid medium.

The finding, that only about 20% of the energy generated by the flagellar beat is translated into the actual propulsion of trypanosomes, might at first sight be surprising. Such huge energy expenditure seems a rather inefficient way to move for a highly adapted parasite. However this perceived inefficiency could be mitigated by the fact, that a trypanosome's flagellum is not merely used for propulsion, but also to transport VSGs to the flagellar pocket, where they are endocytosed and consumed. These VSGs are subsequently replaced by new proteins to counter the host-immune reaction. Such hydrodynamic clearing of the cell surface as described by Engstler *et al.* 2007¹¹, thus warrants the high energy consumption of the trypanosomal flagellum by enabling a high adaptability to the hostile environment of the trypanosome.

Studying the hydrodynamic flow field around trypanosomes swimming in a liquid containing polystyrene beads, we observed that the surrounding particles were being actively pushed along the cell body from the anterior to the posterior end of the trypanosome. Through this observation we could classify trypanosomes as pushers among the unicellular swimmers. This further strengthens the model of hydrodynamically mediated surface-clearing and host-immune

evasion of trypanosomes, since the flow field helps to push the variable surface proteins back to the flagellar pocket at the anterior end where endocytosis takes place.

Like for *Trypanosoma brucei brucei*, the force generated by the flagellar beat of *Caulobacter crescentus* swarmer cells was assessed with a combination of microfluidics and optical trapping. Other than trypanosomes, caulobacter as free living, unicellular organisms do not have the need to evade a hostile immune system. However, surface adhesion is of paramount importance for caulobacter to form biofilms¹²¹. In order to proliferate, caulobacter cells need to differentiate into stalked cells. These stalked cells are then able to produce holdfast to adhere to a surface.⁴¹

In our experiments, we managed to induce this holdfast formation by quickly bringing wild-type *Caulobacter* into contact with a surface. When using mutants lacking pili, we found that some caulobacter still managed to induce holdfast adhesion. However, pili-negative caulobacter that did not form holdfast attachment, nevertheless adhered to the surface with some kind of sticky filament. In this filament-mediated adhesion, the caulobacter were rotating around the adhesion site with a radius of 1-4 μm which is slightly shorter than the length of the caulobacter flagellum (6 μm)⁴⁶. Mutants lacking both pili and flagella still exhibited some sort of unspecific surface adhesion, which did however not show any form of rotational movement. The rotational radius in the pili-negative but flagellum-positive mutant and the lack thereof in the flagellum-negative caulobacter, could potentially indicate that the adhesion filament in the pili-negative mutant is indeed the flagellum. Yet to know for sure, this would have to be investigated in further experiments, for example by labelling the flagellum in order to see whether the flagellum is indeed the filament that adheres to the surface in absence of pili and holdfast.

The above mentioned findings show that microfluidics in combination with other tools such as high-speed microscopy and optical traps, is indeed a powerful tool to answer many questions. But in order to do so, the trap has to be adequately calibrated and the device accordingly designed depending on the matter under study and the research question. Phototoxic and other influencing factors have to be taken into account when working with living matter.

In our work we found that optical traps have to be adapted in order to minimize phototoxic effects on caulobacter. *Caulobacter* within the optical trap were incapacitated after only 10 seconds when using a laser with a wavelength of 808 nm, even with the relatively low power used in our experimental setup. This is an important parameter to account for, when manipulating caulobacter in an optical trap. Our findings are surprising in the light of the works of Liu (2009)⁵⁸ who reported to have optically trapped caulobacter for longer periods of time with wavelengths between 633 and 1064 nm and powers the same and higher as the one used by our setup, without having observed any noteworthy phototoxic effects. Nevertheless, it is advisable to first assess

any possible influences of the specific experimental setup on the organism under study before attempting to manipulate it with optical means

One applied use for our microfluidic setup in combination with high speed microscopy and unicellular pathogens, is studying the influence of chemical substances on the viability of the study organism. Colleagues from our research group have already demonstrated that microfluidic devices can be built in a way that they contain micro chambers with a no-flow condition, even in the presence of high flow velocities in the rest of the device.¹⁰⁹ We used this finding to create a device with which it was possible to test the influence of chemical substances on trypanosomes. Due to the lack of flow within the chamber, the concentration of the chemical substance introduced into the system, is determined purely by diffusion and can thus be very exactly controlled. This experimental setup was used in our work to demonstrate the effect of 2-deoxy-D-glucose, a known glycolysis inhibitor, and of suramin, the hallmark drug against early stage HAT, on *Trypanosoma brucei brucei*. With 2-deoxy-D-glucose, trypanosomes were fully paralyzed at a concentration of 515 mM, whereas for suramin, a concentration of 123 mM was sufficient to reduce the trypanosome's displacement to a level where it equalled mere brownian motion. Furthermore we were able to observe trypanocidal effects of suramin, leading trypanosomes to disintegrate once exposed to a drug concentration of 35 mM. Trypanosomes that had been exposed to this drug concentration, disintegrated independent of whether suramin concentration remained the same or dropped back down to zero again. Creating an experimental tool wherein it is possible to directly observe the effects of chemical substances on the viability and structure of living cellular pathogens in complex fluids, narrows the gap between compound research for new drugs and animal testing.

The geometry of the microfluidic devices itself also plays a role in the control and manipulation of study matter. The layout and size of the micro chambers influences, for example, the dwelling time of trypanosomes within the chamber. We observed that escape from round chambers was much quicker (from 2-12 minutes depending on flow and channel size) than escape from square chambers (retained throughout the whole observation) in our experiments. Analyzing the trajectories of the trypanosomes, we could observe that once trypanosomes hit a wall, they will follow this wall in one direction until they encounter a barrier. In a round chamber this following of the wall will inevitably lead the trypanosomes to an exit, whereas in a square chamber the trypanosome will hit another wall and then change direction randomly. Furthermore, ratchet devices can be used to hinder trypanosomes to exit the chamber once they are inside it. Through a combination of ratchet design and device geometry it should be possible to passively sort and concentrate trypanosomes in a suitable setup. By subsequently introducing a simple cross-flow

through the ratchet devices, the thus concentrated trypanosomes could then be evacuated from the device again for further use. A first attempt to design such a concentration device has been made in this work, leaving us with a preliminary knowledge-base of what to consider when designing cell-sorting devices for living trypanosomes. We learned that material properties and size of the structures have to be adjusted in order to ensure that the ratchets adhere to the surface and enable a concentration of trypanosomes. Yet, by employing arrow-head and gear-wheel ratchet structures, we were able to confine trypanosomes at a predefined place, and subsequently flush them out of the device again for further use. With some additional work, a microfluidic device for the passive concentration of trypanosomes from infected blood or spinal liquor samples is conceivable and would indeed be much wanted in the current search for new diagnostic devices for the sleeping sickness⁸⁹.

11 Outlook and Perspectives

As we did for *Trypanosoma brucei brucei* and *Caulobacter crescentus*, microfluidic devices in combination with optical traps can be used to analyse, manipulate and control the motility of different unicellular organisms.

Based on the results in this work, the combination of microfluidic devices with optical tweezers and high-speed microscopy can be further adapted for standardised testing of the effects of miniscule changes in drug concentrations on pathogenic microorganisms.

The knowledge about the motility of model organisms within a liquid medium deepens our understanding of how locomotion of microscopic organisms in the human blood circulation works. This knowledge is the basis needed by nano-engineers in their attempt to create artificial swimmers that could be used for the delivery of a drug to difficult to reach destinations.

Additionally, with a little more work, a cell sorting device can be created to passively sort and concentrate trypanosomes from infected blood or liquor samples and can be used as a diagnostic tool.

12 Appendix A Recipes

12.1 Soft Lithography:

Photoresist SU-8 3010 is spread on the waver in a spin coater using the following program:

1.	500 rpm for	10 seconds	fast ramping (1)
2.	4000 rpm for	30 seconds	slow ramping (8)
3.	soft baking on a heat plate for	3 minutes	@ 95 °C and cool down to R.T.
4.	align under the chrome mask.		
5.	expose to UV ($\lambda = 345 \text{ nm}$)	4.8-6 seconds	@ 33 mW/mm ²
6.	post-Exposure baking for	1 minute	@ 65 °C
6.b	for	4 minutes	@ 95 °C
7.	cool down to R.T.		
8.	rinse with SU-8 developer for	20-30 seconds	
9.	immerse in SU-8 developer for	4 minutes	
10.	spray wash with 2-propanol for	30 seconds	
11.	blow dry using nitrogen.		

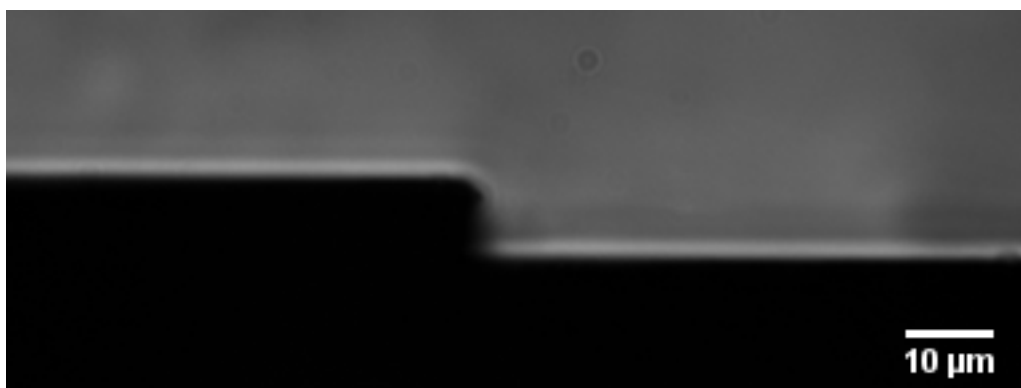


Figure 12.1: Side-on view through a device. The device height (8 μm) is visible as the size of the step between the wall (left) and a square micro chamber (right), resulting from the recipe above.

12.2 Cell Culture

12.2.1 Media

HMI-9 culture medium (HMI-9; 1 litre):

1.	830	mL			H ₂ O
2.	17.66	g			IMDM (+ L-Glutamine, -NaHCO ₃)
3.	3.024	g			NaHCO ₃
4.	028.2	mg	in	10 mL H ₂ O	Bathocuproind
5.	039.0	mg	in	10 mL H ₂ O	Thymidin
6.	014.0	µL	in	10 mL H ₂ O	2-Mercaptoetanol
7.	001.0	mg	in	10 mL H ₂ O	Pen/Strep
8.	136.0	mg	in	20 mL H ₂ O	Hypoxanthine
9.	100	mL			FCS
10.	182.0	mg	in	10 mL H ₂ O	Cysteine

Sterilize by filtration

Culture medium for experiments (50 mL):

1.	50	mL			HMI-9
2.	250	mg			BSA (Bovine Serum Albumin)

Store at 37.0 °C and 95%/5% CO₂ / air (v/v) for at least 4 hours.

Discard left-over after 5-7 days.

Drug solution for experiments (20 mL):

1.	20	mL			HMI-9
2.	100	mg			BSA **
3.	x	mg			drug (glutaraldehyde/2-deoxy- <i>D</i> - glucose/**suramin)
4.	0.02	mL			polystyrene beads

**Since BSA is known to reduce suramin efficacy, drug solutions of suramin contained no BSA

^dsonicated @ 40 °C for 15 min & vortexed prior to adding to solution

Freezing medium (100 mL)

1.	50	mL	FCS
2.	40	mL	CM culture medium
3.	10	mL	Glycerol

Sterilize by filtration

Trypanosome dilution buffer TDB

1.	1000	mL	of pure water
2.	0.37	g	KCl
3.	4.68	g	NaCl
4.	0.62	g	MgSO ₄
5.	3.56	g	Na ₂ HPO ₄ •2 H ₂ O
6.	0.28	g	NaH ₂ PO ₄ •1 H ₂ O
7.	3.96	g	Glucose

Sterilize by filtration

Trypanosome fixation buffer TFB

1.	90	mL	of pure water
2.	0.037	g	KCl
3.	0.468	g	NaCl
4.	0.062	g	MgSO ₄
5.	0.356	g	Na ₂ HPO ₄ •2 H ₂ O
6.	0.028	g	NaH ₂ PO ₄ •1 H ₂ O
7.	10	mL	Glutaraldehyde (25% solution in H ₂ O)

Sterilize by filtration

Trypanosome sleeping buffer TSB

1.	1000	mL	pure water, pH 7.7
2.	0.37	g	KCl
3.	4.68	g	NaCl
4.	0.62	g	MgSO ₄
5.	3.56	g	Na ₂ HPO ₄ •2 H ₂ O
6.	0.28	g	NaH ₂ PO ₄ •1 H ₂ O
7.	3.61	g	2-Deoxy-D-glucose

Sterilize by filtration

12.3 MATLAB codes

12.3.1 Plotting Trajectories in 3D:

To plot the recorded trajectories in 3D, the MATLAB inherent method “plot3” was modified :

```
Figure;  
plot3(Xm,Ym,Ts,'color','black');  
A=[Xm Ym Ts];  
L=size(A,1);  
L2=(round(L/4));  
L3=(round(L/2));  
L4=(round(L*3/4));  
for k=1:L2  
hold on  
plot3(A(k,1),A(k,2),A(k,3),'marker','o','color',[0,0.8,(k/L2)]  
)  
end  
for k=L2:L3  
plot3(A(k,1),A(k,2),A(k,3),'marker','o','color',[0,0.8*(1-  
(k/L3)),1])  
end  
for k=L3:L4  
plot3(A(k,1),A(k,2),A(k,3),'marker','o','color',[.8*(k/L4),0,1  
)  
end  
for k=L4:L  
plot3(A(k,1),A(k,2),A(k,3),'marker','o','color',[.8,0,1-((k-  
L4)/(L2))])  
end
```

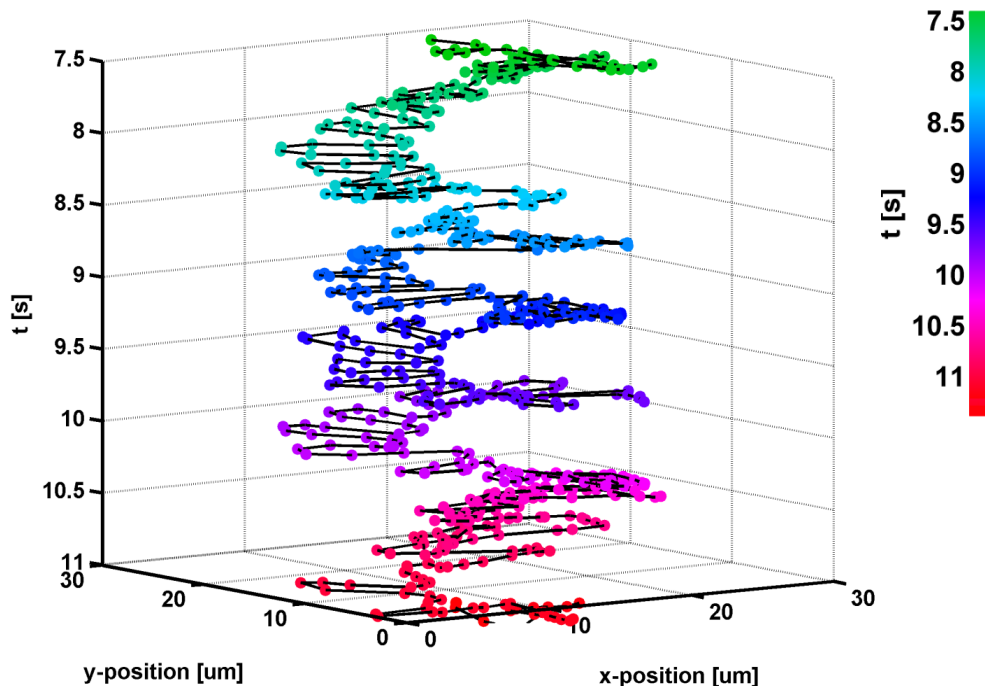


Figure 12.2: This 3-D-trajectory exhibits the rotation of an optically trapped trypanosome. Each dot denotes the position of the flagellar tip. This trajectory was recorded at 150 fps.

12.3.2 Mean squared displacement (MSD) script

The MSDs were calculated and plotted using the x- and y-positions of recorded trajectories employing the following MATLAB script:

```
%% Data Input

Fs=(58.3);                %Frequency of frames
l = length(x);
a=x';
b=y';
ts=1;
te=l-1;

%% x- MSD
xd1=a(1:(end-1));
xd2=(diag(xd1')•hankel(ones(1,length(xd1))))';
xd3=hankel(a(2:end));
msdx=xd3-xd2;

%% y-MSD
yd1=b(1:(end-1));
yd2=(diag(yd1')•hankel(ones(1,length(yd1))))';
yd3=hankel(b(2:end));
msdy=yd3-yd2;

%% total MSD
meansd=(msdx.^2 + msdy.^2);
factor = (size(meansd):-1:1);
msdav2 = ones(1,length(meansd))•(meansd');
msdav = msdav2./factor;
msdav=msdav(1:te);

%% Timescale
incr=1/Fs;                %your time increment
time=0:incr:(size(msdav,2))-1;

%% Fitting & Plotting Data
te=0.9•te;                %cutting off the 10% with least statistical significance;

B=polyfit(log(time(ts:te)),log(msdav(ts:te)),1);
loglog(time(ts:te),msdav(ts:te));
```

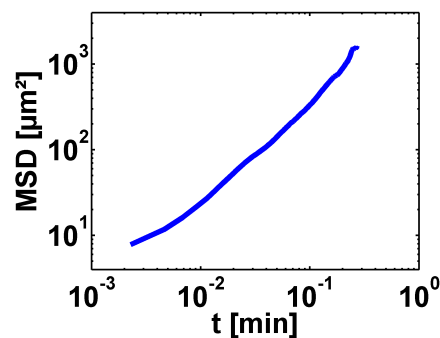


Figure 12.3: MSD of a random walker. The slope is approximately one.

13 References

1. Pfohl, T., Mugele, F., Seemann, R. & Herminghaus, S. Trends in microfluidics with complex fluids. *Chemphyschem* **4**, 1291–8 (2003).
2. Stellamanns, E. Cell motility in microfluidic environments. Georg–August–Universität, Göttingen, Germany (2010). at <<http://ediss.uni-goettingen.de/bitstream/handle/11858/00-1735-0000-0006-B548-9/stellamanns.pdf?sequence=1>>
3. Kitano, H. Systems biology: a brief overview. *Science (80-.)*. **295**, 1662–4 (2002).
4. Zheng, X. T. *et al.* On-chip investigation of cell-drug interactions. *Adv. Drug Deliv. Rev.* **65**, 1556–74 (2013).
5. Shahapure, R., Driessen, R. P. C., Haurat, M. F., Albers, S.-V. & Dame, R. T. The archaeellum: a rotating type IV pilus. *Mol. Microbiol.* **91**, 716–23 (2014).
6. Banusch, B. *Motility and Surface Adsorption of Caulobacter Crescentus*. 1–19 (2012).
7. Bardy, S. L. Prokaryotic motility structures. *Microbiology* **149**, 295–304 (2003).
8. Langousis, G. & Hill, K. L. Motility and more: the flagellum of *Trypanosoma brucei*. *Nat. Rev. Microbiol.* **12**, 505–18 (2014).
9. Rottner, K. & Stradal, T. E. B. Actin dynamics and turnover in cell motility. *Curr. Opin. Cell Biol.* **23**, 569–78 (2011).
10. Ziebert, F. & Aranson, I. S. Modular approach for modeling cell motility. *Eur. Phys. J. Spec. Top.* **223**, 1265–1277 (2014).
11. Engstler, M. *et al.* Hydrodynamic flow-mediated protein sorting on the cell surface of trypanosomes. *Cell* **131**, 505–515 (2007).
12. Levi, A. & Jenal, U. Holdfast formation in motile swarmer cells optimizes surface attachment during *Caulobacter crescentus* development. *J. Bacteriol.* **188**, 5315–8 (2006).
13. Entcheva-Dimitrov, P. & Spormann, A. M. Dynamics and Control of Biofilms of the Oligotrophic Bacterium *Caulobacter crescentus*. *J. Bacteriol.* **186**, 8254–8266 (2004).
14. Ciccarelli, F. D. *et al.* Toward automatic reconstruction of a highly resolved tree of life. *Science* **311**, 1283–7 (2006).
15. Degeneraas, G. The kingdom of life, science hq. Ed. Rod Pierce. accessed: 2014–08–17 (2013). at <<http://www.sciencehq.com/biology/kingdoms-life.html>>
16. Lighthill, J. Flagellar hydrodynamics. *SLAM Rev.* **18**, 161–230 (1976).
17. Maulucioni & Doridí. Phylogenetic-symbiogenetic tree of living organisms. accessed: 2014–10–25 (2013). at <http://en.wikipedia.org/wiki/Protist#mediaviewer/File:Tree_of_Living_Organisms_2.png>
18. Adl, S. M. *et al.* The new higher level classification of eukaryotes with emphasis on the taxonomy of protists. *J. Eukaryot. Microbiol.* **52**, 399–451 (2005).
19. Dauptain, A., Favier, J. & Bottaro, A. Hydrodynamics of ciliary propulsion. *J. Fluids Struct.* **24**, 1156–1165 (2008).
20. Ishikawa, T. Suspension biomechanics of swimming microbes. *J. R. Soc. Interface* **6**, 815–34 (2009).
21. Bravo-Cordero, J. J., Magalhaes, M. a O., Eddy, R. J., Hodgson, L. & Condeelis, J. Functions of cofilin in cell locomotion and invasion. *Nat. Rev. Mol. Cell Biol.* **14**, 405–15 (2013).
22. Melville, S. & Craig, L. Type IV pili in Gram-positive bacteria. *Microbiol. Mol. Biol. Rev.* **77**, 323–41 (2013).
23. Biais, N., Ladoux, B., Higashi, D., So, M. & Sheetz, M. Cooperative retraction of bundled type IV pili enables nanonewton force generation. *PLoS Biol.* **6**, e87:0907–13 (2008).
24. Curran, J. W. Gonorrhoea and the Urethral Syndrome. *Sex. Transm. Dis.* **4**, 119–121 (1977).

25. Einstein, A. Über die von der molekularkinetischen Theorie der Wärme geforderte Bewegung von in ruhenden Flüssigkeiten suspendierten Teilchen. *Ann. d. Phys.* **17**, 549–560 (1905).
26. Przi Bram, K. Über die ungeordnete Bewegung niederer Tiere. *Pflüger, Arch. für die Gesamte Physiol. des Menschen und der Thiere* **153**, 401–405 (1913).
27. Selmeczi, D. *et al.* Cell motility as random motion: A review. *Eur. Phys. J. Spec. Top.* **157**, 1–15 (2008).
28. Seed, J. R., Baquero, M. A. & Duda, J. F. Inhibition of hexose and glycerol utilization by 2-deoxy-d-glucose in *Trypanosoma gambiense* and *Trypanosoma rhodesiense*. *Exp. Parasitol.* **16**, 363–368 (1965).
29. Fenn, K. & Matthews, K. R. The cell biology of *Trypanosoma brucei* differentiation. *Curr. Opin. Microbiol.* **10**, 539–46 (2007).
30. Matthews, K. R., Ellis, J. R. & Paterou, A. Molecular regulation of the life cycle of African trypanosomes. *Trends Parasitol.* **20**, 40–47 (2004).
31. Bakker, B. M. *et al.* The silicon trypanosome. *Parasitology* **137**, 1333–41 (2010).
32. Rusk, N. How parasites do it. *Nat. Methods* **2**, 572–572 (2005).
33. Welburn, S., Picozzi, K., Fèvre, E. & Coleman, P. Identification of human-infective trypanosomes in animal reservoir of sleeping sickness in Uganda by means of serum-resistance-associated (SRA) gene. *Lancet* **358**, 2017–2019 (2001).
34. Fèvre, E. M. *et al.* The origins of a new *Trypanosoma brucei rhodesiense* sleeping sickness outbreak in eastern Uganda. *Lancet* **358**, 625–8 (2001).
35. Picozzi, K. *et al.* Sleeping sickness in Uganda: a thin line between two fatal diseases. *BMJ* **331**, 1238–41 (2005).
36. Welburn, S., Fèvre, E. & Coleman, P. Sleeping sickness: a tale of two diseases. *Trends Parasitol.* **17**, 19–24 (2001).
37. Welburn, S. C. *et al.* Crisis, what crisis? Control of Rhodesian sleeping sickness. *Trends Parasitol.* **22**, 123–8 (2006).
38. Uppaluri, S. Unicellular parasite motility: a quantitative perspective. Georg-August-Universität, Göttingen, Germany (2011).
39. Koyfman, A. Y. *et al.* Structure of *Trypanosoma brucei* flagellum accounts for its bihelical motion. *Proc. Natl. Acad. Sci. U. S. A.* **108**, 11105–8 (2011).
40. Uppaluri, S. *et al.* Impact of microscopic motility on the swimming behavior of parasites: straighter trypanosomes are more directional. *PLoS Comput. Biol.* **7**, e1002058:1–8 (2011).
41. Li, G. *et al.* Surface contact stimulates the just-in-time deployment of bacterial adhesins. *Mol. Microbiol.* **83**, 41–51 (2012).
42. Johnson, R. C. & Ely, B. Isolation of Spontaneously Derived Mutants of *Caulobacter Crescentus*. *Genetics* **86**, 25–32 (1977).
43. Poindexter, J. S. Selection for Nonbuoyant Morphological Mutants of *Caulobacter crescentus*. *J. Bacteriol.* **135**, 1141–1145 (1978).
44. Johnson, R. C. & Ely, B. Analysis of Nonmotile Mutants of the Dimorphic Bacterium *Caulobacter crescentus*. *J. Bacteriol.* **137**, 627–634 (1979).
45. Skerker, J. M. & Laub, M. T. Cell-cycle progression and the generation of asymmetry in *Caulobacter crescentus*. *Nat. Rev. Microbiol.* **2**, 325–37 (2004).
46. Li, G. & Tang, J. X. Low flagellar motor torque and high swimming efficiency of *Caulobacter crescentus* swarmer cells. *Biophys. J.* **91**, 2726–34 (2006).
47. Gravesen, P., Branebjerg, J. & Jensen, O. S. Microfluidics - a review. *J. Micromech. Microeng.* **3**, 168–182 (1993).
48. Atencia, J. & Beebe, D. J. Controlled microfluidic interfaces. *Nature* **437**, 648–55 (2005).
49. Ashkin, a. Optical Levitation by Radiation Pressure. *Appl. Phys. Lett.* **19**, 283–285 (1971).
50. Ashkin, A., Dziedzic, J. M., Bjorkholm, J. E. & Chu, S. Observation of a single-beam gradient force optical trap for dielectric particles. **11**, 288–290 (1986).

51. Galajda, P. & Ormos, P. Complex micromachines produced and driven by light. *Appl. Phys. Lett.* **78**, 249 (2001).
52. Asavei, T. *et al.* Optical angular momentum transfer to microrotors fabricated by two-photon photopolymerization. *New J. Phys.* **11**, 093021 (2009).
53. Marchington, R. F. Applications of Microfluidic Chips in Optical Manipulation & Photoporation. *Library (Lond)*. University of St Andrews, St Andrews, Scotland (2010). at <<http://hdl.handle.net/10023/1633>>
54. Singer, W., Bernet, S. & Ritsch-Marte, M. 3D-Force Calibration of Optical Tweezers for Mechanical Stimulation of Surfactant-Releasing Lung Cells. *Laser Phys.* **11**, 1217–1223 (2001).
55. Zhang, H. & Liu, K.-K. Optical tweezers for single cells. *J. R. Soc. Interface* **5**, 671–90 (2008).
56. Chien, Y.-S., Lin, C.-H., Kao, F.-J. & Ko, C.-W. Micro-flow-cytometer integrated with optical tweezer and DIP technique for cell/particle sorting and manipulation. *Nanosci. Technol. Pts 1 2* **121-123**, (2007).
57. Wang, M. M. *et al.* Microfluidic sorting of mammalian cells by optical force switching. *Nat. Biotechnol.* **23**, 83–7 (2005).
58. Liu, Y. MT Striped Birefringence Pattern Formation and Application of Laser Tweezers in Microrheology , Bacterial Motility and Adhesion. *Diss. Thesis* Brown University, Providence, Rhode Island, USA (2009).
59. Van Mameren, J., Wuite, G. J. L. & Heller, I. in *Single Mol. Anal.* (Peterman, E. J. G. & Wuite, G. J. L.) **783**, 1–20 (Humana Press, 2011).
60. Neuman, K. C. & Nagy, A. Single-molecule force spectroscopy: optical tweezers , magnetic tweezers and atomic force microscopy. *Nat. Methods* **5**, 491–505 (2008).
61. Visscher, K., Gross, S. P. & Block, S. M. Construction of multiple-beam optical traps with nanometer-resolution position sensing. *IEEE J. Sel. Top. Quantum Electron.* **2**, 1066–1076 (1996).
62. Batters, C. & Veigel, C. Single Molecule Enzymology. **778**, 97–109 (2011).
63. Ahluwalia, B., Yuan, X. & Tao, S. Transfer of “pure” on-axis spin angular momentum to the absorptive particle using self-imaged bottle beam optical tweezers system. *Opt. Express* **12**, 5172–7 (2004).
64. Ambrosio, A., Marrucci, L., Borbone, F., Roviello, A. & Maddalena, P. Light-induced spiral mass transport in azo-polymer films under vortex-beam illumination. *Nat. Commun.* **3**, 989 (2012).
65. Padgett, M. & Bowman, R. Tweezers with a twist. *Nat. Photonics* **5**, 343–348 (2011).
66. Litvin, I. A., Dudley, A. & Forbes, A. Poynting vector and orbital angular momentum density of superpositions of Bessel beams. *Opt. Express* **19**, 16760–71 (2011).
67. Padgett, M. & Di Leonardo, R. Holographic optical tweezers and their relevance to lab on chip devices. *Lab Chip* **11**, 1196–205 (2011).
68. Hesseling, C., Woerdemann, M., Hermerschmidt, A. & Denz, C. Controlling ghost traps in holographic optical tweezers. *Opt. Lett.* **36**, 3657–9 (2011).
69. Farré, A. *et al.* Positional stability of holographic optical traps. *Opt. Express* **19**, 21370–84 (2011).
70. Deshpande, S. Dynamics of Emerging Actin Networks. *Diss. Thesis* Universität Basel, Basel, Switzerland (2013).
71. Schindelin, J. *et al.* Fiji: an open-source platform for biological-image analysis. *Nat. Methods* **9**, 676–82 (2012).
72. Th, P., Ruttimann, U. E. & Unser, M. A Pyramid Approach to Subpixel Registration Based on Intensity. *IEEE Trans. Image Process.* **7**, 27–41 (1998).
73. Ramser, K. & Hanstorp, D. Optical manipulation for single-cell studies. *J. Biophotonics* **3**, 187–206 (2010).

74. Li, G., Smith, C. S., Brun, Y. V & Tang, J. X. The Elastic Properties of the *Caulobacter crescentus* Adhesive Holdfast Are Dependent on Oligomers of N -Acetylglucosamine. **187**, 257–265 (2005).
75. Ahmadi, G. Hydrodynamic forces. *Pers. Commun.* 1–11 (2005).
76. Hill, K. L. Parasites in motion: flagellum-driven cell motility in African trypanosomes. *Curr. Opin. Microbiol.* **13**, 459–65 (2010).
77. Heddergott, N. *et al.* Trypanosome motion represents an adaptation to the crowded environment of the vertebrate bloodstream. *PLoS Pathog.* **8**, e1003023:1–17 (2012).
78. Stellamanns, E. *et al.* Optical trapping reveals propulsion forces, power generation and motility efficiency of the unicellular parasites *Trypanosoma brucei brucei*. *Sci. Rep.* **4**, 6515:1–6515–7 (2014).
79. Tirado, M. M., Garcia, J. & Torre, D. Rotational dynamics of rigid, symmetric top macromolecules. Application to circular cylinders. *J. Chem. Phys.* **73**, 1986–1993 (1980).
80. Meinhart, C. D., Wereley, S. T. & Santiago, J. G. PIV measurements of a microchannel flow. *Exp. Fluids* **27**, 414–419 (1999).
81. Valentin, G. Ueber ein Entozoon im Blute von *Salmo fario*. *Arch. für Anat. Physiol. und wissenschaftliche Med.* 435–436 (1841).
82. Thielicke, W. & Stamhuis, E. J. PIVlab - Time-Resolved Digital Particle Image Velocimetry Tool for MATLAB (version: 1.35). at <<http://dx.doi.org/10.6084/m9.figshare.1092508>>
83. Rodríguez, J. A. *et al.* Propulsion of African trypanosomes is driven by bihelical waves with alternating chirality separated by kinks. *Proc. Natl. Acad. Sci.* **106**, 19322–19327 (2009).
84. Park, S., Kim, D., Mitchell, R. J. & Kim, T. A microfluidic concentrator array for quantitative predation assays of predatory microbes. *Lab Chip* **11**, 2916–23 (2011).
85. Galajda, P. *et al.* Funnel ratchets in biology at low Reynolds number: choanotaxis. *J. Mod. Opt.* **55**, 3413–3422 (2008).
86. Mahmud, G. *et al.* Directing cell motions on micropatterned ratchets. *Nat. Phys.* **5**, 606–612 (2009).
87. Elizabeth Hulme, S. *et al.* Using ratchets and sorters to fractionate motile cells of *Escherichia coli* by length. *Lab Chip* **8**, 1888–95 (2008).
88. Beech, J. P., Holm, S. H., Adolfsson, K. & Tegenfeldt, J. O. Sorting cells by size, shape and deformability. *Lab Chip* **12**, 1048–51 (2012).
89. Simarro, P. P., Jannin, J. & Cattand, P. Eliminating human African trypanosomiasis: where do we stand and what comes next? *PLoS Med.* **5**, e55:0174–80 (2008).
90. Steinhäuser, D., Köster, S. & Pfohl, T. Mobility Gradient Induces Cross-Streamline Migration of Semiflexible Polymers. *ACS Macro Lett.* **1**, 541–545 (2012).
91. Neuhäuser, P., Giselbrecht, S., Länge, K., Huang, T. J. & Manz, A. Revisiting lab-on-a-chip technology for drug discovery. *Nat. Rev. Drug Discov.* **11**, 620–32 (2012).
92. Canavaci, A. M. C. *et al.* In vitro and in vivo high-throughput assays for the testing of anti-*Trypanosoma cruzi* compounds. *PLoS Negl. Trop. Dis.* **4**, e87:0907–13 (2010).
93. Van Reet, N., Pyana, P., Rogé, S., Claes, F. & Büscher, P. Luminescent multiplex viability assay for *Trypanosoma brucei gambiense*. *Parasit. Vectors* **6**, 207 (2013).
94. De Rycker, M. *et al.* A static-cidal assay for *Trypanosoma brucei* to aid hit prioritisation for progression into drug discovery programmes. *PLoS Negl. Trop. Dis.* **6**, e1932:1–7 (2012).
95. Yin, H. & Marshall, D. Microfluidics for single cell analysis. *Curr. Opin. Biotechnol.* **23**, 110–9 (2012).
96. Brouzes, E. *et al.* Droplet microfluidic technology for single-cell high-throughput screening. *Proc. Natl. Acad. Sci. U. S. A.* **106**, 14195–200 (2009).
97. Junkin, M. & Tay, S. Microfluidic single-cell analysis for systems immunology. *Lab Chip* **14**, 1246–60 (2014).
98. Engstler, M. *et al.* in *Nature-inspired Fluid Mech.* (Tropea, C. & Bleckmann, H.) 43–61 (2012).

99. Min, T. L. *et al.* High-resolution, long-term characterization of bacterial motility using optical tweezers. *Nat. Methods* **6**, 831–5 (2009).
100. Groisman, A. *et al.* A microfluidic chemostat for experiments with bacterial and yeast cells. *Nat. Methods* **2**, 685–689 (2005).
101. Hsieh, C.-C., Huang, S.-B., Wu, P.-C., Shieh, D.-B. & Lee, G.-B. A microfluidic cell culture platform for real-time cellular imaging. *Biomed. Microdevices* **11**, 903–13 (2009).
102. Ryan, D., Ren, K. & Wu, H. Single-cell assays. *Biomicrofluidics* **5**, 21501–1 – 21501–9 (2011).
103. Wang, D. & Bodovitz, S. Single cell analysis: the new frontier in “omics”. *Trends Biotechnol.* **28**, 281–90 (2010).
104. Asphahani, F. *et al.* Single-cell bioelectrical impedance platform for monitoring cellular response to drug treatment. *Phys. Biol.* **8**, 015006 (2011).
105. Brun, R., Blum, J., Chappuis, F. & Burri, C. Human African trypanosomiasis. *Lancet* **375**, 148–59 (2010).
106. Overath, P. & Engstler, M. Endocytosis, membrane recycling and sorting of GPI-anchored proteins: *Trypanosoma brucei* as a model system. *Mol. Microbiol.* **53**, 735–44 (2004).
107. Mackey, Z. B. *et al.* Discovery of trypanocidal compounds by whole cell HTS of *Trypanosoma brucei*. *Chem. Biol. Drug Des.* **67**, 355–63 (2006).
108. Myburgh, E. *et al.* In vivo imaging of trypanosome-brain interactions and development of a rapid screening test for drugs against CNS stage trypanosomiasis. *PLoS Negl. Trop. Dis.* **7**, e2384:1–12 (2013).
109. Deshpande, S. & Pfohl, T. Hierarchical self-assembly of actin in micro-confinements using microfluidics. *Biomicrofluidics* **6**, 34120 (2012).
110. Chao, Y. & Zhang, T. Optimization of fixation methods for observation of bacterial cell morphology and surface ultrastructures by atomic force microscopy. *Appl. Microbiol. Biotechnol.* **92**, 381–92 (2011).
111. Moloney, M., McDonnell, L. & O’Shea, H. Atomic force microscopy of BHK-21 cells: an investigation of cell fixation techniques. *Ultramicroscopy* **100**, 153–61 (2004).
112. Han, Y. *et al.* Brownian motion of an ellipsoid. *Science* **314**, 626–30 (2006).
113. Lamour, N. *et al.* Proline metabolism in procyclic *Trypanosoma brucei* is down-regulated in the presence of glucose. *J. Biol. Chem.* **280**, 11902–10 (2005).
114. Parsons, M. & Nielsen, B. Active transport of 2-deoxy-D-glucose in *Trypanosoma brucei* procyclic forms. *Mol. Biochem. Parasitol.* **42**, 197–203 (1990).
115. Legros, D. *et al.* Treatment of human African trypanosomiasis — present situation and needs for research and development. *Lancet* **2**, 437–440 (2002).
116. Nok, A. J. Arsenicals (melarsoprol), pentamidine and suramin in the treatment of human African trypanosomiasis. *Parasitol. Res.* **90**, 71–9 (2003).
117. Fairlamb, A. H. Chemotherapy of human African trypanosomiasis: current and future prospects. *Trends Parasitol.* **19**, 488–494 (2003).
118. Vansterkenburg, E. L. M. *et al.* The uptake of the trypanocidal drug suramin in combination with low-density lipoproteins by *Trypanosoma brucei* and its possible mode of action. *Acta Trop.* **54**, 237–250 (1993).
119. Alsford, S., Field, M. C. & Horn, D. Receptor-mediated endocytosis for drug delivery in African trypanosomes: fulfilling Paul Ehrlich’s vision of chemotherapy. *Trends Parasitol.* **29**, 207–12 (2013).
120. Hughes, L. C., Ralston, K. S., Hill, K. L. & Zhou, Z. H. Three-dimensional structure of the *Trypanosome* flagellum suggests that the paraflagellar rod functions as a biomechanical spring. *PLoS One* **7**, e25700:1–10 (2012).
121. Hughes, V. & Jiang, C. Quick guide *Caulobacter crescentus*. *Curr. Biol.* **22**, R507–R509

Curriculum Vitae

Personal Information

Name	Axel Hochstetter
Date of birth	9 October 1985
Place of birth	Aalen, Germany
Nationality	German
Current address	Lothringerplatz 2, 4056 Basel, Switzerland

Education and Employment history

2010 - 2014	PhD in Biophysics University of Basel, Switzerland
2005 - 2010	Diploma in Chemistry Ulm University, Germany
2004 - 2005	Military Service 9. / Transport Battalion 10 Ellwangen (Jagst), Germany
30.06.2004	Abitur Parler Gymnasium Schwäbisch Gmünd, Germany

Publications, Meetings & Awards

Selected Publications

Hochstetter, A., Stellamanns, E., Deshpande, S., Uppaluri, S., Engstler, M. & Pfohl, T. Microfluidics-based single cell analysis reveals drug-dependent motility changes in trypanosomes. *Submitted* (2014).

Stellamanns, E., Uppaluri, S., **Hochstetter, A.**, Heddergott, N., Engstler, M. & Pfohl, T. Optical trapping reveals propulsion forces, power generation and motility efficiency of the unicellular parasites *Trypanosoma brucei brucei*. *Sci. Rep.* **4**, 6515:1–6515–7 (2014).

Hochstetter, A., Stellamanns, E., Uppaluri, S., Heddergott, N., Engstler, M. & Pfohl, T. Tracing the microscopic motility of unicellular parasites. *Eur. Biophys. J.* **42 Suppl 1**, S35-235 (2013).

Selected Meetings

- 2014 Deutsche Physikalische Gesellschaftstagung, Dresden, Germany (Poster)
- 2014 WiBioSE, Arandjelovac, Serbia (Talk)
- 2013 European Biophysical Societies Assosiation, Lisbon, Portugal (Talk + **Grant**)
- 2013 SmBioSE, Sheffield, UK, (Talk and Poster)
- 2013 Deutsche Physikalische Gesellschaftstagung, Regensburg, Germany (Talk)
- 2013 Swiss Soft Days X, PSI Villingen, Switzerland (Talk)
- 2013 Swiss Snow Symposium, Saas Fee, Switzerland (Talk + **Prize**)
- 2013 Rigiworkshop Akademie der Naturwissenschaften, Rigi-Kulm, Switzerland (Poster)
- 2012 Swiss Soft Days IX, Lausanne, Switzerland (Poster)
- 2012 SymBioSE, Szeged & Gödölö, Hungary (Talk, Workshop and Poster)
- 2012 Swiss Soft Days VIII, Geneva, Switzerland (Poster + **Prize**)
- 2011 European Biophysical Societies Assosiation, Budapest, Hungary (Poster)

Awards

Poster Prize (by Givaudan Schweiz AG, at the Swiss Soft Days VIII 2012 in Geneva)

Best Oral Presentation (by Actelion, at the Swiss Snow Symposium 2013 in Saas-Fee)

Travel Grant : Nachwuchs Reisefonds (by the University of Basel for partitipation in EBSA 2013 in Lisbon)

14 Thanks and Acknowledgments

While a dissertation thesis is the product of a single person, it is the effort of more than just that one person. Without support from others, so I believe, no one can nowadays manage to create such a piece of work (and art) as it has to be to pass the examination. So, at first, I want to shout out a great THANK YOU to my parents, Waltraud und Jochen, who made it possible for me to walk this path I chose in my life; to Steffi, Janice, Kai & Yvonne, to Oma, my family and friends, thank you all for being (in) my life!

Thomas, I am so very grateful that you granted me this amazing chance to do research with you and in your group. You literally gave me *carte blanche*, introduced me to curiosity-driven research and let me find my way. You really empowered me to find my way, my style to experiment, learn, teach, write and to present my findings. You actually let me hereby show everyone that I am able to conduct scientific research myself. For me, you were the perfect boss and supervisor, by never tell me which way I had to go, yet you were always there for me to give me advice show me alternatives and even made me defend my ideas and setups. On top of that huge pile, you are also a collegial, social person who knows how to handle a group and how to enjoy a good after-work drink...yet, somehow, that one rum Benni promised never came around, did it ?

Raphael, my Götti, you showed me around in Basel, Switzerland and even the Mensa =). Believe it or not, but you defined "swiss guy" for me: always helpful, a talent in organizing, always on time, friendly, but also sometimes a bit reserved and grumpy if tired. I will never forget how you missed Adriana in Budapest. Or our literally breath-taking hostel in Budapest. All the dust, and mold both in the washing machine and fridge. The electrical cord running along the bath-tub... I still am gratefull we made it out of there alive, you, me and Siddharth.

Siddharth, also called, Sweet-heart, Siddhu, "turkish pimp" or now: Dr. of Panda-nation. I always awed your knowledge of Beatles and books, your escapist love for books, films and Audrey Hepburn. By bringing your food to our parties at Thomas place and our hikes, you sparked the flame that now burns as afire for indian food, both in my heart and - occasionally - in my throat. I still know your recipe for green curry and make good use of it (along with the about two kilograms of eye- and mouth-watering spices you left me).

Nora, you took Siddharth's place in the office and you took to the task of rebuilding and improving "Eric". Always, you come up with a smile and always se the good side of anything.

Natalja, you are a charming and modest person. You were as eager to learn german as you were to teach me russian. □□□□□□ □□□□□□! By joining me in "my" office you made work so much more fun. In our group you found friends and even love, right, Michi? =). It was so much fun to see you two find together, even though you fought in the beginning like cats and dogs.

Cora, you are an inspiring person, always helpful, friendly and with an incredible treasure of experience. It is always a pleasure and an honour to work with you. I am thankful beyond words for your input on scientific writing and I hope we will have some more future projects ⇒).

Zoe Swank, you charming, warm-hearted girl. It was really fun to work and discuss with you.

Michael, tell me, how is it working only one and a half days per week? Just kidding ;)

Liebetanz, you were my first "student", one of many in all the years. Teaching was a very rewarding experience that I was happy to make a lot of times over the last years. From all of my students, very special thanks go to Benjamin Banusch, who not only joined our (and Urs Jenal's) group for almost half a year, but who also assisted me greatly in calibrating the optical trap and basically carried out all the experiments with caulobacter and was drawing the nice Figures. And he - had just as whacky working times as I had during the weekends ⇒).

I also wish to thank all my other students, Joel, Serena, Laura, Reto, Cedric, SM & SM and all the others.

And my friends here in Basel: Silvia, Angi, Flo, Andi, Franzi, Selma, Timo, Urs, Daniel, Peiling & Martin,... you made my life here so much more colorful.

Special thanks go to the Swiss tropical and Public Health Institute in Basel for their support, their gift of Trypanosomes after the -80 °C fridge malfunctioned and thawed, as well as to the many friends I could make there.

...and a special "Thank you!" goes to the Bands Sabaton, Van Canto, Manowar, Blind Guardian and to Lindsey Sterling and Alex "ASP" Spreng (and many more...) for their unbreaking moral support during the long shifts of coding, composing Figures and writing the texts, from their first points to the final version. You guys and girls created acoustic miracles that make endorphins dance tango and waltz with adrenalin in my blood, letting me push on and on and on.

And finally; my heart, my beloved Steffi. Your copious amounts of love, support and friendship empowered me, whenever I needed a boost of energy, motivation or just another point of view. You did more than just help me, you *changed* me. You made me a more understanding, compassionate, trusting and - hardly imaginable - a more relaxed person. Whether we danced together on Peiling and Martins wedding, or took the transsiberian railway for a week and 9288 km, or realized, that there are different ways to communicate, we had fun, and we came a long way :). You also helped me understand the differences between the journalistic way to write (to which I still am accustomed) and the scientific way, that I still have to learn loads about. And also, for your never fading understanding for the very egoistic needs, that arise during the hot-time of a PhD.

Thank You!